GEOTECHNICAL BEARING CAPACITY OF MV PILES

Improving the design based on full scale load tests in the Port of Rotterdam

F.Y.H. Westerbeke

Geotechnical bearing capacity of MV piles

Improving the design based on full scale load tests in the Port of Rotterdam

by

F.Y.H. Westerbeke

to obtain the degree of Master of Science
at the Delft University of Technology,
to be defended publicly on Thursday June 10, 2021 at 12:00 PM.

Student number:	4378628	
Project duration:	September, 2020 – May, 2021	
Thesis committee:	Dr. ir. M. Korff,	TU Delft
	Prof. dr ir. K.G. Gavin	TU Delft
	Dr. Ir. A.A. Roubos,	TU Delft, Port of Rotterdam
	Ir. J. Putteman,	SBE

Port of Rotterdam TU Delft SBE

Preface

In this thesis, I present the results of my research on the bearing capacity of MV piles, conducted in order to obtain the degree of Master of Science in Geo-Engineering at the faculty of Civil Engineering and Geosciences of Delft University of technology. This research was supported in a joint effort by Delft University of Technology, the Port of Rotterdam and SBE. I would like to express my gratitude to all the people that have supported me throughout this process.

First, I would like to thank the Port of Rotterdam for initiating this innovative project and for granting me the opportunity to contribute to it. I would like to thank Alfred Roubos for his guidance and advice and for helping me to connect theory and practice by bringing me into contact with many experts in the engineering industry.

Secondly, I would like to thank SBE for giving me the privilege being their first graduate research intern. Jan Putteman, thank you for your thorough support. You always took the time to review my work and gave me feedback on everything I sent your way (sometimes even before I had taken the time to review it myself). Your enthusiasm and expertise has greatly helped my research. To my colleagues from SBE Nederland, thank you for making me feel part of the team from the start. I could not have wished for a better environment to work in. After communicating from behind a desktop for months, I look forward to working with you all at the office after the summer.

From the TU Delft, I would like to thank my graduation committee. Mandy Korff, I could always ask you for support or opinion. Our online sparring sessions helped me to stay on track and and your input was always helpful. Ken Gavin, thank you for sharing your knowledge and ideas throughout this research. Your expertise and advice helped raising this thesis to a higher level and you were always willing to set a meeting despite your busy schedule. Moreover, I am grateful to Jan van Dalen and Rodriaan Spruit for sharing their knowledge and experience with the specifics of the project with me. I would also like to thank Eva van der Kooij for helping me to improve my Python programming skills and for going through this process with me. Our coffee walks helped me to get out of my so called research-bubble.

Furthermore, I want to thank everyone who supported me throughout my study and during this thesis. Thanks to my roommates and all my friends for going through the pandemic with me and for giving me the necessary distractions. Marijn, thank you for your patience and believing in me. Finally, I would like to thank my parents, Fred en Michèle, and my brother, Michiel, for their infinite love and support.

Fréderike Westerbeke
Rotterdam, May 2020

Abstract

Almost 4000 MV piles are used as anchorage of quay walls in the port of Rotterdam. The current design method of MV piles in Dutch practice is a CPT-based method that correlates the cone resistance to the shaft friction by a factor α_t. In the port of Rotterdam, the cone resistance is restricted under the assumption that no shaft resistance higher than 250 kPa is mobilised. Consequently, α_t is used in combination with a limiting value for the cone resistance of 18 MPa. Moreover, the value of α_t that is currently used in the port of Rotterdam (1.4%) is derived after limiting the cone resistance at 18 MPa. Since this design method was developed in the 1980s', many more MV piles were tested in the port of Rotterdam. The maximum test load was generally at least two times the characteristic value of the required anchor force. None of these full-scale tests were loaded up to failure and no significant creep effects were observed. Consequently, the design standard was never updated as ultimate bearing capacity remained undetermined.

Recently, the Port of Rotterdam has executed failure load tests in the Maasvlakte area. The tests allowed detailed strain readings along the full length of the test piles and offer the possibility to accurately determine the local mobilisation of shaft friction in addition to the ultimate failure load. Apart from describing the successful instrumentation with BOTDA fiber optical sensors (Brillouin Optical Time Domain Analysis), this study addresses the assessment of the obtained data in detail.

Multiple relations are considered in this thesis. Analysis of CPT's indicates an increase in cone resistance due to pile installation. Investigation of pile driving data shows that installation energy correlates well with the cone resistance. Soil-structure interaction is analysed and a mobilisation curve is composed. This curve illustrates that mobilisation of shaft friction as a function of displacement of MV (tension) piles is similar to the Dutch standard for small and non-displacement compression piles.

This thesis presents proof that limiting the cone resistance based on a maximum shaft friction of 250 kPa is not correct. The derivation of α_t without limiting the cone resistance results in a value of 1.2%. Installation energy proves to be a good indicator of the soil conditions. The piles that give good predictions for the bearing capacity with α_t = 1.2% present similar ratio's between the installation energy and the cone resistance. Future research may establish a consistent relation between CPT-based bearing capacity and pile driving energy to reduce uncertainty. This thesis will contribute to an update on the design method for MV-piles in dense sand layers of the Maasvlakte area.

List of abbreviations and symbols

- MV = Müller Verpress
- OTR = Offshore Tank Terminal
- HTT = Hartel Tank Terminal
- LVDT = Linear Variable Differential Transducer
- FOS = Fiber Optic Sensors
- BOTDA = Brillouin Optical Time Domain Analysis
- CPT = Cone Penetration Test
- IE = Installation energy
- q_c = Cone resistance
- q_s = Shaft resistance
- α_t = Coefficient for tensile bearing capacity

Contents

1

Introduction

1.1. Problem description

The Port of Rotterdam is the gateway to Europe thanks to its favourable geographical position right on the North Sea and at the mouth of the river Rhine. Because of this strategic location, its large depth and good hinterland connections, the port of Rotterdam continues to grow in container throughput. Along with this growth, the demand for deep-sea quay wall and terminal capacity space increases.
Figure 1.1 shows a a typical quay wall structure in the port of Rotterdam. MV (Müller Verpress) piles are frequently used as anchorage for these quay walls. MV piles are steel piles that are driven into the soil, while grout is injected at the tip of the pile. The grout reduces friction during installation, but ensures large shaft friction after hardening. MV piles up to 70 meters can be installed, providing a very high bearing capacity.

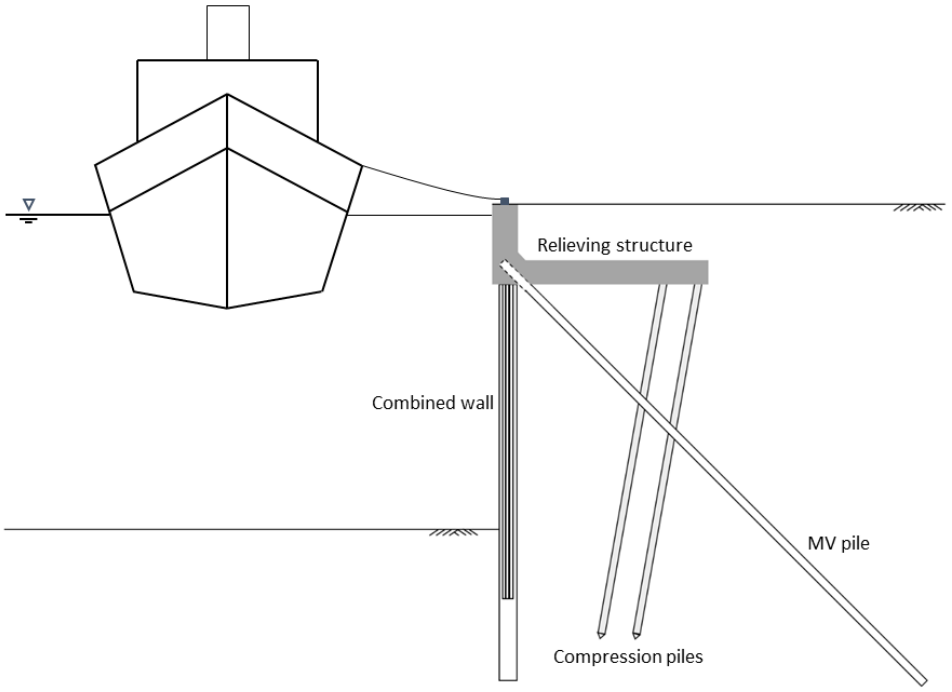

Figure 1.1: Quay wall structure

The design method that is used for the bearing capacity of MV piles in Dutch practice is based on the results of pile load tests from the 1980's. Since then, many full scale static load tests have been performed to evaluate the design of the MV piles along with the construction of quay walls in the port of Rotterdam. In many of these tests, piles remained far from geotechnical failure at maximum testing load. This indicates that the design method is too conservative and underestimates the ultimate bearing capacity of the piles. In a competitive domain such as port infrastructure it is crucial that the design of all components of infrastructure is optimised.

1.2. Project background

Between 2016 and 2019, the Port of Rotterdam executed 11 full scale pile load tests along with the construction of two major deep sea quay walls in the Maasvlakte area. The locations of the test sites are marked in Figure 1.2. The tested piles were not part of the quay construction, enabling loading until geotechnical failure to determine the ultimate bearing capacity. All test piles were instrumented with optical fibres, allowing detailed strain distributions along the full length of the piles to accurately determine the local mobilisation of shaft friction in addition to the ultimate failure load.

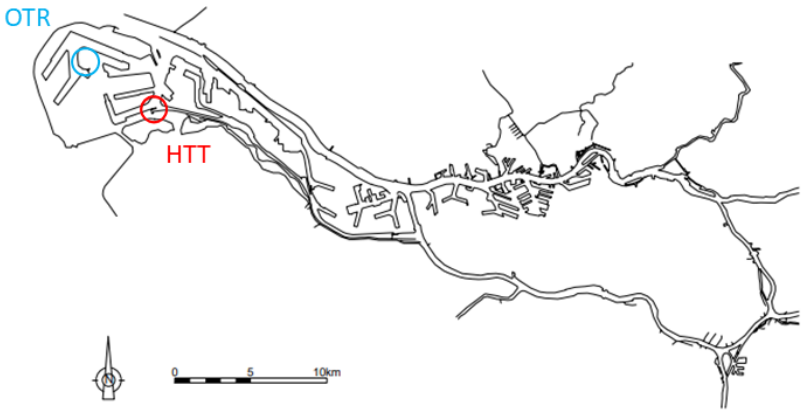

Figure 1.2: Location of the Offshore Terminal Rotterdam (OTR) and Hartel Tank Terminal (HTT).

The design method that is used in Dutch practice for the design of MV piles is a CPT-based design method, correlating the cone resistance (q_c) from the Cone Penetration Test directly to the shaft friction (q_s). The shaft resistance (equivalent to the bearing resistance for tension piles), is determined using a factor $\alpha_t = q_s/q_c$. This factor is limited to a maximum q_s of approximately 250 kPa, corresponding in effect to a limiting the cone resistance at a value of 18 MPa in Maasvlakte soil conditions (15 MPa in the rest of the Netherlands). The cone resistance is restricted under the assumption that no shaft resistance higher than 250 kPa is mobilised. Moreover, the value of α_t that currently used in the port of Rotterdam is derived after limiting the cone resistance at 18 MPa. As the retaining heights of quay walls have increased over the years, soil strengths have also increased and values of q_c exceeding 50 MPa are commonly encountered. Analysis of recent failure load tests, opens the route to an improved design method.

1.3. Research objective and questions

The objective of this thesis is to evaluate and improve the design method of MV piles. The main research question of this thesis is formulated as follows:

> "**How can the data acquired from full scale load tests upon failure be used to improve the design bearing capacity of MV-piles?**".

To achieve the objective of this research, the following is investigated:

1. Is the imposed limited value on cone resistance appropriate for determination of the ultimate bearing capacity?
2. What are the effects of installation on the cone resistance?
3. Can installation parameters of MV piles be correlated to their bearing capacity?
4. What CPT-based design method is most appropriate to determine the bearing capacity of MV piles in Maasvlakte soil conditions?
5. Can the full scale test data be used to validate finite element models for research and design purposes?

1.4. Scope and limitations

The scope of this research is focused on MV piles that are loaded axially in tension. All test piles are installed under an angle of 42.5°or 47.5°in the similar soil conditions. The scope of this research is therefore limited to MV piles located in the dense Pleistocene sand layer in Maasvlakte-area.

1.5. Outline

This chapter is followed by 6 chapters as schematically illustrated in Figure 1.3. Chapter 2 contains the literature study of this thesis and provides the relevant background information to support assumptions, methodologies, analysis in this research. Chapter 3 describes the test setup and presents an overview of all obtained data. The fourth chapter describes how the test data is processed. The processed data is analysed in Chapter 5. The derived results are presented and discussed in Chapter 6. In the final chapter, conclusions are drawn and recommendations regarding future research are proposed.

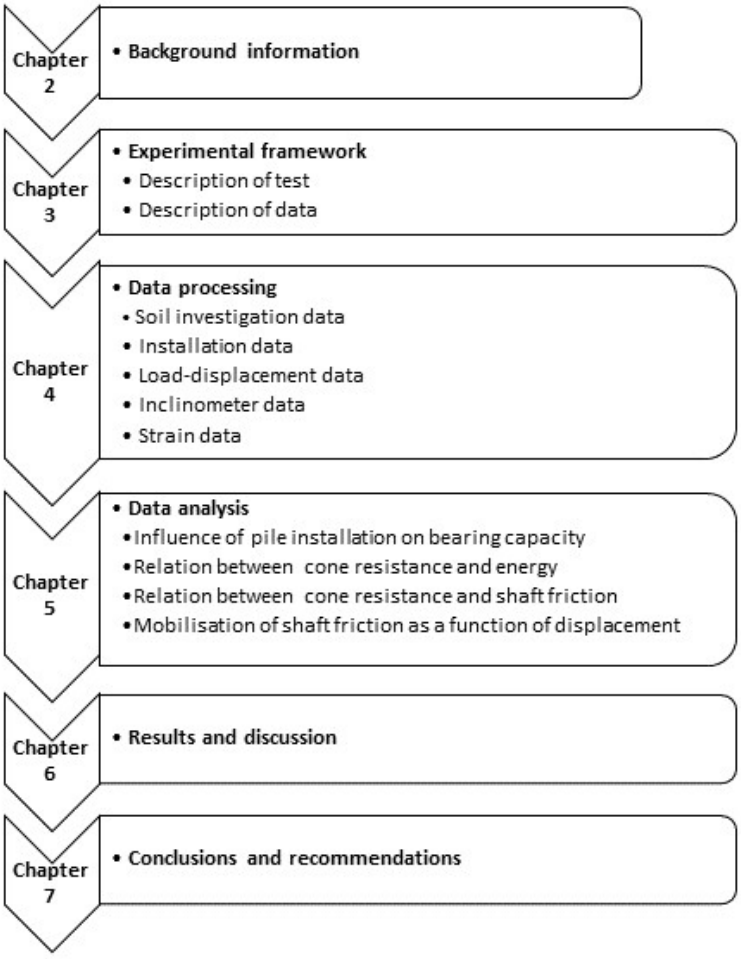

Figure 1.3: Structure of report.

2

Background information

This chapter contains the relevant background information that is conducted as part of the literature study of this thesis. The information in this chapter provides general background and supports assumptions, analysis and interpretations in this research.

2.1. MV piles in the port of Rotterdam

Almost 4000 MV piles are used as anchorage of quay walls in the port of Rotterdam. Figure 2.1 shows at which quay walls MV piles are used as anchorage. A table containing the number of piles per quay wall can be found in Appendix A. To evaluate the design of the MV piles, full scale static load tests are performed prior to construction. Since 1980, MV piles have been tested at almost every project. The maximum test load was generally at least a factor two higher than the characteristic value of the required anchor force. None of the tested piles were considered to have geotechnically failed and most of the test piles did not yet show significant creep effects. A table containing an overview of all historic load tests on MV piles in the port of Rotterdam can be found in Appendix A.

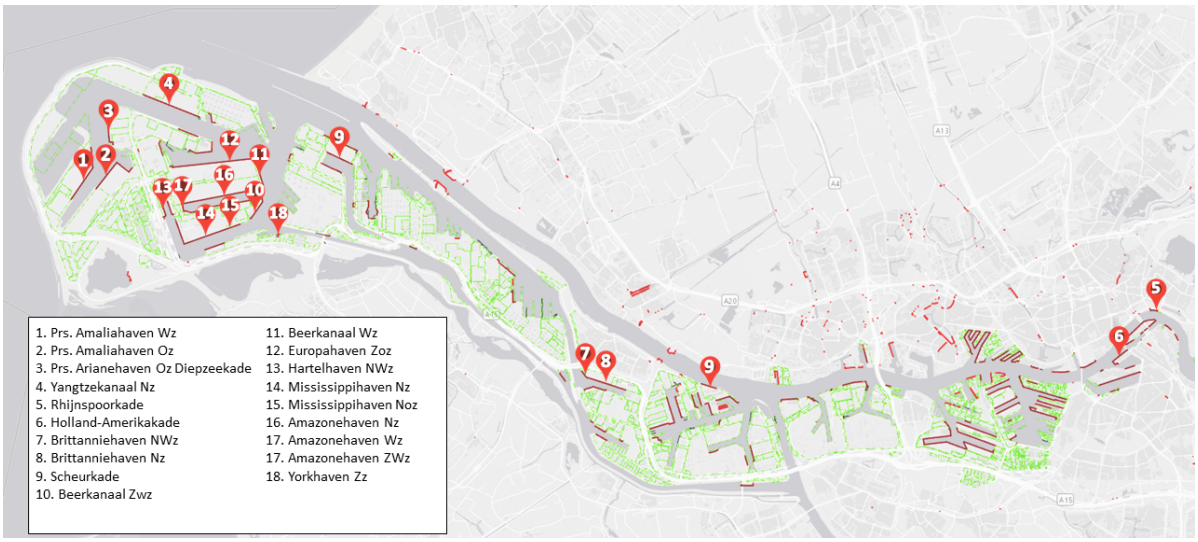

Figure 2.1: Map of quay walls with MV piles as anchorage in the port of Rotterdam.

2.2. MV-piles

2.2.1. General description

The MV pile can be described as an in situ driven and grouted displacement pile. MV piles consist of a steel profile with a widened tip (see Figure 2.2). The soil that is pushed away by the widened tip during installation is filled up by grout that is injected just above the tip. The liquid grout column improves the driveability of the soil during installation. After hardening, the grout improves the attachment between pile and soil as it acts as glue between the steel profile and the surrounding soil. Moreover, the shell of grout provides protection against corrosion. MV piles are tension piles as they are installed by driving and are often used for quay wall anchorage as they can withstand substantial tensile forces.

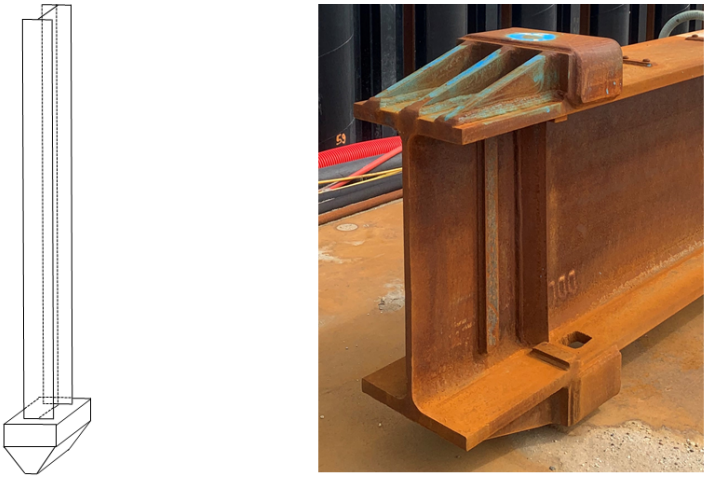

Figure 2.2: Schematisation of MV pile (left) and picture of pile tip (right).

2.2.2. Installation method

MV piles are installed under and angle of ca 45 °to the horizontal. MV piles can be up to 70 meters long and are installed by driving. The steel profile is driven into the soil by repeated blows provided by a hydraulic hammer. This is done by a piling rig as can be seen in Figure 2.3. Grout is continuously pumped to the pile toe during hammering.The grout is supplied through pipes that are attached to the flanges of the profile. Close to the tip, the grout is injected into two steel reservoirs [6].

Figure 2.3: Installation of MV pile (personally taken photograph: Putteman, J.).

2.3. Pile design

2.3.1. Bearing capacity of single piles

The ultimate bearing capacity of a single pile is generally determined from one or a combination of three approaches [12]:

- Static bearing capacity design.
- Dynamic bearing capacity design.
- Empirical pile design.

Static bearing capacity design

Static bearing capacity design methods are based on in situ soil strength parameters. The ultimate pile capacity (Q_u) is usually expressed as the sum of the shaft friction (Q_s) and the base resistance (Q_b).

$$Q_u = Q_s + Q_b \tag{2.1}$$

The bearing capacity of a tension pile is entirely derived from friction between the pile shaft and soil (Q_s). The amount of friction depends on [17]:

- The roughness of the pile shaft.
- The angle of internal friction and cohesion of the soil.
- The density of the soil.
- The stress level in the soil.

Dynamic bearing capacity design

Dynamic bearing capacity formulas are based on the effects of the dynamics of pile installation on the system. Dynamic pile analysis generally involves driving a pile, recording the driving history and performing a pile load test. Nearly all dynamic equations are based on the rational pile formula, which is derived from the principle that the total dynamic soil resistance must at least equal the effective impact force (impulse-momentum theorem). However, most dynamic pile formulas are derived under various assumptions and are coupled with a wide variability in soils and hammer conditions. No dynamic equation has been consistently reliable over a certain range of pile capacities. It is generally accepted that dynamic predictions are not very reliable [2].

Empirical pile design

Empirical pile design is based on installation and testing of trial piles. Full scale load testing is usually performed as part of larger contracts as it is relatively expensive and time consuming. Relationships with in situ test techniques, often involving CPT penetrometers (see Section 2.5.1), are often studied for the argument that the penetration resistance can be correlated to pile bearing capacity. CPT based pile design is also favourable as CPT's are frequently used during site investigation of a project [12]. The longer-term effects of installation on soil stress are usually not included in empirical pile design as bearing capacity is determined based on the characteristics of the soil before the piles are installed [17].

2.3.2. Dutch design standard for tension piles (CUR166)

In Dutch practice, MV piles are designed with the design method described in CUR166 [27] for grouted anchors [32]. The CUR166 [27] is composed in accordance with the NEN9997-1 [22] and is more explicit for sheet pile constructions and quay wall anchorage. The method for calculating the bearing capacity is a CPT-based method correlating the cone resistance (q_c) to the shaft friction. The value of correlation factor α_t is determined from test loads. Moreover, it is assumed that soil parameters influencing the bearing capacity are implicitly included in the value of α_t. Effects of neighbouring pile installation, large tensional loads during the operation phase are not included in this α-value and are incorporated into the design by design factors (f). The design value of the bearing capacity of a tension pile can be calculated with equation 2.2 [27]:

$$F_{r;tension;d} = \int_O^L q_{c;z;d} \cdot f_1 \cdot f_2 \cdot O_{p;z} \cdot \alpha_t dz \tag{2.2}$$

Where:

$F_{r;tension;d}$ = design value of the tensional capacity [kN];
$q_{c;z;d}$ = design value for the cone resistance at depth z [kPa];
f_1 = group effect of installation of neighbouring piles (f_1 > 1.0);
f_2 = group effect of tensional load (f_2 < 1.0);
$O_{p;z}$ = circumference of the shaft at depth z [m];
α_t = coefficient for shaft friction at depth z;
L = length of the pile over which shaft friction is taken into account [m].

If a CPT is executed close to the pile after installation, f_1 = 1.0. For a single pile: $f_1 = f_2 = 1.0$ [17]. The design value of the cone resistance is generally determined using the following equation:

$$q_{c;z;d} = \frac{\xi}{\gamma_{m;b4} \cdot \gamma_{m;var;qc}} \cdot q_{c;z;lim} \tag{2.3}$$

In which:

$q_{c;z;d}$ = representative cone resistance [MPa];
$q_{c;z;lim}$ = cone resistance at depth z below ground level, in which peaks in the CPT diagram are cut off;
ξ = factor for the number of CPT's and the redistribution capacity of the structure;
$\gamma_{m;b4}$ = material factor for tension piles (1.35 for tension piles according to NEN 9997 [22]);
$\gamma_{m;var;qc}$ = partial factor for load variations ($\gamma_{m;var;qc} \leq 1.5$).

The measured cone resistance from the CPT's is limited to account for effects that impact the soil resistance after construction. In Dutch practice, the cone resistance is limited to between 12 MPa and 15 MPa, depending on the thickness of the bearing layers. Design codes allow a higher q_c value of approximately 18 MPa in Maasvlakte area because of the history of load testing by the Port of Rotterdam [27]. Research has shown that limiting the cone resistance has a large impact in dense sand profiles, which can lead to underestimation of the pile capacity [10].

2.4. Pile load testing

The objective of a pile load test is to obtain as much information as possible to assess the behaviour of the pile. For grouted anchors in sand, a loading procedure with one unloading/reloading cycle per load step is to be preferred. This testing procedure gives information about the creep and the permanent displacement, while the ultimate capacity or the creep behaviour of the anchor is least affected by the loading cycles [31]. The following test boundaries apply to tension piles [29]:

1. The applied load equals the limit of the test system.
2. The pile experiences structural failure.
3. The pile is no longer able to resist the target load (geotechnical failure).

The test will be terminated if one of the boundaries is reached. Figure 2.4 illustrates the three failure mechanisms.

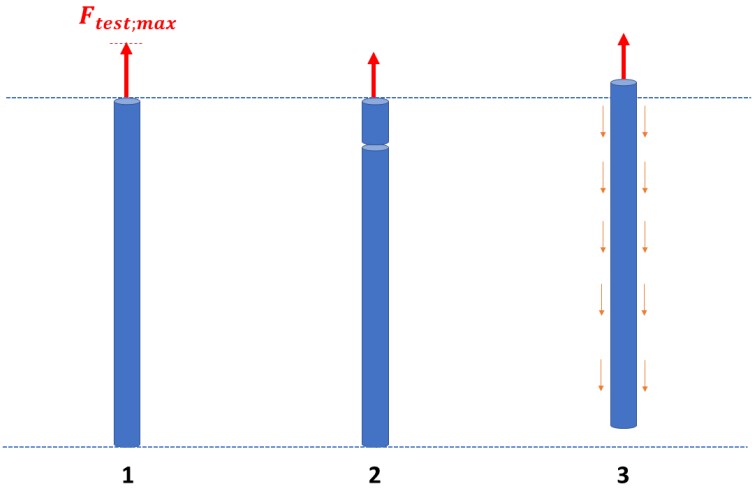

Figure 2.4: Boundaries of load test on tension piles: maximum test load (1), structural failure (2) and geotechnical failure (3).

2.4.1. Dutch design standard for load testing (CUR166)

The testing procedure for tension piles is described in CUR166. This Dutch design standard is All pile load tests in the port of Rotterdam are carried out according to this standard. At more recent tests, the number of load steps and maximum test load is increased as larger test loads were applied. In Dutch practice, the axial displacement of the pile over time is used as indicator of failure. This indicator is known as the creep criterion. The threshold of failure is set by the creep coefficient (c), which is equal to the slope of the pile head displacement (δ) plotted on a logarithmic timescale:

$$c = \frac{\delta_1 - \delta_2}{log(t_1) - \log(t_2)} \tag{2.4}$$

Where:

c = coefficient of creep;
δ_1 = pile head displacement at time t_1;
δ_2 = pile head displacement at time t_2.

The creep coefficient is not allowed to exceed 2 mm in the Netherlands. To prevent structural failure of the pile maximum test load is limited by [27]:

$$P_p \leq 0.9 \cdot R_{t;d} \tag{2.5}$$

In which:

P_p = maximum test load;
$R_{t;d}$ = the design value of the strength of the anchor.

Figure 2.5 shows the standard loading scheme including the force and duration per step. An initial force (P_i) of 10% of the maximum test load is applied first to check if the reaction frame needs to be realigned. After this, the maximum test load is raised in steps to the maximum test load. After each step, the force is reduced back to the initial force.

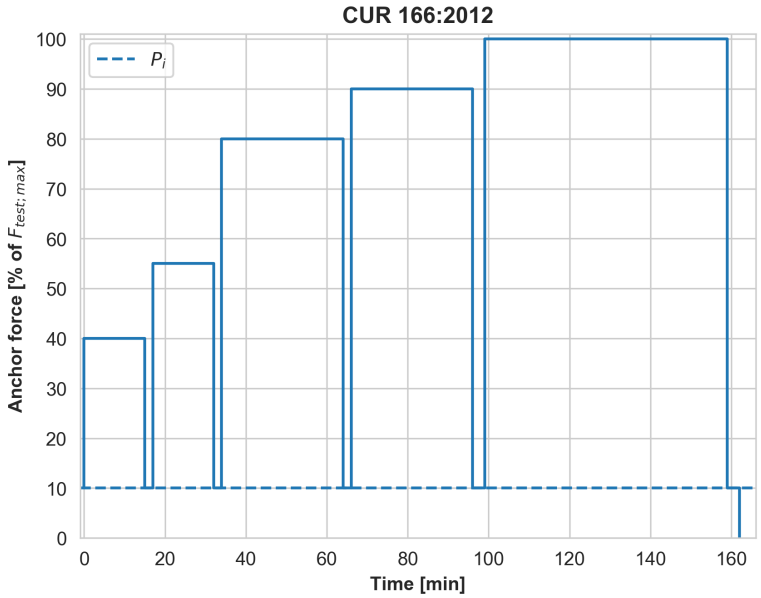

Figure 2.5: Procedure of failure load test.

2.5. Measurement techniques

Different measurement techniques are used during the pile load tests that are analysed in this research. This section provides as background for the assessment and processing of the data obtained from these techniques in following chapters.

2.5.1. Cone Penetration Test (CPT)

The Cone Penetration Test (CPT) is an in-situ test method used to investigate the underground stratigraphy and to determine the geotechnical properties of the soils present. Due to low cost, continuous data and well established correlations with soil properties, it is one of the most widely used and accepted test methods in the geotechnical engineering practice [18]. Cone penetration testing is performed by pushing an instrumented cone into the ground at a controlled rate. Parameters obtained generally include the cone resistance (q_c), sleeve friction (f_s) and piezocone pore pressure (u). The cone resistance is determined by dividing the total force acting on the cone over the projected area of the cone. Sleeve friction (f_s) is the force acting on the sleeve divided by its surface area. Pore pressure is typically measured behind the cone, as indicated in Figure 2.6.

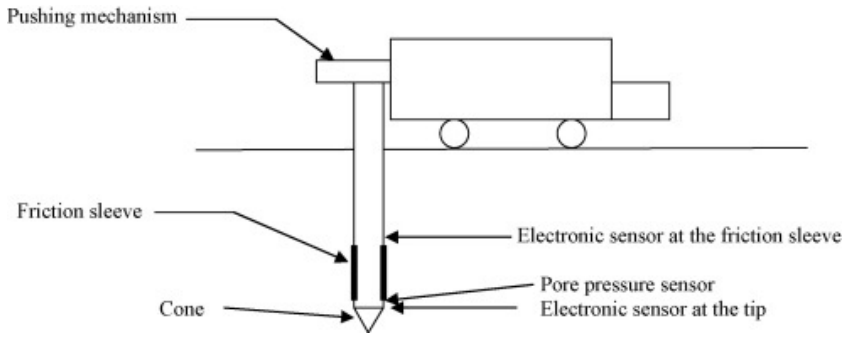

Figure 2.6: Principle of Cone Penetration Testing [7].

2.5.2. Linear Variable Differential Transducer (LVDT)

Linear Variable Displacement Transducers (LVDTs) are used to measure movement in one direction along a single axis. An LVDT consists of a core and three coils of wire wound on a hollow form (see Figure 2.7). The core is a metal rod attached to the moveable object whose position is to be determined. If the primary core is moved out of the centre of the object, the voltage rises in one secondary coil and decreases in the other secondary coil. When the primary core is positioned in the middle, the voltages of secondary coils are equal. The output of the LVDT is the measured distance the objective has traveled. LVDTs provide reliable position measurements. Their main advantage over other types of displacement transducer is the high degree of robustness as there is no physical contact with the sensing element [15].

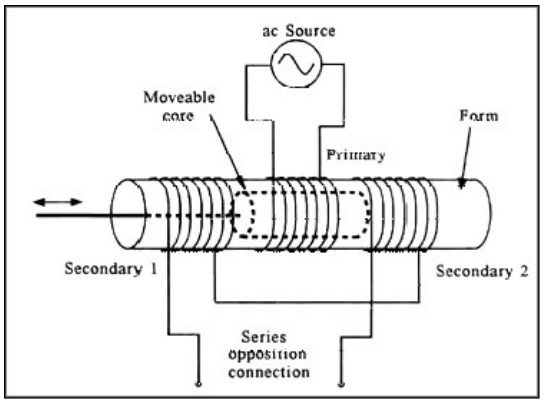

Figure 2.7: Components of Linear Variable Displacement Transducers [15].

2.5.3. Fiber optic sensors (FOS)

Over the last years, the use of Fiber optic sensors (FOS) has grown in the geotechnical industry. Measuring the wave propagation in fibers provides a direct method of measuring the changes in strain along the entire length of piles, whereas the conventional strain gauges only provided measurements at certain locations within the piles [5]. Two FOS technologies that are commonly used are Brillouin Optical Time Domain Re-flectometry (BOTDR) and Brillouin Optical Time Domain Analysis (BOTDA) [33]. The BOTDR systems consists of only one fiber end while the BOTDA requires two fiber ends which are connected in a loop. The BOTDA system has two lightwaves injected into the optical fiber: a pulsed-optical wave (pump pulse) and a counter propagating light (prope signal). By measuring the frequency of either wave with respect to the other, the difference can be translated to strain or temperature at each point along the sensing fiber [23]. Figure 2.8 illustrates the BOTDA measurement principle.

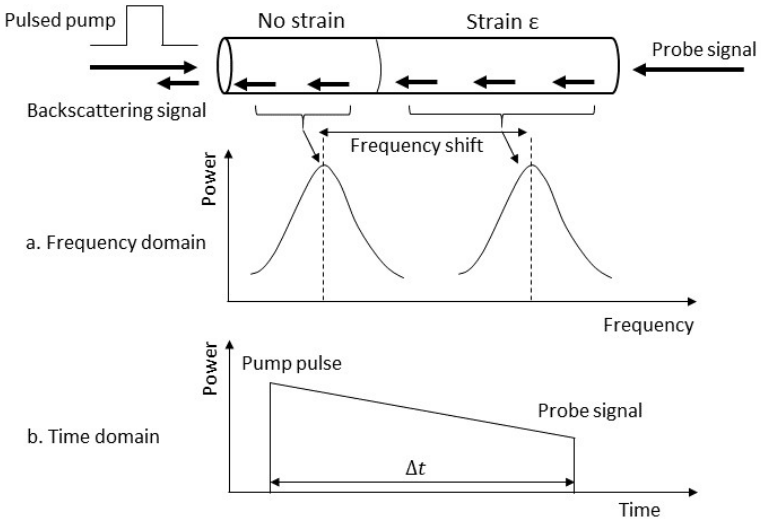

Figure 2.8: BOTDA measurement system with frequency (a) and time (b) domain analysis.

For pile instrumentation, it is recommended to install more than one fiber per pile for redundancy purposes and for verification in case damage occurs. For steel piles, fibers are commonly glued to the pile and protected by an additional steel bar that is welded to the pile.

Figure 2.9: Photo of MV test pile illustrating the loop configuration of BOTDA sensor and protection by a welded steel bar (personally taken photograph: Putteman, J.).

2.6. Static pile capacity from load-displacement data

The static pile bearing capacity can be back-calculated from load-transfer data obtained from full scale load tests equipped with strain gauges and/or fiber optics.The stress-strain relationship for axially loaded pile can be divided into three parts [4]:

- The skin friction acting along the shaft
- The axial deformation of the pile
- The soil end-bearing (not relevant for tension piles).

The soil skin friction along the pile shaft
The soil skin friction is equal to the load transferred to the soil over a pile segment. Pile segments are determined by the measurement intervals of the strain gauges or fiber optics. The load transferred to the soil difference in measured load or stress. As the pile diameter and measurement interval are known, the shear resistance can be easily computed.

The axial deformation of the pile
If the point displacement is known, the axial deformation of each segment can be computed using the average axial load [2].

The soil end-bearing
The soil end-bearing is not relevant for this research, as MV piles are tension piles.

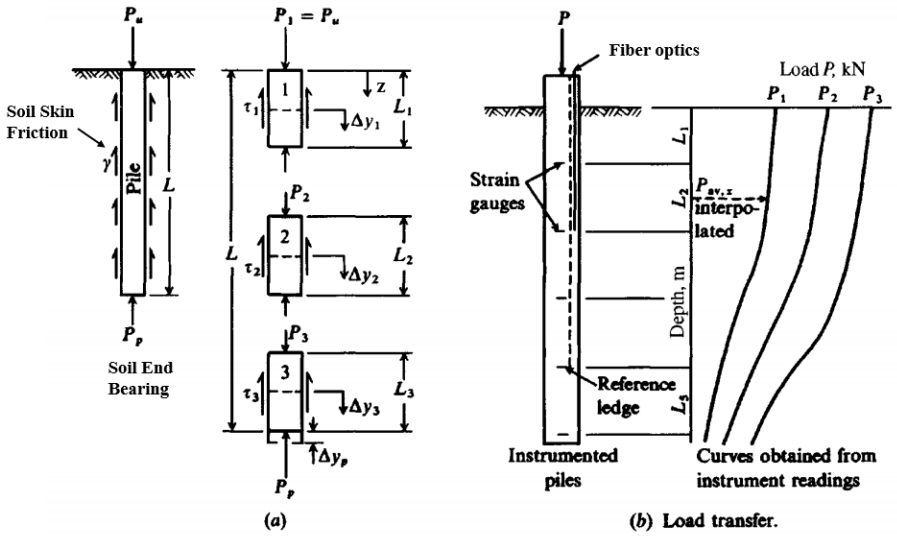

Figure 2.10: Load-transfer method for axially loaded piles [4].

The previously described load-transfer method is visualised in Figure 2.10. A load-transfer curve can be developed by applying several load increments to the pile. In general, multiple curves are required to model the pile-soil response. A load-transfer curve can be developed for each pile segment of the pile.

2.7. Strain-to-load interpretation

Static full-scale load tests on instrumented piles can provide valuable information about the actual bearing capacity and shear characteristics of the pile. As mentioned in section 2.5, fiber optic sensors provide distributed strain sensing along the entire length of the pile. These sensors measure the changes in strain during conventional top load pile testing [13]. Changes in strain can also be caused by uneven load increments, variations in load-level duration and unloading actions. Therefore, static load tests should be executed without disruptions and continuously in load and direction. When test data is secured, a detail that is often overlooked is the determination of loads from strains. This is not as simple as the multiplication of strain (ϵ) by the Young's modulus (E) and cross sectional area of the pile (A) [8]. This section provides background for the assessment and interpretation of strain data.

2.7.1. Residual loads

It is common to assume a "no-load" condition before the start of a test. This means a start with zero conditions. However, assuming that the reading before the start of the test represents the "no-load" condition neglects the existence of residual loads in the pile [9]. Residual loads are the locked-in loads that exist in the pile after installation before loading. The development of residual loads can be divided into two stages for driven piles [9].

(a) During pile driving.

(b) During relaxation of the surrounding soil.

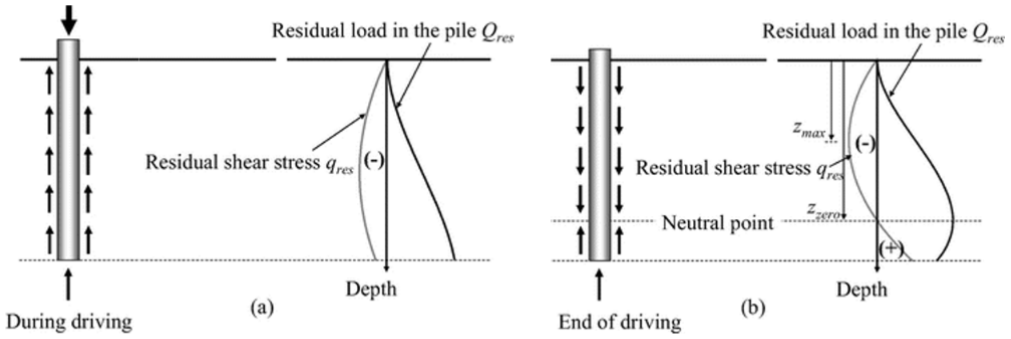

Figure 2.11: Residual load and shear stress distribution during pile driving (a) and at the end of driving [28].

During driving, compression and rebound result in relative displacements between pile and soil. Due to a difference in stiffness between the pile and soil, the rebounding deformation of the pile is locked by the surrounding soil, resulting in locked-in stresses in the pile. As illustrated in Figure 2.11, this results in negative direction shear forces along the upper part of the pile and positive direction shear forces in the lower part of the pile plus some toe resistance. For piles loaded in tension, this results in an underestimation of shaft friction and relative movement above the neutral plane and an overestimation in toe resistance and below the neutral plane [21].

2.7.2. Pile stiffness

The stiffness of a MV pile is determined by the combination of the grout and the steel profile. However, determining the stiffness is not as simple as adding them up. Grout can only sustain low tension stresses and will crack under increasing stress. If the grout body is uncracked, it will contribute fully to the stiffness. The contribution of the grout part deteriorates with increasing strain until the stiffness of the pile only consists of that of the steel. Design standards commonly use the steel stiffness to calculate displacements. Taking the contribution of grout into account could overestimate the longer term stiffness [19].

2.7.3. Pile cross section

The circumference of the MV pile is equal to the shape of the grout body. As described in section 2.2, the grout body of a MV pile is formed during installation. The grout is continuously injected in two steel trays above pile tip and the entire steel profile is encased in grout (see Figure 2.12). Results of modelled simulations have shown that the shape and circumference of the grout body is approximately constant in sandy soils [30].

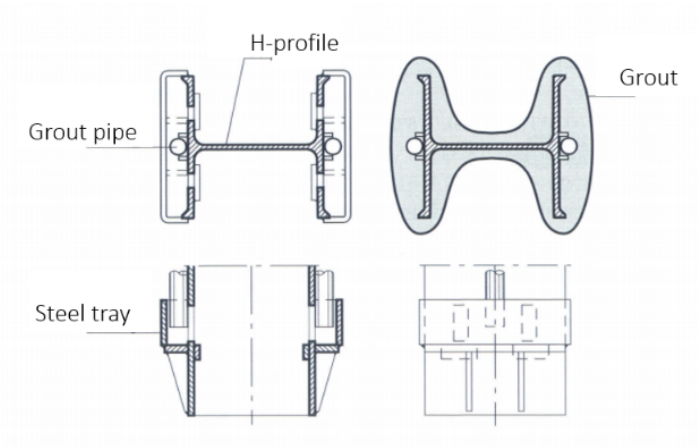

Figure 2.12: Principle of MV pile cross-section [6]

3

Experimental framework

This chapter presents the setup and procedure of the testing framework of this research and provides an overview of the data obtained.

3.1. Description of test

3.1.1. Testing framework

The setup of the full scale tensile load tests at OTR and HTT is schematized in Figure 3.1. It is assumed that the geotechnical resistance is entirely provided by the dense Pleistocene sand layer. The contribution of the soil on top is disregarded because of the adverse effect of the active soil wedge on the shaft friction. Consequently, only the shaft friction mobilized in the Pleistocene sand is considered for the design bearing capacity of the pile. In order to mobilize the maximum amount of skin friction in this layer during the test, an oversized casing was driven around the MV pile directly after the MV pile was driven into the soil with a bentonite injection. The oversized casing is indicated in green in Figure 3.1. The soil and grout inside the casing were removed by hydrojetting.

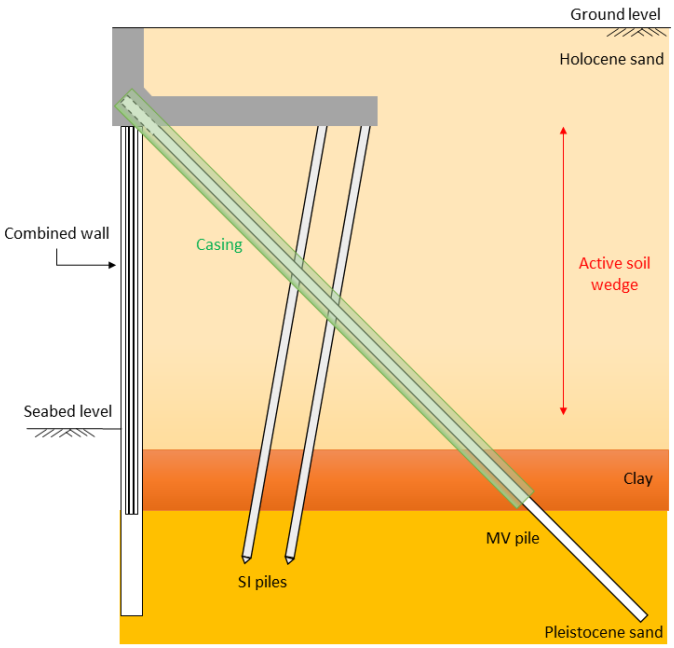

Figure 3.1: Overview of HTT testing framework.

In 2016, 5 full scale pile load tests were executed at the Offshore Terminal Rotterdam (OTR). Different measures were taken at each test to debond the pile from the surrounding soil. Only the last pile (OTR5) was loaded to geotechnical failure based on the creep criterion according to CUR 166 [27]. In the other tests, structural failure criterion of the steel pile was decisive. It was concluded that using a flushed oversized casing driven with bentonite injection was the best test setup [25]. As a result, it was decided

to apply this debonding strategy to all test piles at the Hartel Tank Terminal (HTT) in 2018. During this test campaign, all 6 test piles were loaded successfully to geotechnical failure. Furthermore, strain was recorded over smaller intervals (0.25 m instead of 1 m), resulting in more data and higher reliability of the measurements. Consequently, this thesis is focused on the 6 load tests at HTT.

3.1.2. Design of test piles

The design of the test piles at OTR and HTT is made on the basis of the Dutch standards according to CUR166 [27] (see section 2.3.2):

$$F_{pile} = \alpha_t \cdot O \cdot \Delta L \cdot q_{c,avg} \tag{3.1}$$

In which for these tests specifically:

α_t = 1.4% (Brassinga, 1987) [26];
O = 2.23 m (HEB600) ;
ΔL = length of pile between the end of the casing and pile tip [m];
$q_{c,avg}$ = $min(q_{c;av}$, 18 MPa).

The design parameters for α_t and $q_{c;avg}$ are determined based on historic pile load tests in the port of Rotterdam [11]. The circumference of the pile can either be taken as the enveloping outline of the pile or the ”Diabolo” circumference (see Figure 3.2). The enveloping outline, which is the conventional method in the Netherlands, is taken for the design of the test piles. All results in this research are derived based on this assumed circumference shape.

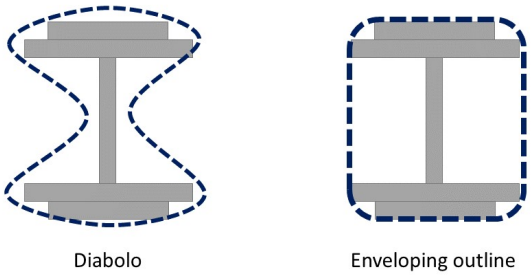

Figure 3.2: Schematization of the Belgian (left) and Dutch (right) method for calculation of the pile circumference

The design parameters of the MV piles are summarized in Table 3.1.1.

Test pile	Name	Zone	Profile	Δ L [m]	Depth pile tip [m NAP]	Depth casing [m NAP]	Angle [° w.r.t. hor.]
HTT1	MV-A-12b	A	HEB600	8.14	-30.0	-24.50	42.5
HTT2	MV-A-48b	A	HEB600	7.46	-29.5	-22.25	47.5
HTT3	MV-A-60b	A	HEB600	8.13	-32.0	-26.00	47.5
HTT4	MV-B-48b	B	HEB600	8.48	-29.0	-22.75	47.5
HTT5	MV-C-6b	C	HEB600	8.48	-29.0	-22.75	47.5
HTT6	MV-C-54b	C	HEB600	8.48	-29.5	-23.25	47.5

Table 3.1.1: Overview HTT test pile parameters

3.1.3. Testing procedure

The maximum test load was 10770 kN (95% of the yield strength of the HEB600 profile S420M/S420N) and the option of an extra load step to 11300 kN. This is different the standard procedure (see Chapter 2.3.2). Consequently, the number of load steps is increased from 6 to 10 (shown in Figure). F_i is the initial load that is put on the pile one day before the start of the test.

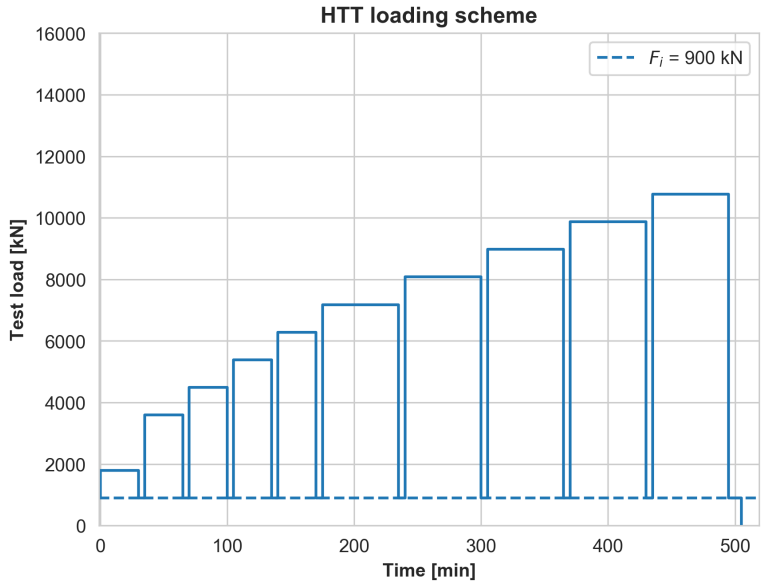

Figure 3.3: Loading scheme at HTT (creep not taken into account).

The creep was monitored during the test to check if the duration of the load steps needed to be altered.

Criterium	Action
c < 1.0 mm	Start next step after unloading.
1.0 ≤ c ≤ 2.0 and decreasing	Reduce the length of the next load step by half.
1.0 ≤ c ≤ 2.0 and increasing	Increase the length of the next load step by 30 minutes.
c > 2.0 and decreasing	The test is extended for a minimum of 60 minutes and a maximum of 4 x 60 minutes. If after 4 x 60 minutes c > 2.0 mm the test is terminated.
c > 2.0 and increasing	The test is terminated.

Table 3.1.2: Monitoring and action plan w.r.t. creep observations during the load test.

The procedure and results of the 6 pile load tests at HTT is presented in Table 3.1.3. Graphs illustrating the monitoring of creep can be found in Appendix B.2.1.

Test pile	Name	Load steps	F_i [kN]	F_{max} [kN]	Installation date	Test date	t_0
HTT1	MV-A-12b	10	100	8727	06-07-2018	28-07-2018	7:46:21
HTT2	MV-A-48b	9	100	10027	10-08-2018	25-08-2018	8:44:20
HTT3	MV-A-60b	11	100	10726	17-08-2018	01-09-2018	12:44:05
HTT4	MV-B-48b	10	100	10266	28-09-2018	13-10-2018	06:30:26
HTT5	MV-C-6b	10	100	11719	16-11-2018	01-12-2018	05:15:42
HTT6	MV-C-54b	10	100	7125	30-11-2018	15-12-2018	05:17:53

Table 3.1.3: Test overview HTT

3.2. Description of research data

3.2.1. Soil investigation data

All piles are installed in in typical Maasvlakte-area soil conditions. The subsoil can be divided into three layers from top to bottom:

- Holocene sand layer with cone resistances up to 30 MPa.
- Wijchen clay layer of 1 to 3 m thick with low cone resistances.
- Pleistocene sand starting from ± 21-25 m below NAP with cone resistances up to 50 MPa.

At least two CPT's are executed before and after installation of each MV pile (see Figure 3.4). The CPT's completed before pile installation are used for the design of the test piles. The CPT's after pile installation are executed at least one week after the test pile and surrounding piles are constructed. All CPT profiles are plotted in one graph for each test pile (see Appendix B.1.4). The top view of the global location of the test piles and CPT's can also be found in Appendix B.1.4.

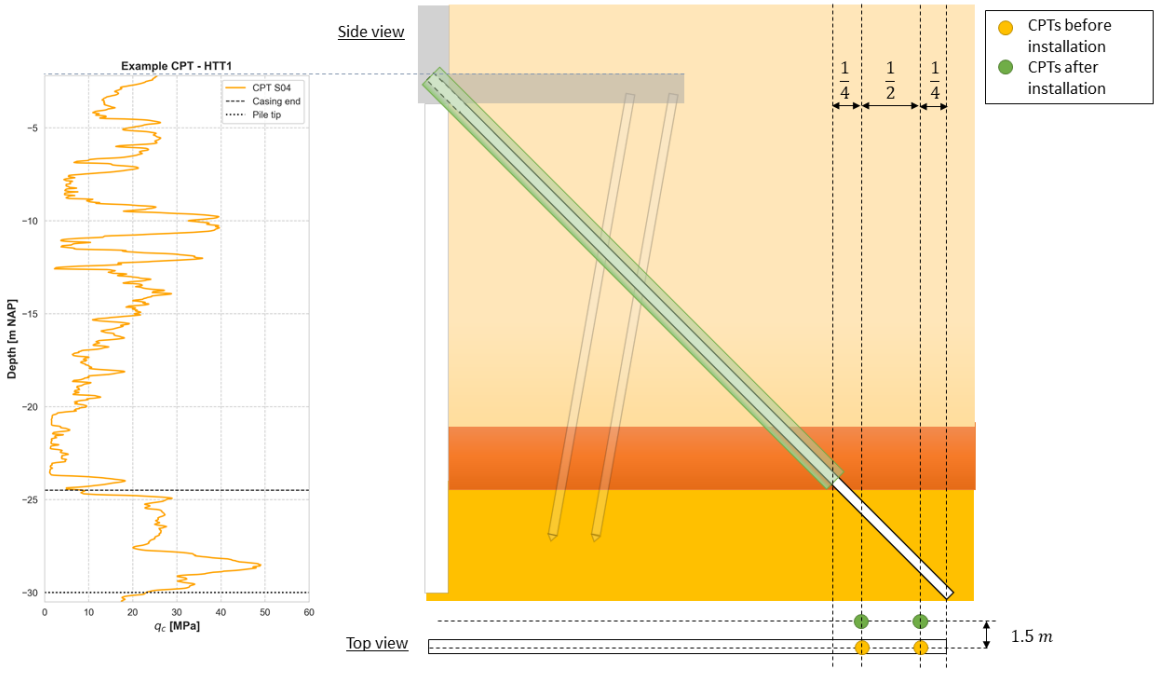

Figure 3.4: Example CPT near HTT1 and schematic overview of the location of CPTs before and after installation of MV pile

3.2.2. Installation data

All HTT test piles are installed by hammering a hydraulic hammer (type S-120) with a ram weight of 6.2 ton. The drop height of the hammer can be be adapted during installation to enable the contractor to control the energy and blow rate. Grout is supplied throughout the installation process through two tubes towards the toe of the pile. The amount of grout that is injected is registered per tube. The spill of grout that was pumped away above ground level has not been registered. Consequently, the measured volume of grout is not necessarily equal to the amount around the pile. The installation data is registered every 0.25 m (in the same direction as the axis of pile) and consists of:

- Grout pressures [bar]
- Volume of grout [L]
- Piling duration [sec]
- Piling energy [Ton*meter]
- Blow count [-]

All installation data per pile can be found in Appendix D.

3.2.3. Load-cell and LVDT data

The tensile load is powered by 4 hydraulic jacks and transferred to the pile by a steel reaction frame. For each jack, the tensile load is recorded by a load cell with integrated LVDT sensors on the corners of the pile head. The resolution of the load-cells is 0.36 m. During the test, the deviation with the increased oil pressures in the tubes connected to the load-cell is monitored. This deviation from the load-cell data is verified to be less than 1%.The pile head displacement is measured with respect to a reference frame. The position of the reference frame is periodically monitored during the test using a total station. The position of the reaction frame, top of the casing and pile head is also measured. Figure 3.5 presents an overview of all relevant components.

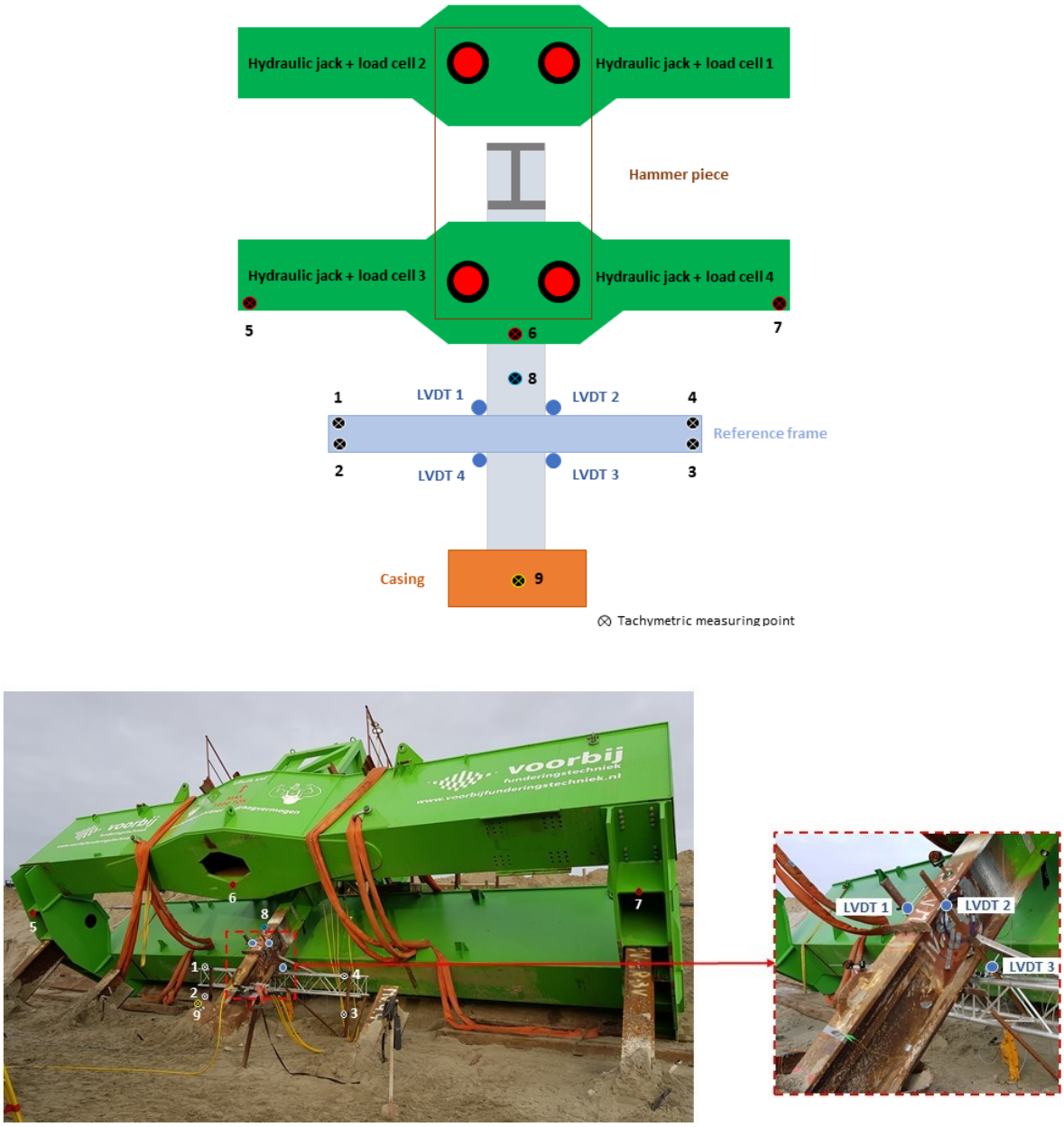

Figure 3.5: Schematic overview and pictures of testing frame and relevant components (personally taken photograph: Putteman, J.)

3.2.4. Inclinometer data

In order to determine the lateral deflections of the piles, a digital inclinometer system (model DIS-500) is used. Lateral deformation of the pile is measured by lowering an inclinometer probe in the inclinometer tube. Measurements are taken in the A axis, in the direction of the wheels, and the B axis, which is perpendicular to the A axis. The tube starts ±0.5 m from the tip of the pile and takes readings every 0.5 m. After obtaining the first set of measurements (A^+ and B^+), the probe is removed from the casing, rotated 180°and a second set (A^- and B^-) of readings is recorded. By combining the data sets, offset from the vertical position of the probe is eliminated. As measurements A and B are not in the X and Y direction of the pile, measurements are rotated 45°clockwise. A schematic view of the inclinometer system and previously discussed directions is visualised in Figure 3.6 below.

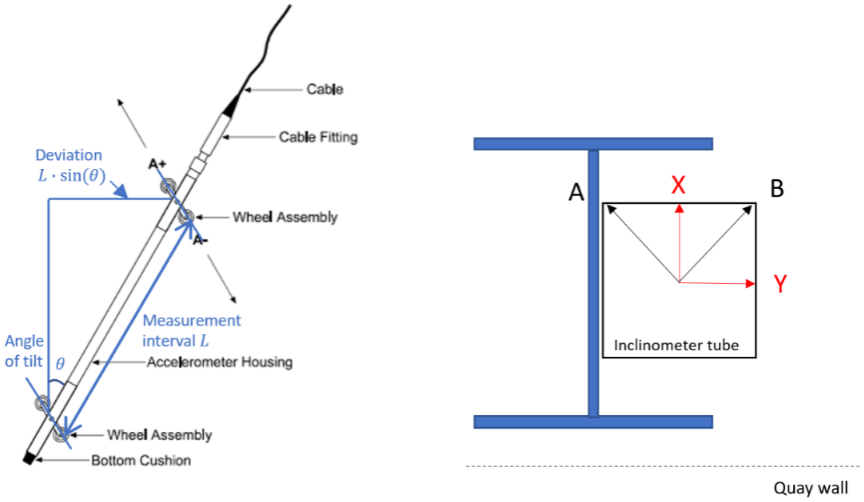

Figure 3.6: Schematic view of inclinometer system and orientation (for clarity, the right figure is not drawn to scale).

3.2.5. Strain data

The strain is measured using Brillouin Optical Time Domain Analysis (BOTDA) sensors. BOTDA sensors are capable of measuring the stress distribution of over the pile as a function of distance and applied load [1]. Each pile is equipped with three sensors. Figure 3.7 shows the position of the sensors on the pile profile. The sensors are attached to the steel profile using epoxy and covered by a steel tube before pile installation. The strain is recorded along the complete length of the pile, except for the last 0.5 meter. The loop of the sensor is located at the deepest point (see Figure 3.7). The strain recorded every 25 cm with a resolution of 5 micro-strain.

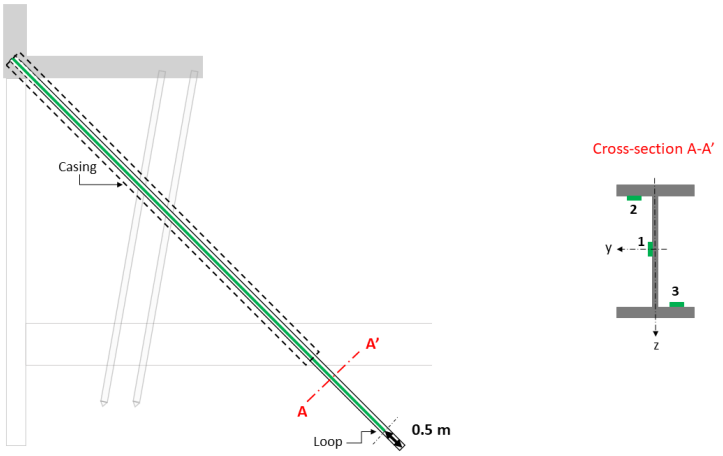

Figure 3.7: Position of strain sensors (indicated in green)

4

Data processing

This chapter describes how the HTT test data is processed. Furthermore, this chapter outlines which fundamentals influence the analysis of this research. The assessment methods of the following data sets are discussed:

1. Soil investigation data
2. Installation data
3. Load-displacement data
4. Inclinometer data
5. Strain data

4.1. Assessment of soil investigation data

During the installation of the test piles, soil is displaced around the tip. As a result of this, the state of the soil is significantly different from the initial conditions. Further insight into the installation effects is useful for improvement of CPT-based methods as CPT's used for design represent the initial soil conditions. If the sand around the pile compacts (closer packing of particles) due to soil displacement, the density increases and the cone resistance will be higher. This is analysed by comparing the CPT profiles prior to and after installation. As the MV pile is installed under an angle and the CPT profile is made vertically, the cone resistance is compared at the depth where the CPT intersects the pile as visualised in Figure 4.1. The depth at which the axis of the MV-pile intersects the CPT's is calculated based on location of the pile head and installation angle. This depth is interpreted as a zone of ±1 meter to account for the height of the pile profile.

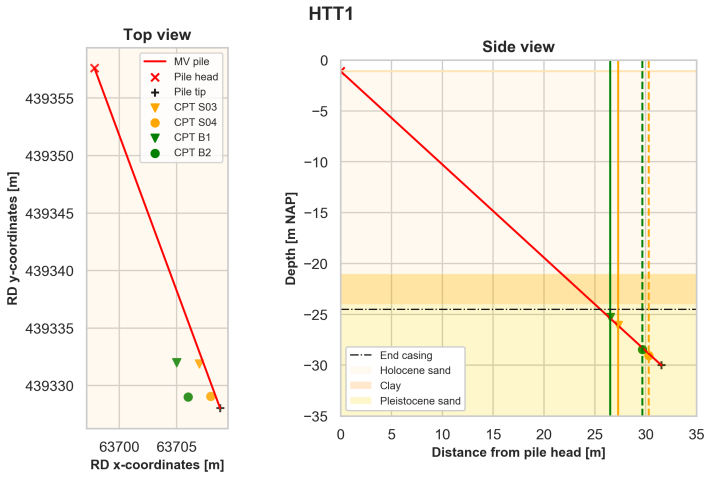

Figure 4.1: Left: top view of pile and CPT's. Right: side view displaying intersection of pile and CPTs.

The CPT's prior to pile installation are combined as the cone resistance profiles per pile are similar. Computing the average q_c value reduces the uncertainty of spatial variability of the soil. The q_c values per pile and the computed average can be found in Appendix B.1.3.

4.2. Assessment of installation data

The energy required for installation can be interpreted as an indicator of the soil resistance and therefore the pile bearing capacity. During installation, the impact from the hammering block generates an elastic compression wave through the pile inducing the motion of the pile. This pile motion is counteracted by the resistance of the soil. The pile will penetrate the soil if the stress wave in the pile is high enough to overcome the soil resistance and long enough to overcome elastic deformations [14]. It must be noted that the installation energy reflects the conditions during installation, similarly to the CPT's prior to installation. The installation energy (IE) is computed by multiplying the blow count by the average piling energy. Figure 4.2 illustrates the results as a function of vertical depth (m NAP) per test pile.

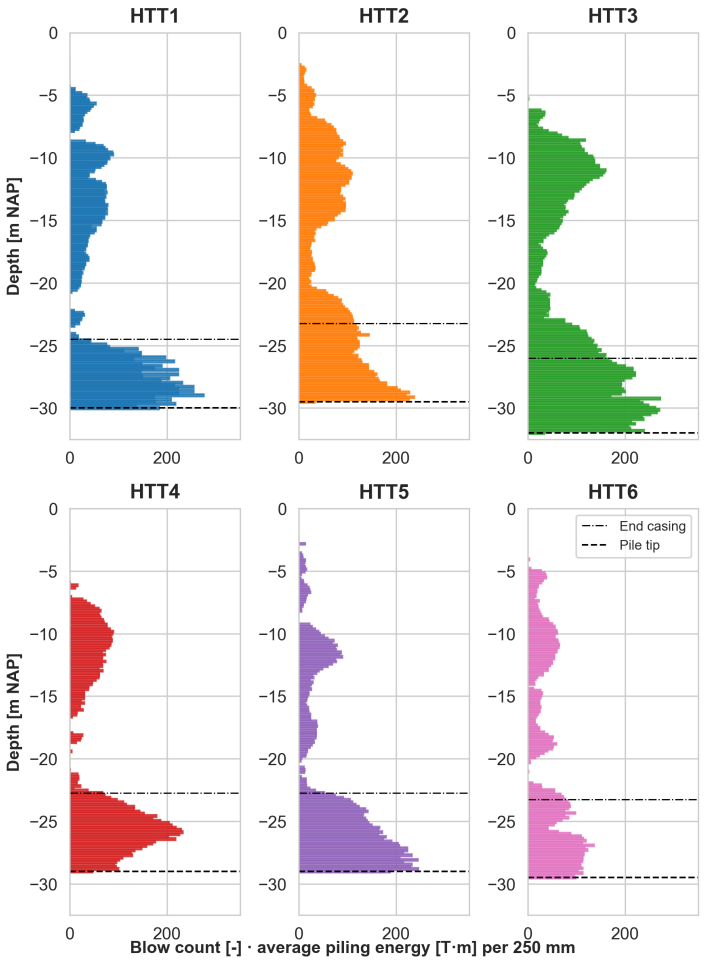

Figure 4.2: Installation energy profile per test pile computed by multiplying the blow count with the average pile energy.

4.3. Assessment of load-displacement data

The load and displacement data of the first test piles is displayed in Figure 4.3. The load scheme of this test consisting of 11 steps can be clearly observed. The total applied load is computed by taking the sum of the four load cells. Load-cell 3 of HTT1 (see orange line, 4.3) and load-cell 1 of HTT2 did not work properly. For these piles, the total load is computed by multiplying the average of the other three load-cells by four. This was checked with the registrations of the increased oil pressures. LVDT measurement are separately checked and corrected if the position of the jacks was adjusted during the test. The load-displacement graphs of all HTT test piles can be found in Appendix B.2.2.

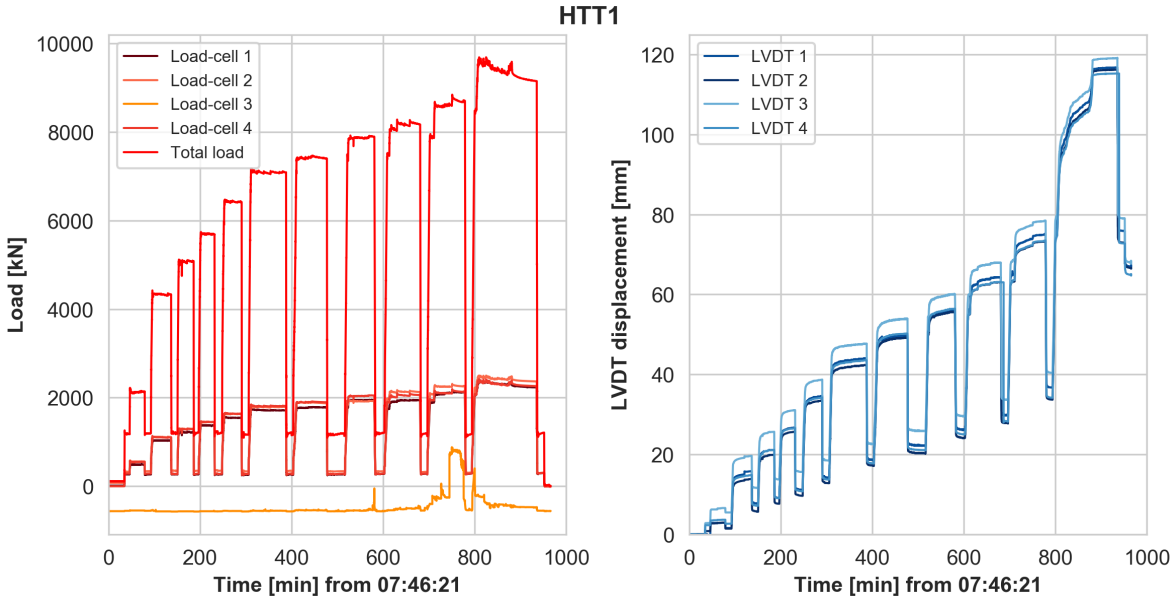

Figure 4.3: Corrected LVDT and load-cell measurements at HTT1.

4.4. Assessment of inclinometer data

First, the installation angle of the piles is checked by computing the angle between the measurements in X-direction and the depth (see left part Figure 4.4). No inclination measurements were executed on test pile HTT1. The design angle of installation of the other piles was 47.5°. The deviation in angle with respect to the horizontal is less than 0.3° for all five piles. Because the small deviation, the installation angle is not adapted for the data interpretation. Next, the measurements are converted to RD-coordinates. In Figure 4.5, the actual location (dashed blue line) is compared to the design location of the pile (continuous line). It can be observed that the curvature is different for each pile. Pile HTT 6 has the largest deviation from the designed location of the pile tip (2.7 meters).

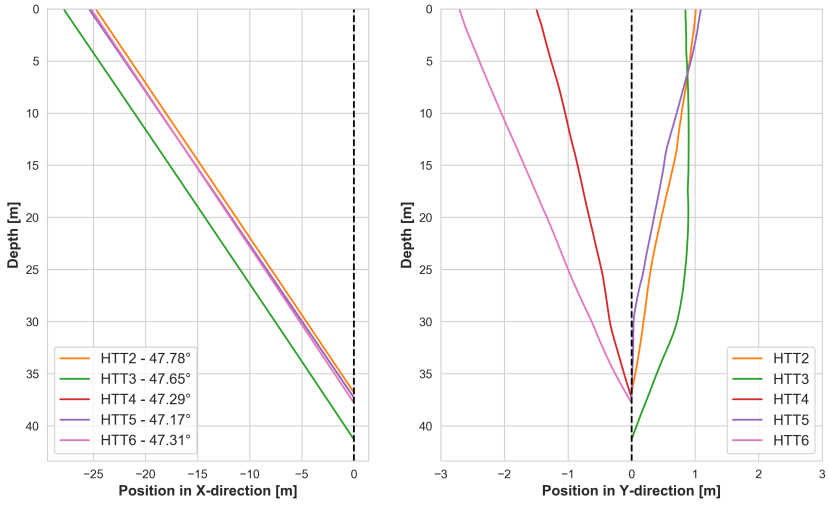

Figure 4.4: Absolute position of HTT test piles in X and Y direction. Note: no inclination measurement was performed on test pile HTT1.

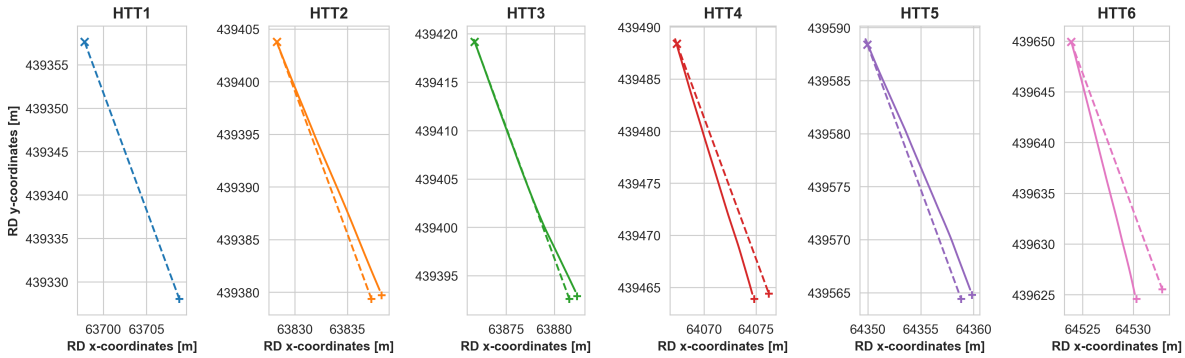

Figure 4.5: Top view of HTT test piles in design (dashed line) and in practice (continuous line) in RD coordinates. Note: no inclination measurement was performed on test pile HTT1.

4.5. Assessment of strain data

As discussed in Chapter 3, all test piles are equipped with three BOTDA fiber optic sensors that record the strain as a function of time with intervals of 25 cm. These measurements are linked to the depth [m NAP] based on the location of the loop in the sensor (0.5 from the tip of the pile). This depth of the loop in m NAP is calculated for every pile based on the level of the pile tip and the installation angle. The location of the loop in the cable data is determined at the point of minimum strain as illustrated in Figure 4.6. Strain readings at equal depth before and after the loop are averaged to increase the accuracy of the interpretation.

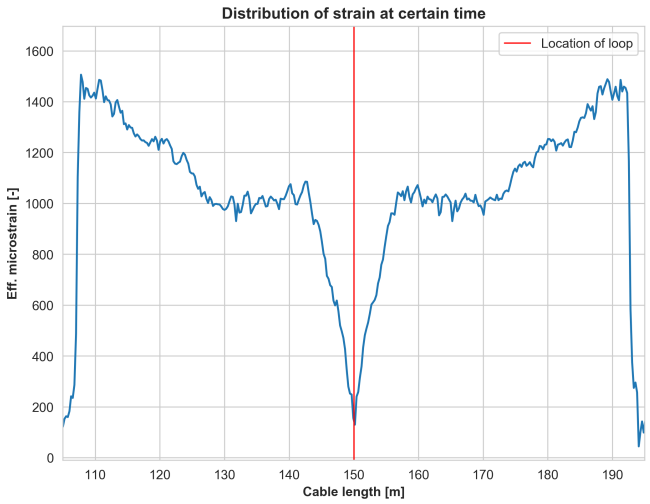

Figure 4.6: Distribution of strain at certain time of HTT1.

Normal force

The measured strains are converted into normal forces with the following equations:

$$F_n = \epsilon \cdot EA_{steel} \tag{4.1}$$

$$\epsilon = \epsilon_{measured} - \epsilon_0 \tag{4.2}$$

Where:

F_n = Normal force [kN];
$\epsilon_{measured}$ = Measured strain [-];
ϵ_0 = Reference strain [-];
E_{steel} = Elasticity modulus of steel (210 kN/mm^2);
A_{steel} = Surface area of HEB600 steel profile (27000 mm^2).

Reference measurement
The reference strains (ϵ_0) are determined by computing the average of he first 6 strain readings (i.e. the average over ±24 minutes before the test). This is after application of the initial load of 100 kN. The effect of residual loads is analysed on five production piles prior to this thesis. Appendix A.1 contains the test results of one production piles. First, a reference measurement was conducted for each pile in four different positions (see Figure A.1) to account for possible effects of bending. The effect of residual loads due to installation is analysed by comparing the average of these reference measurement to the measurement directly after installation. The effect of installation on the stresses in the piles was clearly visible. Comparison of the reference measurements to a measurement 30 days after installation showed that the residual loads have disappeared. The residual loads loads in the test piles is not determined as no reference measurements are taken prior to testing.

Verification of EA
The correlation between the theoretical value of EA (210 GPa x 27000 mm^2 = 5670 MN) and the applied load measured by the load cells is analysed based on the strain readings in the top 2.5 m of the pile. The strains in this part of the pile (near the pile head) are fully determined by the applied load. At deeper levels, the measured strains decrease as a result of force transfer from the pile to the soil due to friction. The average effective strain at the top of the pile is plotted against the applied load in Figure 4.7. It is concluded that the strain readings give reasonable results. For all test piles, the relationship between the load and the measured strains is slightly lower than the theoretical relationship. This suggests that the stiffness is slightly overestimated. Practical aspects that could be the explanation of deviations are:

- Initial calibration offset of the sensors.
- Efficiency of the load cells. Deviations can be caused by eccentricity of the force near the pile head. Possibly not all force was transferred into the pile.
- Locked in stresses caused by of pile driving. However, the locked in stresses are not expected to be significant as explained in the previous subsection.
- Temperatures around the sensors can affect the frequency signal and therefore the measured strains.

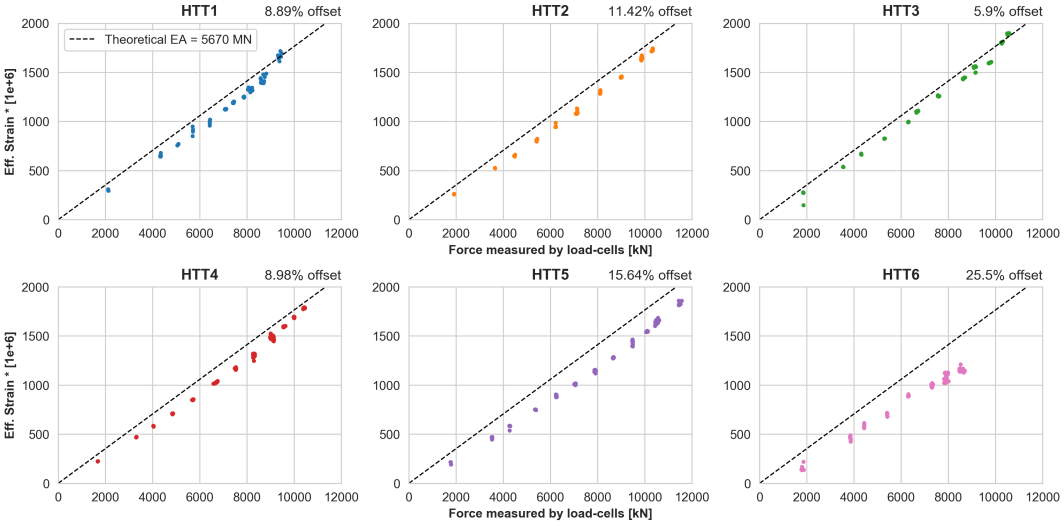

Figure 4.7: Comparison of the measurements at the pile head with the theoretical EA relation (5670 MN).

The offset of HTT6 increases in the last load steps. This is most likely caused by eccentricity of the applied force as the reaction frame was twisting during the test. If the efficiency of the load cells caused the deviation from the theoretical EA of steel, correcting would result in an underestimation of shaft friction. Moreover, it is conceivable that the efficiency of the load cells caused deviations as it was observed that the reaction frame was twisting during most tests. Consequently, the theoretical EA of steel is used for strain-to-load interpretation for all piles without individual corrections per pile.

Combining fiber optic sensors
As explained, every pile is equipped with three BOTDA fiber-optic sensors. The first sensor is located at the web and the other two at the flanges of the steel profile. The effect of bending on the distribution of forces is clearly visible when the readings of at the flanges are compared. When these two readings are combined, the effect of bending cancels out and is almost equal to the reading of the sensor at the web. For HTT6, the readings of the sensors on the flanges deviate strongly from the readings of the sensor at the web. This is most likely the result of deflection of the pile, as this pile has the strongest inclination (see section 4.4). For this pile, only the reading of the sensor on the web is used in further analysis. For the other piles, the strain readings of all three sensors are combined.

Shaft friction
From the distribution of normal force, calculated with Equation 4.3, the shaft friction is derived every 0.25 m [3]:

$$q_s = \frac{F_n}{\Delta L \cdot O} \tag{4.3}$$

Where:

q_s = Shaft friction [kPa];
F_n = Normal force [kN];
ΔL = Distance between two measurements (along pile axis) [m];
O = Circumference of the grout body [m].

Localized spikes in measured strains during the test are observed. These sudden increases of strain at a short distance are typical for pile load tests using BOTDA fiber-optic sensing [20]. To filter out the noise for computation of the shaft friction, the data is processed by taking the moving average over three measurements.

Maximum shaft friction
The distribution of maximum mobilised shaft friction is determined as this is equivalent to the bearing capacity of the pile and required for analysis of the design method. To identify this point in time, an interactive slider plot in Python is used (see Figure 4.8). The maximum shaft friction is mobilised the point in time at which the normal force below the casing is maximum. To account for small fluctuations over time, three consecutive measurements are combined. This corresponds with a period of ±12 minutes.

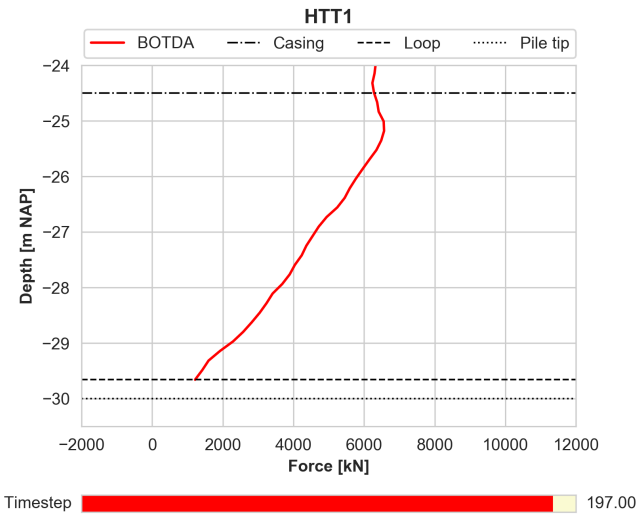

Figure 4.8: Interactive slider plot of normal force below the casing (HTT1). The red slider bar can be used to slide through time (measurement intervals are ±4 min.)

5

Data analysis

This chapter contains the analysis and findings derived from the processed data in the previous chapter. The aim of this chapter is to find relations that can be used to compose a new design method and to improve understanding about the mobilisation of shaft friction as a function of displacement. The following relationships are analysed:

1. The influence of pile installation on bearing capacity.
2. The relation between cone resistance and installation energy.
3. The relation between cone resistance and shaft friction.
4. Mobilisation of shaft friction as a function of displacement.

5.1. Influence of pile installation on bearing capacity

Figure 5.1 illustrates the average cone resistance (q_c) before and after installation of all test piles. CPT's before pile installation are indicated in orange and CPT's before installation are indicated in green. This figure shows a significant increase in q_c at most of the test piles.

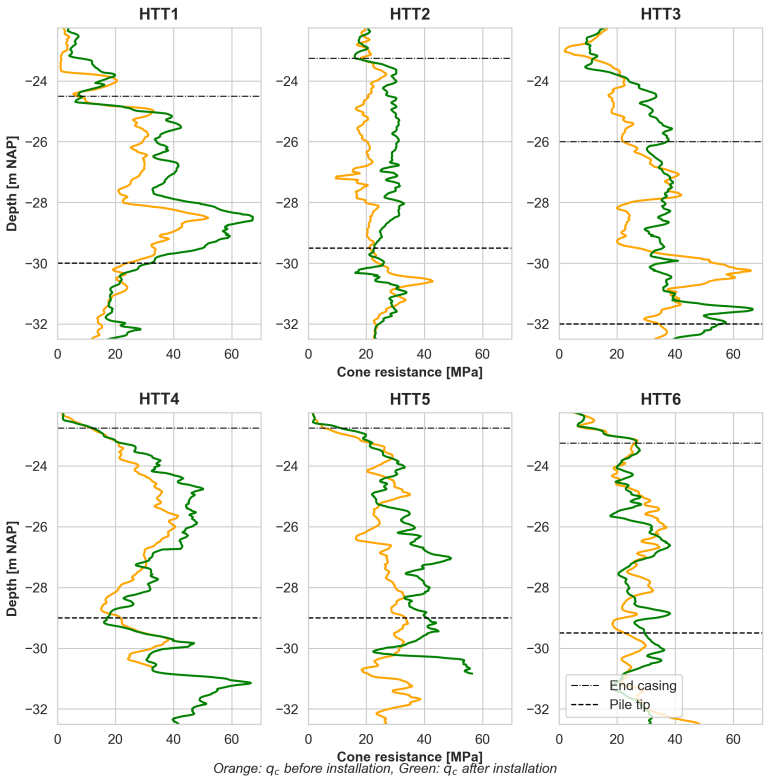

Figure 5.1: Cone resistance before (orange) and after (green) pile installation at each test pile. The start of the Pleistocene sand layer (end of casing) and the pile tip level are indicated by dashed lines.

Table 5.1.1 presents an overview of the average increase in q_c of each test pile. This is determined between the end of the casing and the pile tip (in the Pleistocene sand layer). For assessing soil variability, the difference between the CPT's prior to pile installation and the average q_c is determined. The deviation from q_{avg} was around 10%, which is considerably less than the increase in the average q_c after installation for test pile 1, 2, 4 and 5 (between 24 and 42% increase). The after CPT's at test pile HTT3 and HTT6 differed from this. At HTT3, CPT's S4 and S5 showed a similar ranges of q_c compared to before installation, while CPT 60b shows a large increase (±50%) until -30 m NAP and a decrease (±35%) between -30 and -31 m NAP.
At HTT 6, the cone resistance after pile installation is nearly the same as before pile installation. The only remark is that CPT b2 indicates a weak clay layer between -25 and -26 m NAP, that was not detected in the CPT's before installation.

Test pile	**Name**	**CPT's** (before instal.)	**CPT's** (after instal.)	**Increase in** $q_{c,avg}$ (before and after instal.)
HTT1	MV-A-12b	2	2	36 %
HTT2	MV-A-48b	2	3	42 %
HTT3	MV-A-60b	2	3	8 %
HTT4	MV-B-48b	4	2	24 %
HTT5	MV-C-6b	2	3	26 %
HTT6	MV-C-54b	2	2	0 %

Table 5.1.1: Quantification of installation effects on q_c

As described in Chapter 4.1, it was investigated if the depths at which the pile intersects the CPT's coincide with the depths at which the q_c has increased. This would indicate that the soil has compacted due to installation of the test pile. However, this hypothesis is not supported by this analysis. The installation of the production piles next to the test piles (h.t.h. distance of 3.3 m) may have affected the soil conditions in the Pleistocene sand layer.

5.2. Relation between cone resistance and installation energy

Pile driving analysis can be used to predict the capacity of the pile. Although it is generally accepted that dynamic relations for predicting pile capacity are not very reliable due to various reasons (see Chapter 2.3), pile driving energy is a convenient indicator of the soil resistance and, therefore, bearing capacity [14]. Analysis of the installation energy allows more insight in the soil conditions around the piles. The measured q_c might deviate from the q_c along the axis of the piles, as all CPT's were executed straight down near the pile tip. In this section, it is investigated how well the installation energy correlates to the q_c from the CPT's from before pile installation.

The installation energy is computed by multiplying of the average piling energy with the blow count, which is the same principle as the the Standard Penetration Test (SPT). Various studies suggest linear relationships between the blow count the SPT and the cone resistance of the CPT [16]. The q_c/IE ratio is determined iteratively and resulted in the best fit when IE was multiplied by 0.2 (please note that this number is significantly affected by various conditions and is specifically computed for this test). Figure 5.2 shows the installation energy (indicated by colored bars) correlates extremely well with q_c (indicated by a black line).

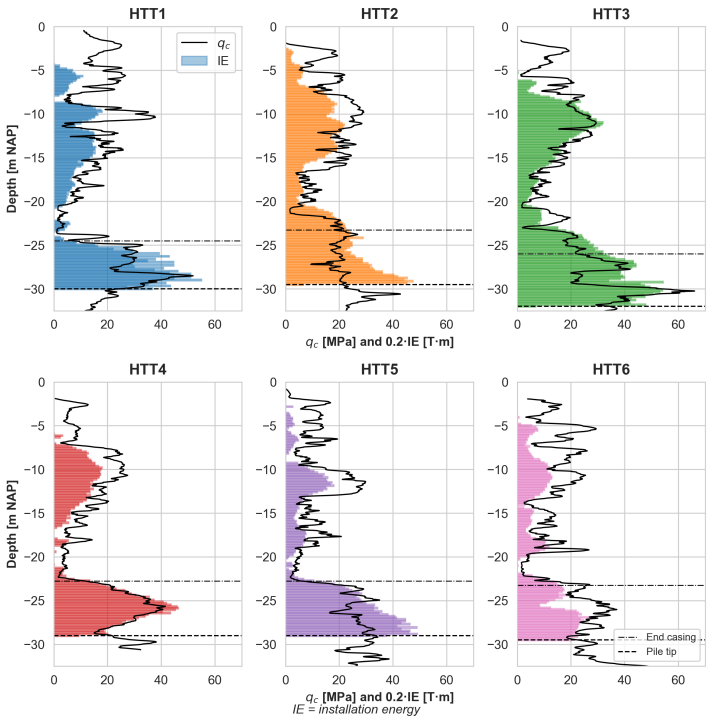

Figure 5.2: Correlation between cone resistance (q_c) and installation energy (IE) per test pile.

By means of comparison, the ratio between the average q_c and 0.2 · IR is computed for each test pile. This derivation is visualised in Appendix C.1. Table 5.2.1 presents the obtained results.

Test pile	**Name**	$q_{c,avg}$ [MPa]	$0.2 \cdot IE$ [tons]	**ratio** [-]
HTT1	MV-A-12b	30	35	1.2
HTT2	MV-A-48b	20	30	1.5
HTT3	MV-A-60b	35	42	1.2
HTT4	MV-B-48b	28	29	1.1
HTT5	MV-C-6b	26	34	1.3
HTT6	MV-C-54b	27	19	0.7

Table 5.2.1: Ratio between q_c and 0.2· IE (between end of casing and pile tip)

5.3. Relation between cone resistance and shaft friction

In this section, the cone resistance (q_c) from the Cone Penetration Test is correlated to the maximum mobilised shaft friction (q_s), which is equivalent to the bearing resistance. This analysis consists of the following steps:

- Definition of boundaries and intervals.
- Computing the average cone resistance before pile installation (see Chapter 4.1).
- Computing the maximum mobilised shaft friction (see Chapter 4.5).
- Computing the correlation factors.

Boundaries and intervals

As measurements of shaft friction are influenced by test conditions (i.e. circumstances of the surrounding soil and configuration of fiber optic sensors), not all measurements represent the 'normal circumstances'. For this reason, boundaries for the analysis are defined. Figure 5.3 illustrates the transition of force in the casing and below casing. The shaft friction in the first meter below the casing is strongly reduced at all test piles. It is investigated if the presence of the compressible clay layer caused this decrease. In Appendix B.1.2, the location of this clay layer is indicated in the force profile of each test pile. However, no clear relationship between the transfer of forces and the presence of the clay layer is found. It assumed that the bentonite suspension around the casing influences the shaft friction just below the casing. For this reason, it is decided to exclude the first meter below the casing for the derivation of α_t.

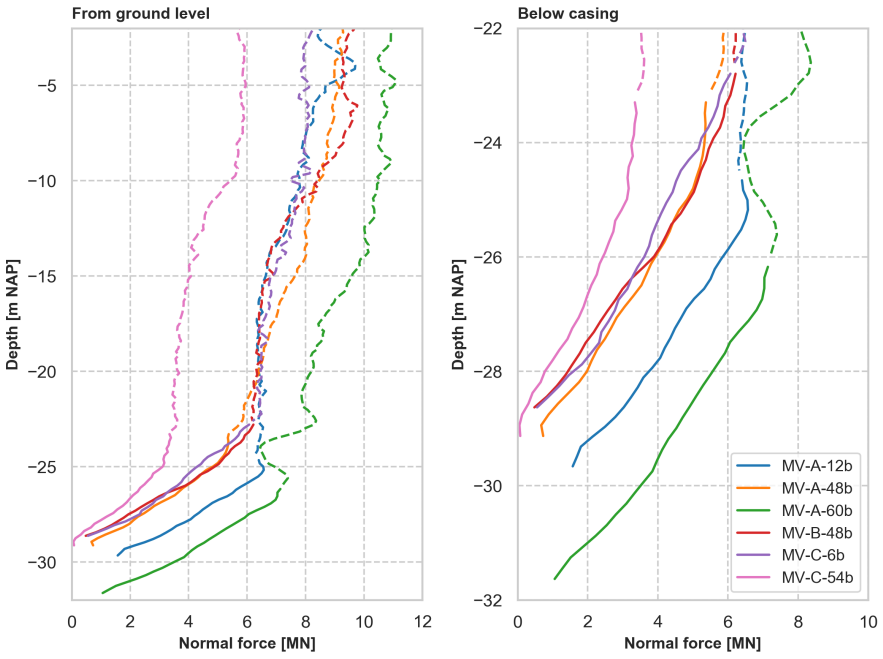

Figure 5.3: Distribution of normal force along the pile profile at the point that α_t is derived. The forces in the casing are indicated by dashed lines

Figure 5.4 shows the defined intervals over the which the average q_s and q_c are computed. The inaccurate measurement at the loop is excluded by computing the last interval until 0.5 m NAP above pile tip. The interval size is 0.5 meter as this eliminates local fluctuations, while retaining an appropriate representation of q_s and q_c along depth.

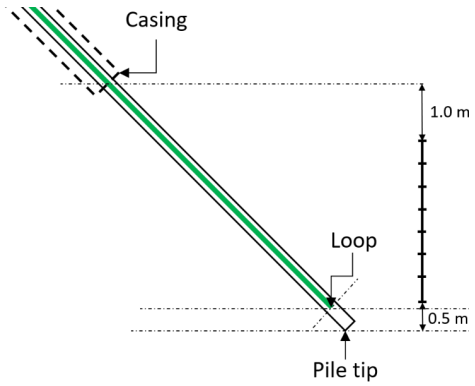

Figure 5.4: Boundaries of depth intervals over which the average q_s and q_c are computed and α_t is derived.

To determine the correlation factor, the cone resistance and mobilised shaft friction are computed at corresponding depths. Figure 5.5 illustrates how the average values of maximum q_s and q_c are computed over the defined intervals.

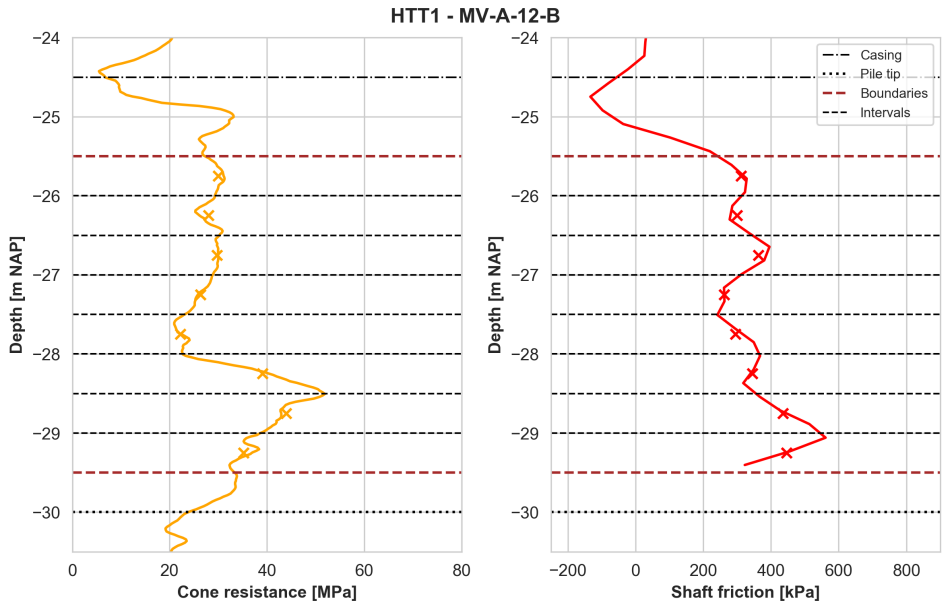

Figure 5.5: Illustration of depth intervals at test pile HTT1. Average values q_c (left) and q_s (right) per interval are indicated by markers

Correlation factors

As discussed in the previous chapter, the average cone resistance (q_c) is computed from all CPT's prior to pile installation. The average value is computed over the intervals defined in the previous subsection. For each interval, the correlation factor between the cone resistance (q_c) and shaft friction (q_s) is determined with equation 5.1. The mean value of α_t per pile (average of intervals) is checked by dividing the average q_s by the average q_c. Graphs illustrating the derivation of α_t, including the shaft friction and cone resistance per pile are presented in Appendix C.2.

$$\alpha_t = \frac{q_s}{q_c} \tag{5.1}$$

The computed α_t factors per interval of 0.5 meter are displayed in Figure 5.6. As described, intervals start 1 meter below the end of the casing and stop 0.5 meter above the pile tip. The mean of all intervals is indicated by a dashed line. The distributions of q_c and q_s correlate quite well, resulting in more or less constant values α_t per pile. Only in the last interval of HTT4, α_t is reasonably higher. This could be attributed to an underestimation of the cone resistance or due to measurement error. Despite the fact that scatter is evident, using a constant factor of α_t is most appropriate for correlating q_s and q_c.

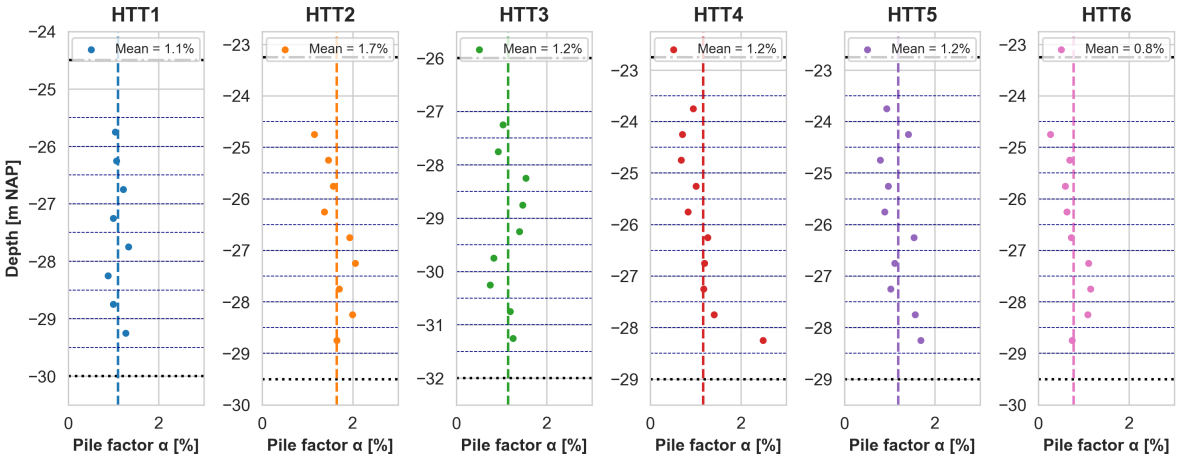

Figure 5.6: Derived values of α_t per interval

The left graph of Figure 5.7 shows that the mean values of α_t of four HTT test piles (1, 3, 4 and 5) are almost equal (around 1.2%). The results of HTT2 and HTT6 deviate from this. At the second test (HTT2), q_s is significantly larger than q_c, resulting in an α_t of 1.7%. At the last test (HTT6), the opposite is observed, resulting in an α_t of 0.8%. The right graph shows the average relation between shaft friction and cone resistance per pile. The average relation is indicated by a continuous black line. As only the dense Pleistocene sand layer is considered in this analysis, the amount shaft friction mobilised at cone resistances lower than ±18 MPa is not determined. It is evident that limiting the cone resistance under the assumption that no shaft resistance higher than 250 kPa is mobilised is not correct for the dense Pleistocene sand layer.

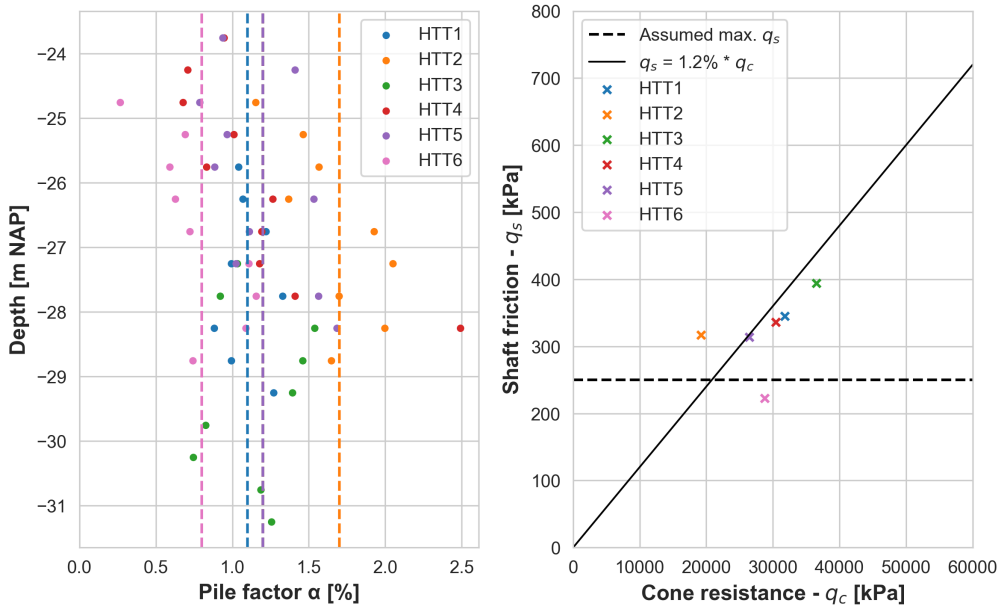

Figure 5.7: Left: Derived values for α_t per interval (mean of each pile is indicated by a dashed line), Right: Average shaft friction plotted against the average cone resistance of per pile (with derived relation and assumed maximum q_s).

5.4. Mobilisation of shaft friction as a function of displacement

Geotechnical finite element software is commonly used in engineering practice to model soil-structure interaction. The use of these models has evolved from a research tool into regular engineering tool. Despite the development of advanced user-friendly models, providing an accurate representation of non-linear and heterogeneous soil response is difficult. Validation of outcomes is very important to verify that the model is a good representation of reality. The goal of this section is to improve understanding of soil-structure interaction and to develop a mobilisation curve that can be used to calibrate and validate finite element models.

Methodology

The LVDT and strain data are combined to compute the mobilisation of shaft friction as a function of relative pile-soil displacement. The mobilisation of shaft friction is computed over intervals of 1 meter within the same boundaries as the previous analysis. After matching the start time (t_0) of the two data sets, the following steps are taken:

- The average shaft friction is computed per interval (see left graph of Figure 5.8).
- The elongation of the steel profile is computed by integrating the strains along the axis of the pile until halfway each interval.
- The relative displacement is computed by subtracting the pile elongation from the LVDT measurement (see right graph of Figure 5.8).
- Measurement during loading and unloading are taken out.
- The shaft friction is plotted against the relative-pile soil displacement at corresponding times. A moving average over five measurements is used to smooth out fluctuations.

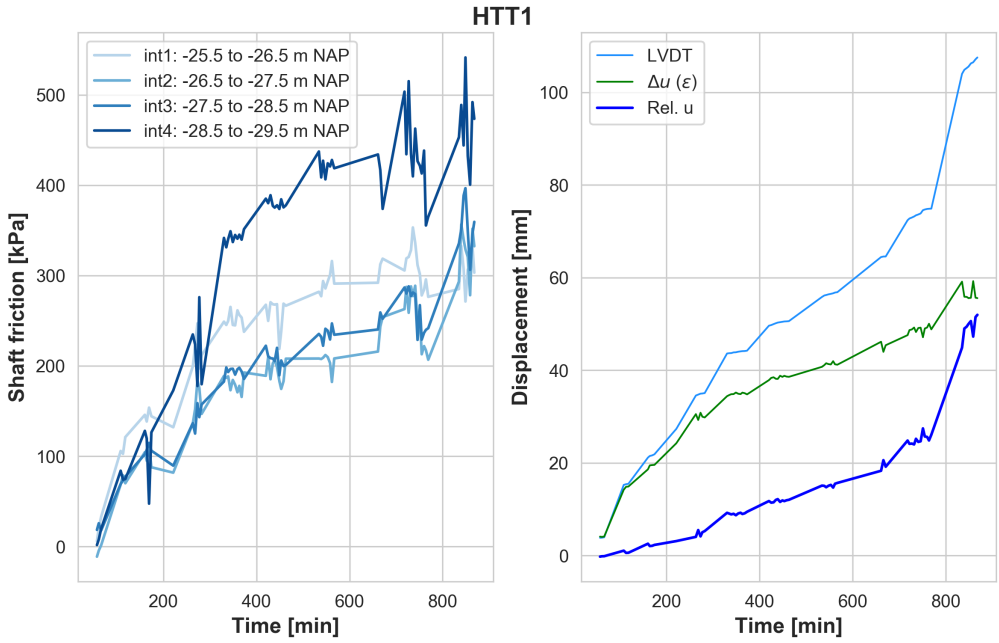

Figure 5.8: Left: Development of shaft friction over time per interval, Right: Computation of relative pile-soil displacement (dark blue line) by subtracting the integrated strains (green line) from the LVDT displacement (light blue line).

The output for each test pile is displayed in Appendix C.3. Figure C.2 illustrates that the maximum amount of shaft friction is mobilised at a relative displacement of approximately 25 mm. Figure C.3 shows the curves that are normalised based on this maximum. This data is combined to develop one general curve, which is presented in the next chapter.

6

Results and discussion

This chapter presents and discusses the results of the findings of Chapter 5 with reference to the objective of this research, which was to re-evaluate and improve the current design method for bearing capacity of MV piles. The first section of this chapter illustrates the composition of a new design method and mobilisation curve. The second section reflects on the obtained results and discusses the potential value of this research to the Port of Rotterdam.

6.1. Results

6.1.1. Design method

In this section, a new design method is presented by analysing the findings of Chapter 5. The derived values of α_t are summarized in Table 6.1.1, are adopted into a new pile factor. The relationships between the cone resistance, installation resistance and the bearing capacity are used to reflect on the derived results.

Test pile	Name	α_t [%]
HTT1	MV-A-12b	1.1
HTT2	MV-A-48b	1.7
HTT3	MV-A-60b	1.2
HTT4	MV-B-48b	1.2
HTT5	MV-C-6b	1.2
HTT6	MV-C-54b	0.8

Table 6.1.1: Overview derived values of α_t

The derived values of α_t result in predictions very close to the true measurements (see Appendix C.4). However, not the same value of α_t was obtained at every test. The Dutch NPR 7201 guideline (Determination of the axial bearing capacity of foundation piles by pile loading tests) [24] prescribes the following method for determination of pile factor α_t:

$$\alpha_{t;terrain;j} = \frac{\sum_{g=1}^{G} \alpha_{t;g;j}}{G} \tag{6.1}$$

Where:

$\alpha_{t;g;j}$ = Pile factor for test pile g, friction in soil layer j [%];
G = Number of test piles [-];

The mean value of α_t = 1.2%. Moreover, it is stated that if pile factors differ more than 20% from the mean value, the lowest value of $\alpha_{t;j}$ is decisive [24]. This is prescribed to ensure a safe design. As this research is focused on finding the most representative value of $\alpha_{t;j}$, the mean value of 1.2% is further analysed.

Figure 6.1 compares the predictions of the following design methods to the BOTDA measurements:

- CUR166 method: α_t = 1.4% (q_c limited at 18 MPa)
- Proposed method: α_t = 1.2% (q_c not limited)

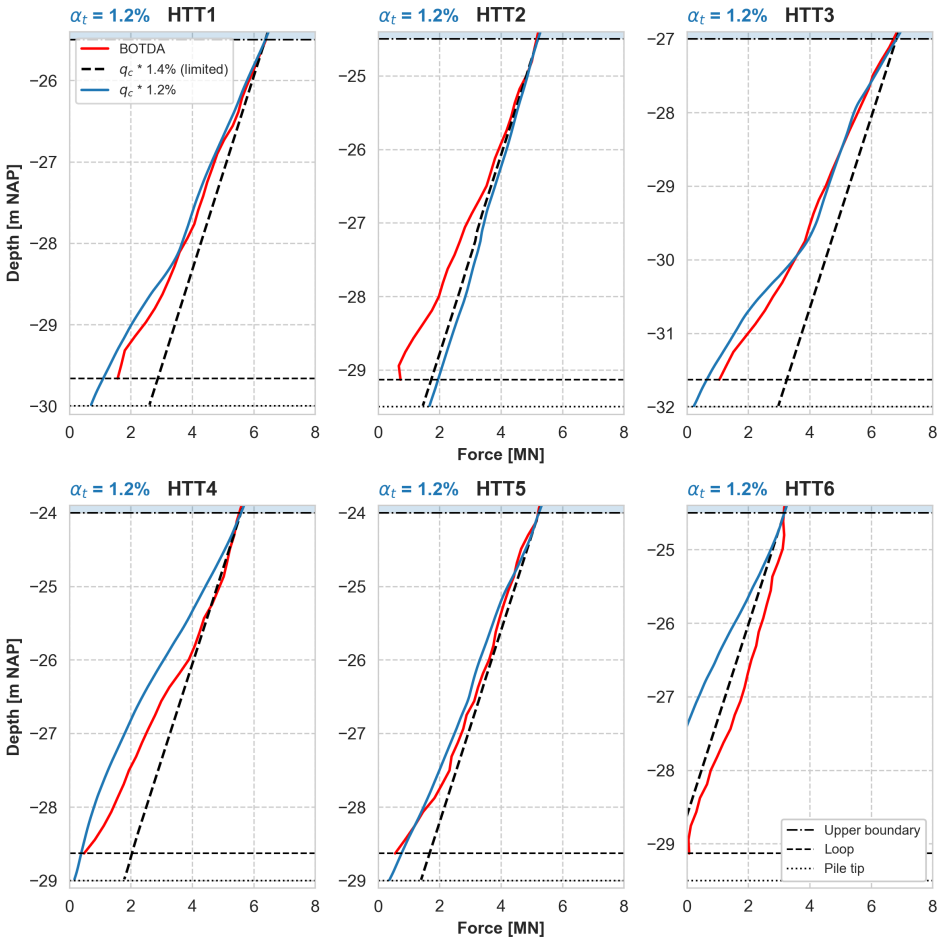

Figure 6.1: Predictions for bearing capacity based on the proposed and CUR166 design method compared to the BOTDA measurements. Predictions are fitted starting from upper boundary at which α_t is derived.

The CUR166 design method is indicated with a dashed black line and the proposed method with a blue line. Predictions are made based on q_c starting at the upper boundary. If the predicted force deviates to the left of the red line, it means that the transfer of forces, and thus the bearing capacity, is overestimated. If the predicted force deviates to the right, the bearing capacity is underestimated. The figure clearly shows that limiting the cone resistance results in a poor prediction and a significant underestimation of the shaft friction. The proposed method, α_t of 1.2% without limiting the cone resistance, gives a good fit for HTT test pile 1, 3, 4 and 5. This illustrates that the derived values of α_t provide a good estimate of bearing capacity. However, the proposed method results in an underestimation of the bearing capacity for HTT2 and an overestimation for HTT6. Possible explanations for this are:

- The circumference of the injected grout body was different than assumed.
- The cone resistance has increased due to installation of the neighbouring production piles.
- The soil surrounding of the piles behaves different from the soil in which the CPT was performed.

Differences in grout body diameter
The possible deviation in circumference of the injected grout body is investigated with the grout discharge data. If more grout is injected at one of the piles and the circumference is larger, the shaft friction may be overestimated. It must be noted that grout discharge data is not a direct indicator of the grout body circumference as soil conditions may also affect this. However, it is expected that the shape and circumference of the grout body is approximately constant in the dense and stiff Pleistocene sand layer. However, no relation between the measured grout discharges and the shaft friction is observed. As discussed in Chapter 3.2.2, it is not certain if the grout discharge data is reliable as grout may have discharged back to ground level, where it was pumped away (and this was not registered).

Effect of pile installation on cone resistance
Table 6.1.2 shows the average increase in cone resistance per pile. The cone resistance seems to have increased the most at HTT2 and the least at HTT6. However, it is uncertain how the cone resistance is affected due to installation as test and production piles deflected in different directions. The distance between the piles was 3.3 m and the measured deflection of pile HTT6 was 2.7 m. Furthermore, the deflection of a CPT at this depth can also be several meters. Therefore, CPT's after pile installation can not be used to explain deviations in bearing capacity.

Incorrect representation of cone resistance
The last explanation can be the result of the change of pile location due to deflection and because CPT's are not executed along the axis of the pile. Chapter 5.2 illustrates that pile installation energy (IE) is a good indicator of the soil conditions. The piles that give good predictions for the bearing capacity with α_t = 1.2% present similar ratio's between the installation energy and the cone resistance. The ratio's at HTT2 and HTT6 suggest that the cone resistance is underestimated at HTT2 and overestimated at HTT6.

Test pile	**Name**	$q_{c,increase}$* [%]	**IE/q_c ratio** [-]	α_t [%]
HTT1	MV-A-12b	36	1.2	1.1
HTT2	MV-A-48b	42	1.5	1.7
HTT3	MV-A-60b	8.0	1.2	1.2
HTT4	MV-B-48b	24	1.1	1.2
HTT5	MV-C-6b	26	1.3	1.2
HTT6	MV-C-54b	0.1	0.7	0.8

Table 6.1.2: Overview of findings Chapter 5.
*Due to pile installation.

6.1.2. Mobilisation curve

As discussed in Chapter 5.4, all normalised data is combined to develop one general curve illustrating the mobilisation of shaft friction as a function of relative pile-soil displacement. This curve can be used to validate and calibrate finite element models for research and design purposes. The mobilisation curve shown in Figure 6.2 is derived according to a second degree polynomial fit function in Python. The function of this mobilisation curve is denoted in Equation 6.2:

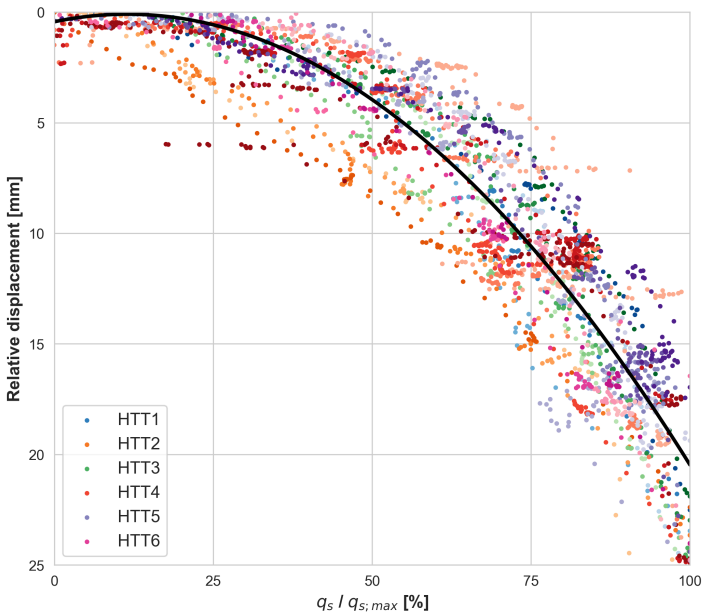

Figure 6.2: Mobilisation curve for shaft friction as a function of relative pile-soil displacement.

Due to measurement scatter, the curve does not start exactly at (0,0). However, an appropriate fit is obtained. The standard deviation of the slope parameters of the fitted function is presented in Table 6.1.3). The fitted curve illustrates the relation between mobilised shaft friction and pile tip displacement of MV piles. This relation is similar for compression piles. Figure 6.3 illustrates this as the derived curve for tension piles is similar to the standardised curve for small and non-displacement compression piles as described in the NEN 9997-1 [22].

Fit parameter			Standard deviation
a	=	-0.05931	±0.0055
b	=	0.00260	±0.0005
c	=	0.43206	±0.1316

Table 6.1.3: Standard deviation of fit parameters.

$$y = -a \cdot x + b \cdot x^2 + c \tag{6.2}$$

Where:

$a = 0.05931$
$b = 0.00260$
$c = 0.43206$

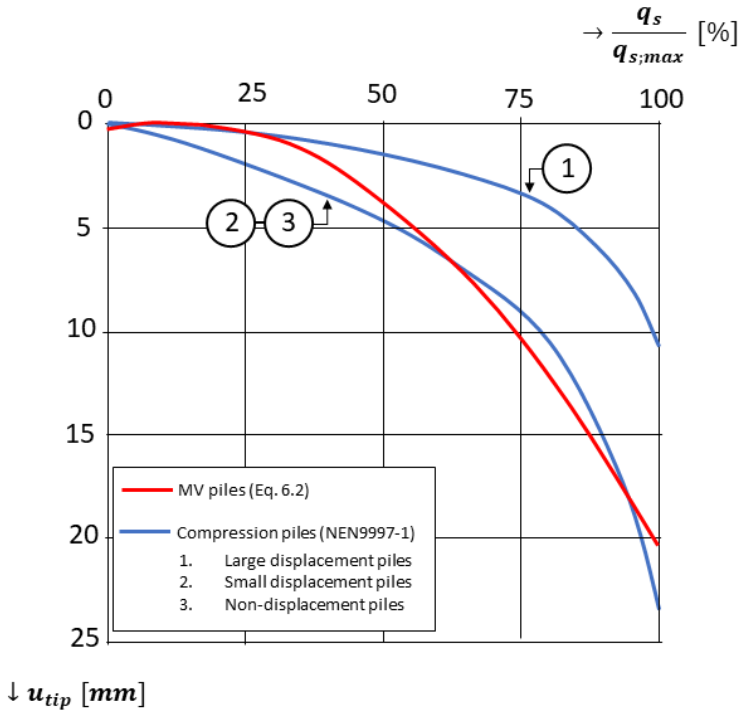

Figure 6.3: Comparison between derived mobilisation curve for MV piles and NEN 9997-1 curve for compression piles [22].

6.2. Discussion

6.2.1. Safety of design method

It is evident that the proposed method with α_t = 1.2% and without limiting the cone resistance may result in an unsafe design. The coefficient of variation of the derived values of α_t is 22%. This same variation applies to the bearing capacity as this is directly dependent of α_t. This means that the risk that the bearing capacity is underestimated is always present. Safety factors are applied in foundation design to compensate for uncertainties. However, one should realize that the uncertainties in foundation design are generally substantial, and most of the historical pile factors have been derived from limited data sets without strain measurements. On the contrary, the α_t value derived in this thesis is based on a state of the art load test with accurate strain measurements. Furthermore, a good correlation between the installation energy and the CPT data was observed. If a consistent relation between CPT-based bearing capacity and pile driving energy is established, uncertainty can be reduced, resulting in a lower factor of safety.

6.2.2. Potential value to the Port of Rotterdam

Significant economic savings for MV-piles in dense sand layers can be achieved by MV pile design with α_t = 1.2% and without limiting the cone resistance. To illustrate the potential value, the required length for geotechnical bearing capacity of HTT production piles is re-calculated. The length reduction is determined per section based on the same number of piles (308 in total). The D-Foundation models used for the original design of the test piles are adapted by modifying α_t and $q_{c;lim}$. The required pile length is re-determined for each quay wall section based on the normative CPT. This resulted in an average reduction of approximately 7 meters per pile (see Appendix C.5). The production and installation costs of 1 meter MV-pile is roughly estimated to be in the range of €300 - €400. This results in a total saving of approximately €750,000 - €1,000,000 for the 1 km long HTT quay wall.

7

Conclusions and recommendations

7.1. Conclusions

The main objective of this thesis is to evaluate and improve the design method of MV piles. The bearing capacity of these anchor piles is determined by a CPT-based method that correlates the cone resistance to the shaft friction by a factor α_t. This factor is limited by a maximum shaft friction of 250 kPa, corresponding in effect to a limiting value of the cone resistance of 18 MPa. Since the formulation of this standard in the 1980's, retaining heights of quay walls have grown and encountered soil strengths have increased and values of q_c exceeding 50 MPa are commonly encountered.

Analysis of the recent failure load tests in the port of Rotterdam allowed accurate determination of the local mobilisation of shaft friction. Detailed strain readings showed values of shaft friction up to 600 kPa near the tip of the piles. This is significantly higher than the assumed maximum value of 250 kPa. It is evident that this assumption is not valid and that limiting the cone resistance results in an underestimation of the bearing capacity.

Comparison between CPT's before and after pile installation showed increasing values of q_c ranging between 24 and 37 % at 4 out of 6 tests. This is significantly more than the range of deviation due to variability of the soil, which was around 10%. Local increases in cone resistance could not be linked to installation of the piles. Installation of production piles next to the test piles has most likely affected the soil conditions in the bearing layer.
Multiplication of the blow count by the energy per blow to compute the installation energy correlated well with the cone resistance. The best-fit was achieved when the installation energy was multiplied by 0.2 for this S-120 type hammer with a ram weight of 6.2 ton.

Derivation of pile factor α_t resulted in a value of 1.2% without limiting the cone resistance. Predictions based on this method provided a good fit with the accurate strain measurements for 4 out of 6 piles. If a consistent relation between CPT-based bearing capacity and pile driving energy is established, uncertainty can be reduced.

A normalised curve for the mobilisation of shaft friction as a function of relative displacement is derived. This curve is similar to the NEN 9997-1 curve for small and non-displacement compression piles. This curve can be used to validate and calibrate finite element models.

7.2. Recommendations

This research proposes a new prediction method for the bearing capacity of MV piles. It is regarded as a first step towards a new design standard. The Port of Rotterdam has planned a new test campaign this year at the Offshore Tank Terminal (OTR). The results of these test can be used to verify and further improve the proposed method. The following is recommended regarding these test:

- Strain recordings before and after pile installation may provide more insight about the existence and time dependent behaviour of residual loads. Reference measurements and measurements after installation should be taken on the test piles instead of the production piles as this allows determination of residual loads and their possible effect on the load distribution.
- Analysis of the soil investigation data of the new tests may provide more insight about the effects of pile installation. Finite element models may improve understanding on the effects of installation and their effect on the bearing capacity.
- The relation between CPT-based bearing capacity and pile driving energy can be further investigated. Analysis of pile installation data may contribute to a better quality control on foundation piles.

Furthermore, future research could investigate how soil-structure interaction finite element models can improve understanding of behaviour and design of MV piles. The derived mobilisation curve can be used to validate and calibrate these models.

Bibliography

[1] Dexin Ba, Benzhang Wang, Dengwang Zhou, Mingjing Yin, Yongkang Dong, Hui Li, Zhiwei Lu, and Zhigang Fan. Distributed measurement of dynamic strain based on multi-slope assisted fast botda. *Optics Express*, 24(9):9781–9793, 2016.

[2] LE Bowles et al. *Foundation analysis and design*. McGraw-hill, 1996.

[3] HE Brassinga. Proefbelasting van twee m.v.-palen aan de brittaniëhaven te rotterdam. Technical report, Gemeentewerken Rotterdam, 1987.

[4] Harry M Coyle and Lymon C Reese. Load transfer for axially loaded piles in clay. *Journal of the Soil Mechanics and Foundations Division*, 92(2):1–26, 1966.

[5] N De Battista, C Kechavarzi, and K Soga. Distributed fiber optic sensors for monitoring reinforced concrete piles using brillouin scattering. In *Sixth European Workshop on Optical Fibre Sensors*, volume 9916, page 99160U. International Society for Optics and Photonics, 2016.

[6] Jacob Gerrit de Gijt and ML Broeken. *Quay walls*. CRC Press, 2013.

[7] Abolfazl Eslami, Sara Moshfeghi, Hossein Molaabasi, and Mohammad M Eslami. *Piezocone and Cone Penetration Test (CPTu and CPT) Applications in Foundation Engineering*. Butterworth-Heinemann, 2019.

[8] Bengt H Fellenius. From strain measurements to load in an instrumented pile. *GEOTECHNICAL NEWS-VANCOUVER-*, 19(1):35–38, 2001.

[9] Bengt H Fellenius. Determining the true distributions of load in instrumented piles. In *Deep Foundations 2002: An International Perspective on Theory, Design, Construction, and Performance*, pages 1455–1470. ASCE, 2002.

[10] Kenneth Gavin, Meho Sasa Kovacevic, and David Igoe. A review of cpt based axial pile design in the netherlands. *Underground Space*, 6(1):85–99, 2021.

[11] JG de Gijt and HE Brassinga. Geotechnische aspecten van de zeekade en de bewerkingskade voor de euroterminal op de maasvlakte. *Polytechnisch Tijdschrift Civiele Techniek*, 1990.

[12] John Evelyn Guy. *Behaviour of a model MV pile in sand bearing capacity implications*. PhD thesis, University of the Witwatersrand, Johannesburg, 1988.

[13] J Hayes and T Simmonds. Interpreting strain measurements from load tests in bored piles. In *Proceedings of the Ninth International Conference on Piling and Deep Foundations*, pages 663–669, 2002.

[14] MH Hussein. Pile driving resistance and load bearing capacity. *Soil and Rock America 2003*, 2003.

[15] N Instruments. Measuring position and displacement with lvdts, 2018.

[16] Fauzi Jarushi, S AlKaabim, and Paul Cosentino. A new correlation between spt and cpt for various soils. *International Journal of Environmental, Ecological, Geological and Geophysical Engineering*, 9(2):101–107, 2015.

[17] M Korff. Reader deep excavations. *Reader, TU Delft*, 2018.

[18] Tom Lunne, John JM Powell, and Peter K Robertson. *Cone penetration testing in geotechnical practice*. CRC Press, 2002.

[19] LA Meerdink. Performance of micropiles under axial tensile loading. 2013.

[20] Hisham Mohamad, Bun Pin Tee, Koh An Ang, and Mun Fai Chong. Characterizing anomalies in distributed strain measurements of cast-in-situ bored piles. *Jurnal Teknologi*, 78(8-5), 2016.

[21] Rusong Nie, Wuming Leng, Qi Yang, and Y Frank Chen. Effects of pile residual loads on skin friction and toe resistance. *Soil Mechanics and Foundation Engineering*, 55(2):76–81, 2018.

[22] Nederlands Normalisatie-instituut. *Geotechnisch ontwerp van constructies - Deel 1: Algemene regels/Geotechnical design of structures - Part 1: General rules*. NEN, Delft, 2017.

[23] Yair Peled, Avi Motil, and Moshe Tur. Fast brillouin optical time domain analysis for dynamic sensing. *Optics express*, 20(8):8584–8591, 2012.

[24] Nederlandse praktijkrichtlijn. *NPR 7201 - Determination of the axial bearing capacity of foundation piles by pile load testing*. Koninklijke Nederlandse Normalisatie-instituut, Delft, 2017.

[25] J Putteman, EJ Broos, HE Brassinga, R Spruit, M De Vos, and ALJ Timmermans. Mv tension pile load tests in the port of rotterdam: practical aspects and geotechnical behaviour. In *Proceeding of the European Conference on Soil Mechanics and Geotechnical Engineering, Reykjavik*, 2019.

[26] SBRCURnet. *CUR 166 damwandconstructies/sheet pile constructions*. 3rd edition. CUR, Gouda, 1997.

[27] SBRCURnet. *CUR 166 damwandconstructies/sheet pile constructions*. 6th edition. CUR, Gouda, 2012. ISBN 9780198520115.

[28] Hoyoung Seo, Irem Zeynep Yildirim, and Monica Prezzi. Assessment of the axial load response of an h pile driven in multilayered soil. *Journal of Geotechnical and Geoenvironmental Engineering*, 135(12):1789–1804, 2009.

[29] Timothy C Siegel. Load testing and interpretation of instrumented augered cast-in-place piles. *DFI Journal-The Journal of the Deep Foundations Institute*, 4(2):65–71, 2010.

[30] Jay Srigopal. *Comprehending the behaviour of a Muller Verpress pile under tensional loading*. PhD thesis, Delft University of Technology Delft, 2018.

[31] J.P. van der Meer and A.H. Rol. Vergelijkende belastingsproeven op groutankers. *LGM-Mededelingen*, 1984.

[32] S. van Dijk Hoofd. Mag het ietsje meer zijn? ervaringen met ontwerpen, maken en testen van mv palen. *Vakblad geotechniek*, 14(12):28–33, 2010.

[33] Dong-sheng Xu, Jian-hua Yin, and Hua-bei Liu. A new measurement approach for deflection monitoring of large-scale bored piles using distributed fiber sensing technology. *Measurement*, 117:444–454, 2018.

A

MV-piles in the Port of Rotterdam

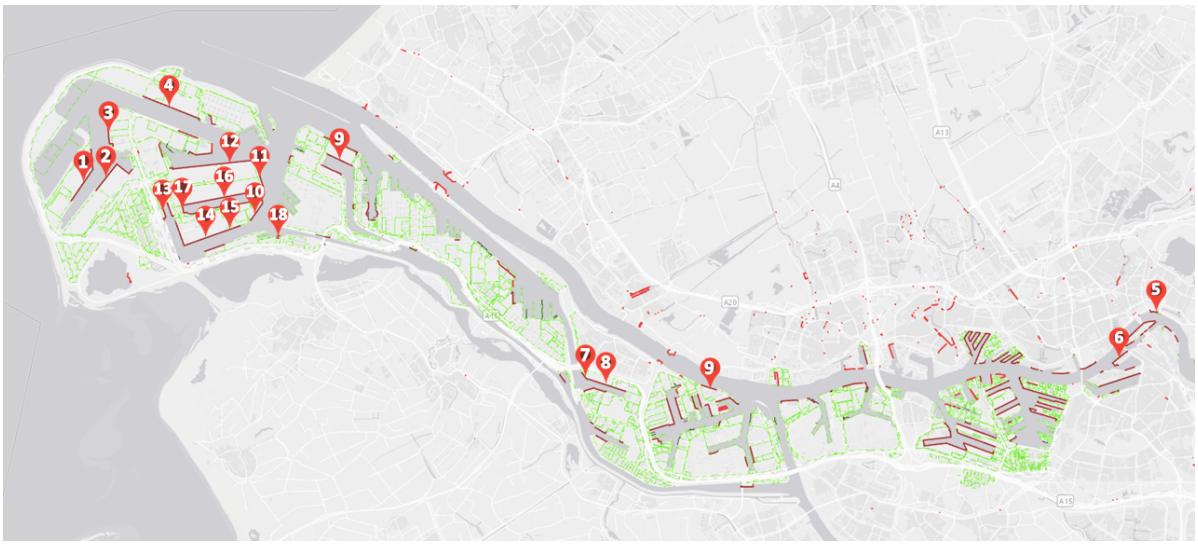

#	Location	Name of quay wall	Number of MV piles
1	Maasvlakte 2	Prinses Amaliahaven Wz	201
2	Maasvlakte 2	Prinses Amaliahaven Oz	185
3	Maasvlakte 2	Prinses Arianehaven Oz Diepzeekade	113
4	Maasvlakte	Yangtzekanaal Nz	361
5	City	Rhijnspoorkade Nz	116
6	City	Holland-Amerikakade	205
7	Europoort	Brittanniehaven NWz	30
8	Europoort	Brittanniehaven Nz	152
9	Botlek	Botlek CG Rosilcokade	681
10	Maasvlakte	Beerkanaal Zwz	217
11	Maasvlakte	Beerkanaal Wz	313
12	Maasvlakte	Europahaven ZOz	276
13	Maasvlakte	Hartelhaven NWz	114
14	Maasvlakte	Mississippihaven Nz	224
15	Maasvlakte	Mississippihaven NOz	3
16	Maasvlakte	Amazonehaven Nz	914
17.1	Maasvlakte	Amazonehaven Wz	72
17.2	Maasvlakte	Amazonehaven ZWz	25
18	Maasvlakte	Yorkhaven Zz	18
19	Maasvlakte	Yangtzekanaal Nz	361

Table A.0.1: Overview of full scale MV pile load tests in the Port of Rotterdam

Test location	Pile name	Year	Depth pile tip [m NAP]	Angle [°]	Max. test load [kN]	Max. creep coeff. [mm]
Ekom kade	A-1	1890	-25.0	45	4500	ND
Ekom kade	A-2	1890	-27.8	45	3600	ND
Ekom kade	B-5	1890	-23.2	45	2500	ND
Ekom kade	C-3	1890	-25.5	45	4500	ND
Ekom kade	C-4	1890	-26.7	45	3500	ND
Ekom kade	C-7	1890	-29.3	45	4500	ND
Hartelhaven	Pile 1	1983	-11.0	45	5500	0.125
Hartelhaven	Pile 2	1983	-11.0	45	5500	0.9
Britanniëhaven	Pile 6	1988	-20.0	45	4000	1.5
Britanniëhaven	Pile 36	1988	-18.0	45	4000	1.5
Swarttouw - ZK	Pile 1	1989	-28.3	45	5000	0.2
Swarttouw - ZK	Pile 2	1989	-25.0	42.5	5000	0.13
Swarttouw - ZK	Pile 3	1989	-29.2	42.5	5000	0.14
Swarttouw - ZK	Pile 4	1989	-30.3	47.5	4000	0.15
Swarttouw - ZK	Pile 5	1989	-30.3	47.5	3000	0.09
Swarttouw - BK	Pile 6	1989	-27.5	47.5	4000	0.11
Swarttouw - BK	Pile 7	1989	-28.2	46.5	4000	0.09
Swarttouw - BK	Pile 8	1989	-27.5	46.5	3000	0.04
Swarttouw - BK	Pile 9	1989	-25.0	45	4000	0.08
Amazonehaven - 1A	mv1	1993	-25.0	45	6000	0.547
Amazonehaven - 1A	mv2	1994	-25.1	45	6000	0.654
Amazonehaven - 1A	mv3	1994	-25.1	45	6000	0.7
Amazonehaven - 1A	mv4	1994	-27.5	45	6000	0.562
Amazonehaven - 1A	mv5	1994	-28.0	45	6000	1.508
Amazonehaven - 1A	mv6	1994	-26.5	45	6000	1.824
Amazonehaven - 1A	mv7	1994	-26.0	45	6000	2.069
Amazonehaven - 1A	mv8	1994	-28.0	45	6000	2.511
Amazonehaven - 1B	mv1	1995	-26.0	45	6000	0.545
Amazonehaven - 1B	mv2	1995	-25.0	45	6000	0.878
Amazonehaven - 1B	mv3	1995	-27.0	45	6000	0.889
Amazonehaven - 2A	119	1996	-26.5	45	6000	0.68
Amazonehaven - 2A	164	1996	-26.5	45	6000	1.64
Amazonehaven - 2A	191	1996	-28.0	45	6000	0.58
Amazonehaven - 2A	227	1996	-29.0	45	6000	0.66
Amazonehaven - 2B	272	1997	-27.0	45	5950	0.65
Amazonehaven - 2B	308	1997	-27.0	45	5500	0.65
Amazonehaven - 2B	326	1997	-28.0	45	5950	0.65
Botlek ”Het Scheur”	11A3	1994	-28.0	45	5000	0.37
Botlek ”Het Scheur”	10A12	1994	-28.0	45	5000	0.14
Botlek ”Het Scheur”	6B43	1994	-29.0	45	5000	0.27
Wilhelminakade	TC60	1995	-25.0	72	5000	0.907
Wilhelminakade	TC147	1995	-25.0	72	5000	1.942
Euromax	H007	2006	-34.0	45	9100	0.7
Euromax	H031	2006	-34.0	45	9100	1.8
Euromax	H118	2006	-34.0	45	9100	0.7
Euromax	H142	2006	-34.0	45	9100	1.4
Euromax	H220	2006	-34.0	45	9100	1.0
BAVO - kade 5.1	08H2	2006	-44.4	45	9100	1.12
BAVO - kade 5.1	25H2	2006	-43.9	45	8800	0.84
BAVO - kade 5.3	08H3	2006	-45.2	45	9100	0.96

Table A.0.2: Overview of full scale MV pile load tests in the Port of Rotterdam

A.1. Additional HTT test report results

The two graphs in this section are copied from test report HHTT-008415 (revision date: 09-03-2020).

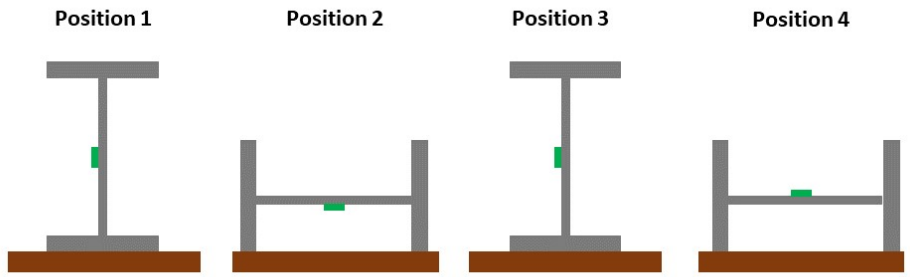

Figure A.1: Positions of reference measurements (strain sensor indicated in green)

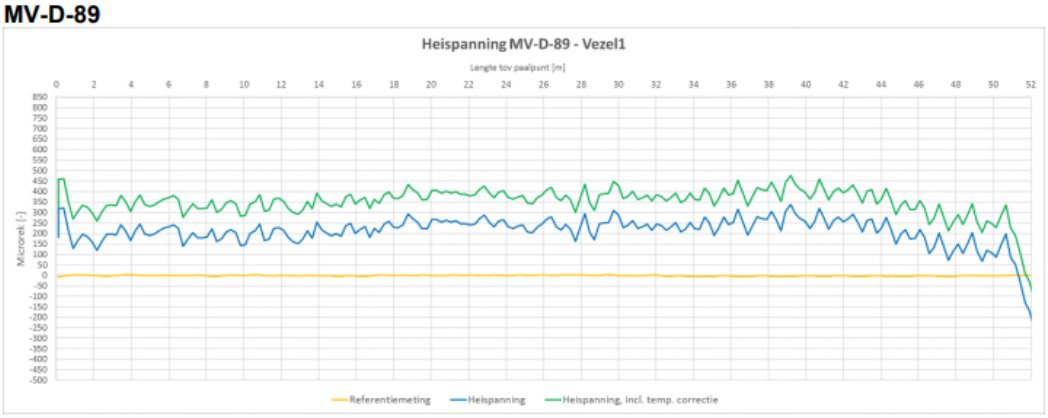

Figure A.2: Residual stresses after installation (blue line) compared to reference measurements (yellow line).The green distribution represents the residual stress distribution after installation including corrections for temperature differences.

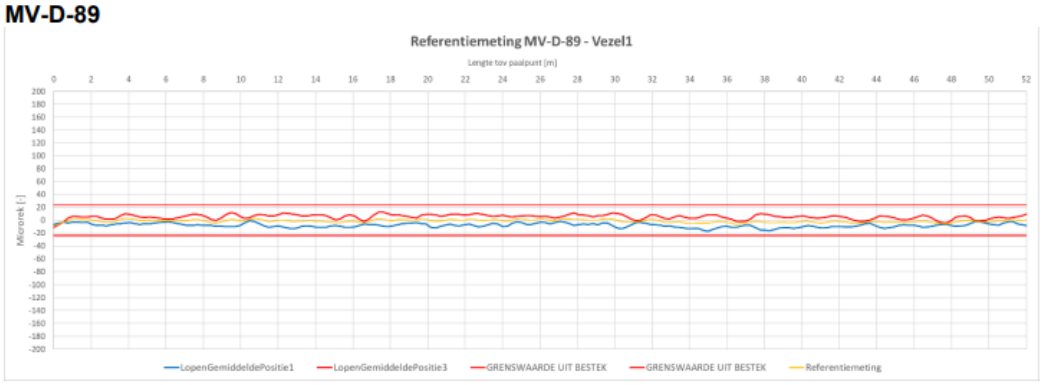

Figure A.3: Residual stresses 30 days after installation compared to reference measurements (yellow line). The red lines represent the imposed limits (±23 micro strain).

B

HTT test data

B.1. Soil investigation

B.1.1. CPT profiles

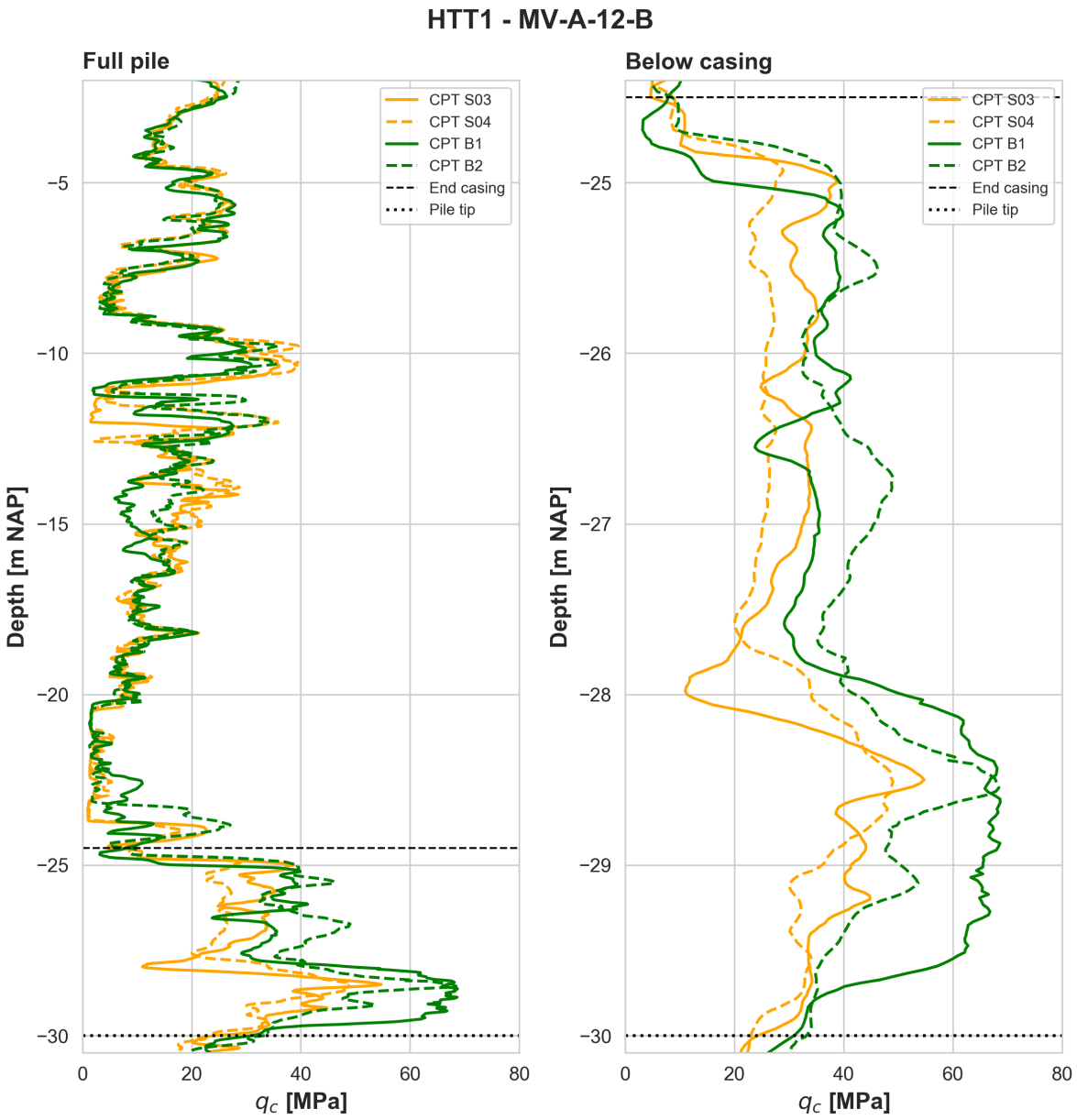

Figure B.1: HTT1 (orange: CPTs before pile installation, green: CPTs after pile installation)

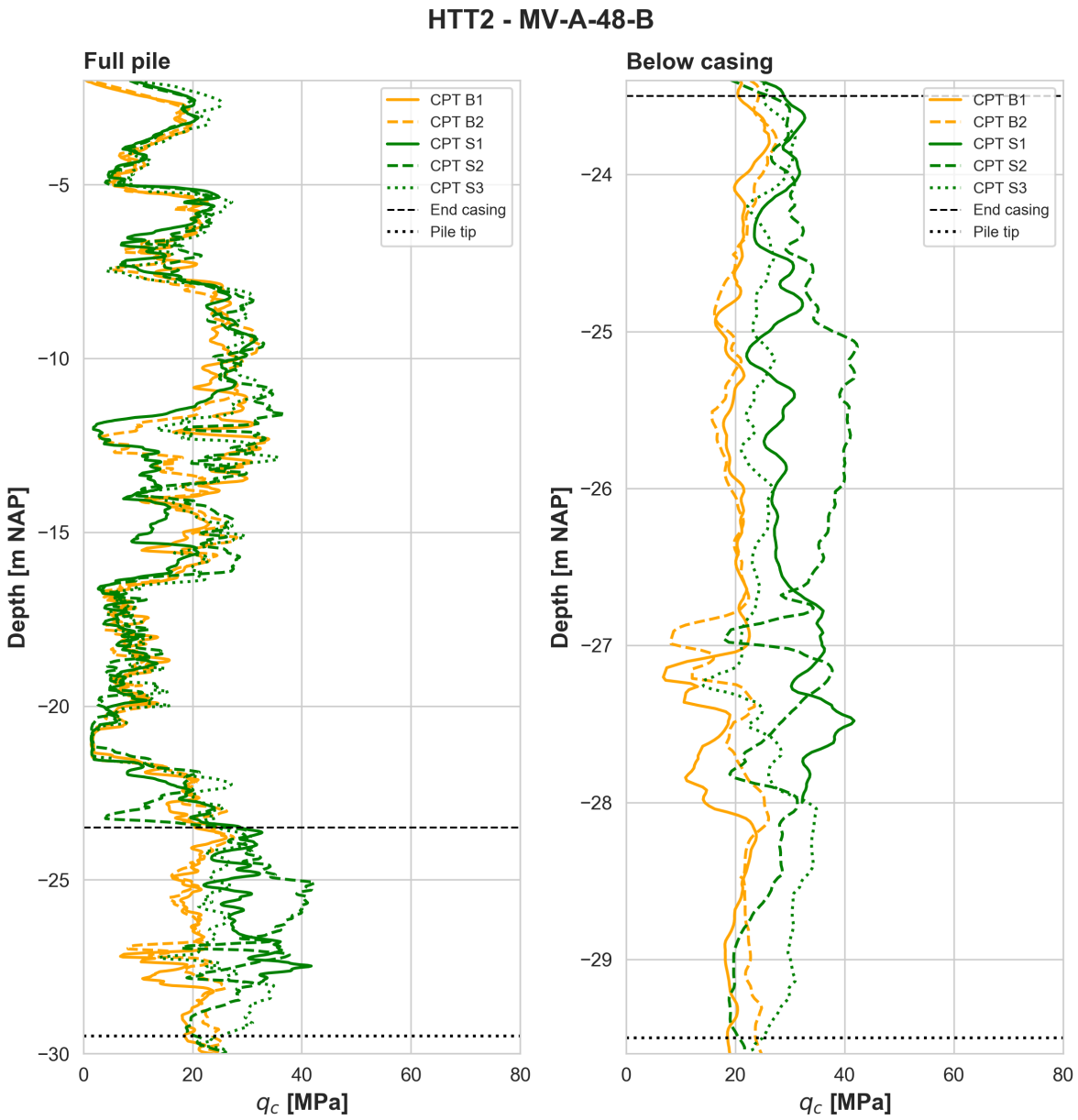

Figure B.2: HTT2 (orange: CPTs before pile installation, green: CPTs after pile installation)

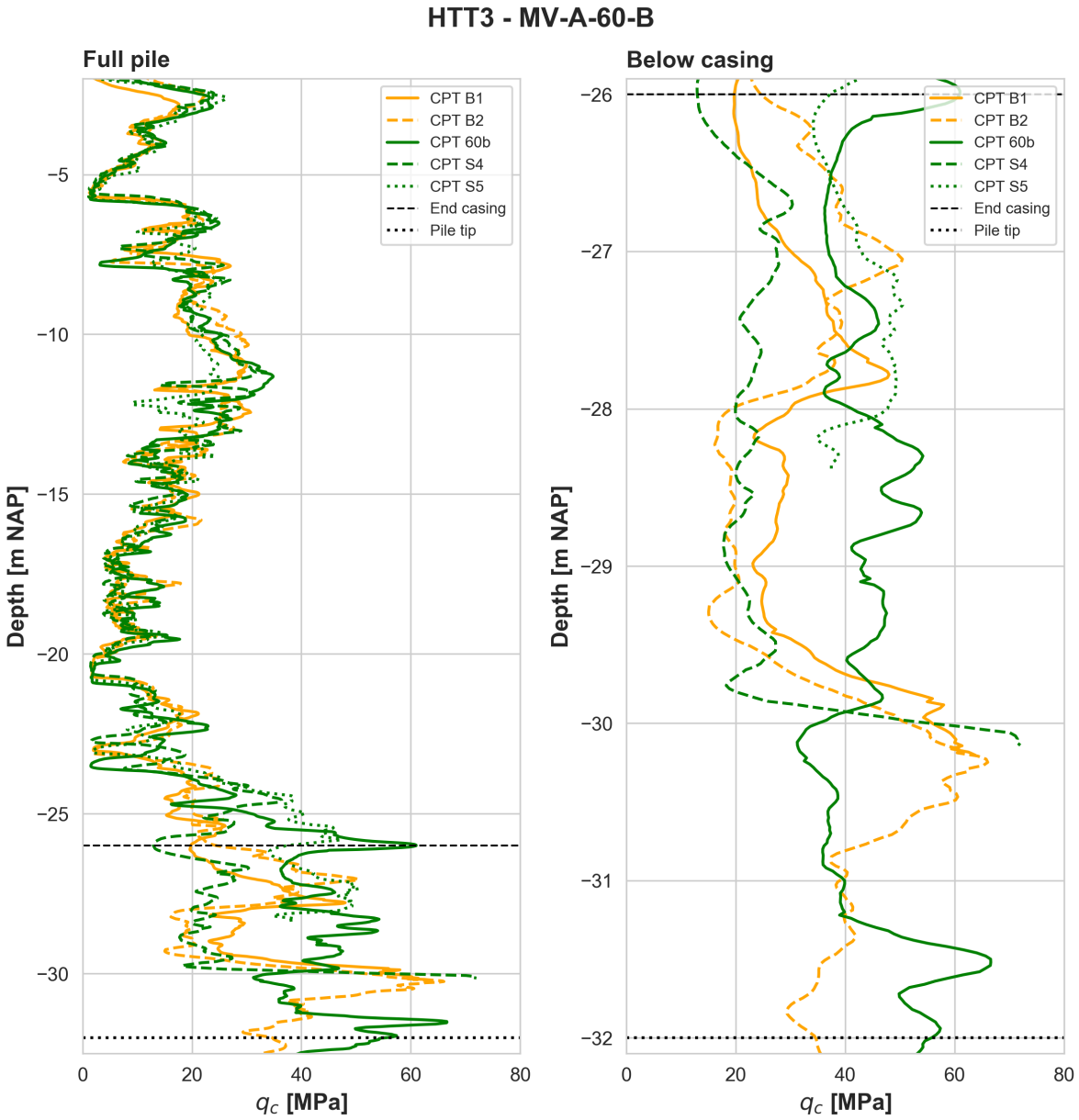

Figure B.3: HTT3 (orange: CPTs before pile installation, green: CPTs after pile installation)

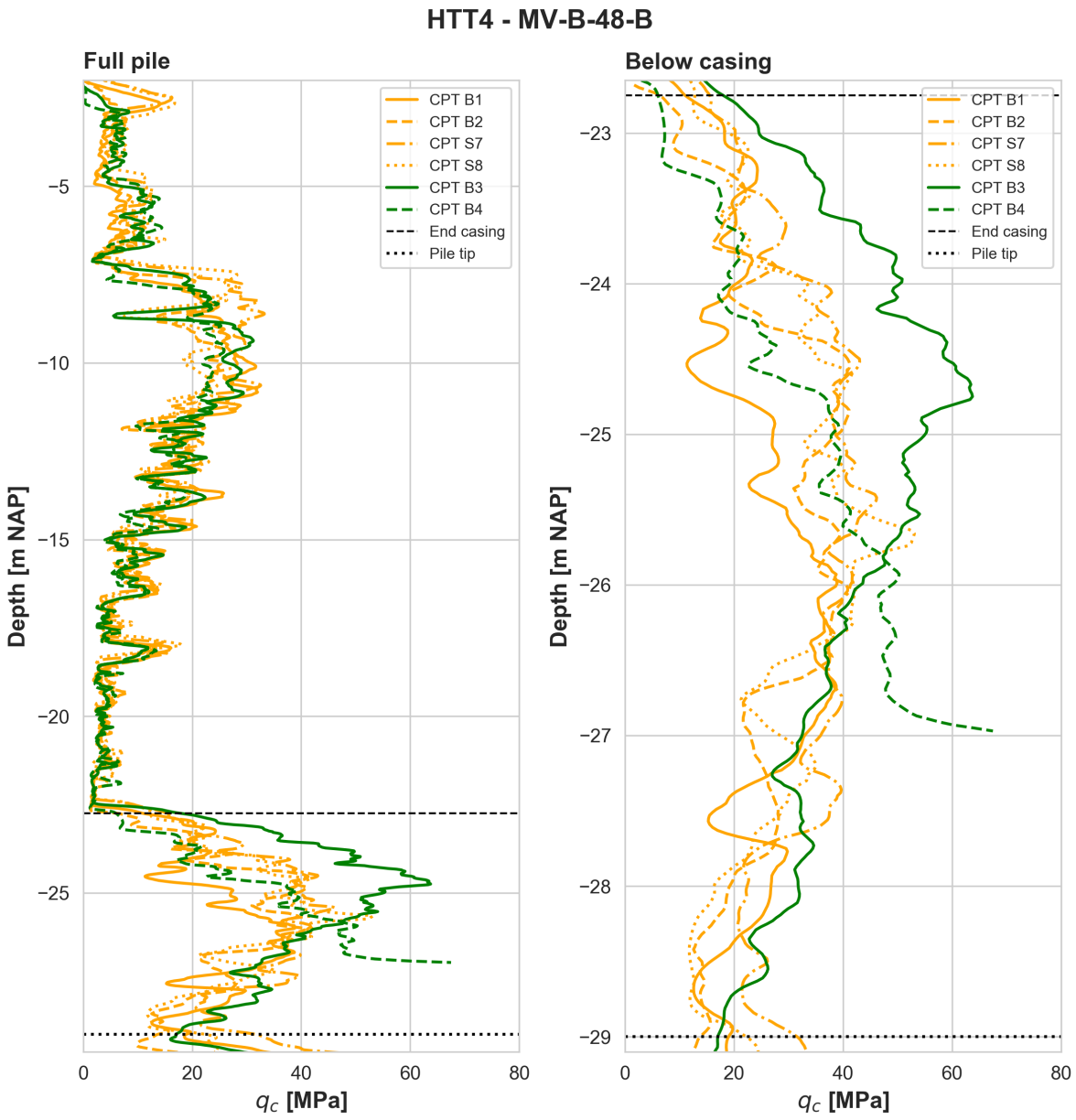

Figure B.4: HTT4 (orange: CPTs before pile installation, green: CPTs after pile installation)

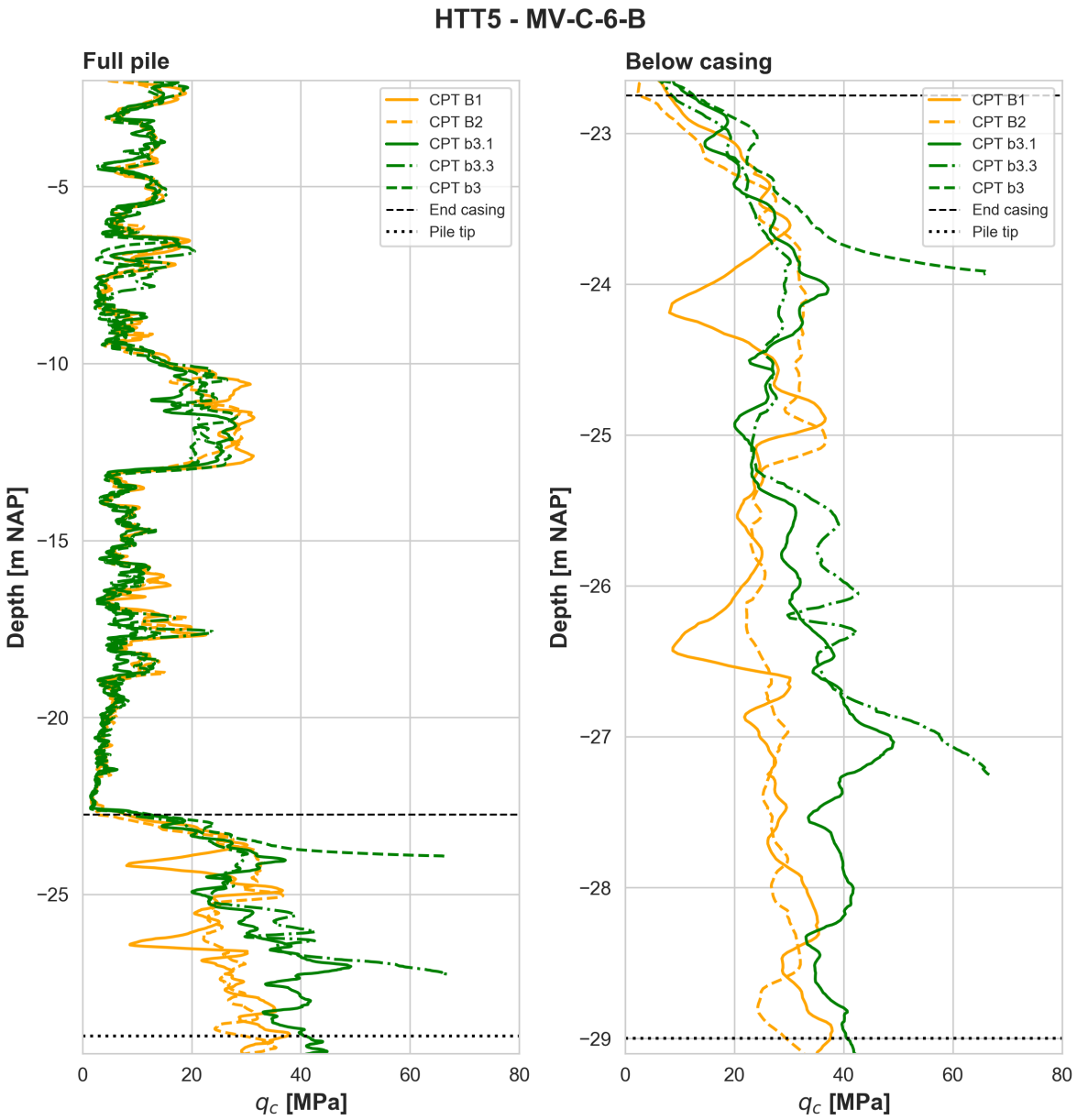

Figure B.5: HTT5 (orange: CPTs before pile installation, green: CPTs after pile installation)

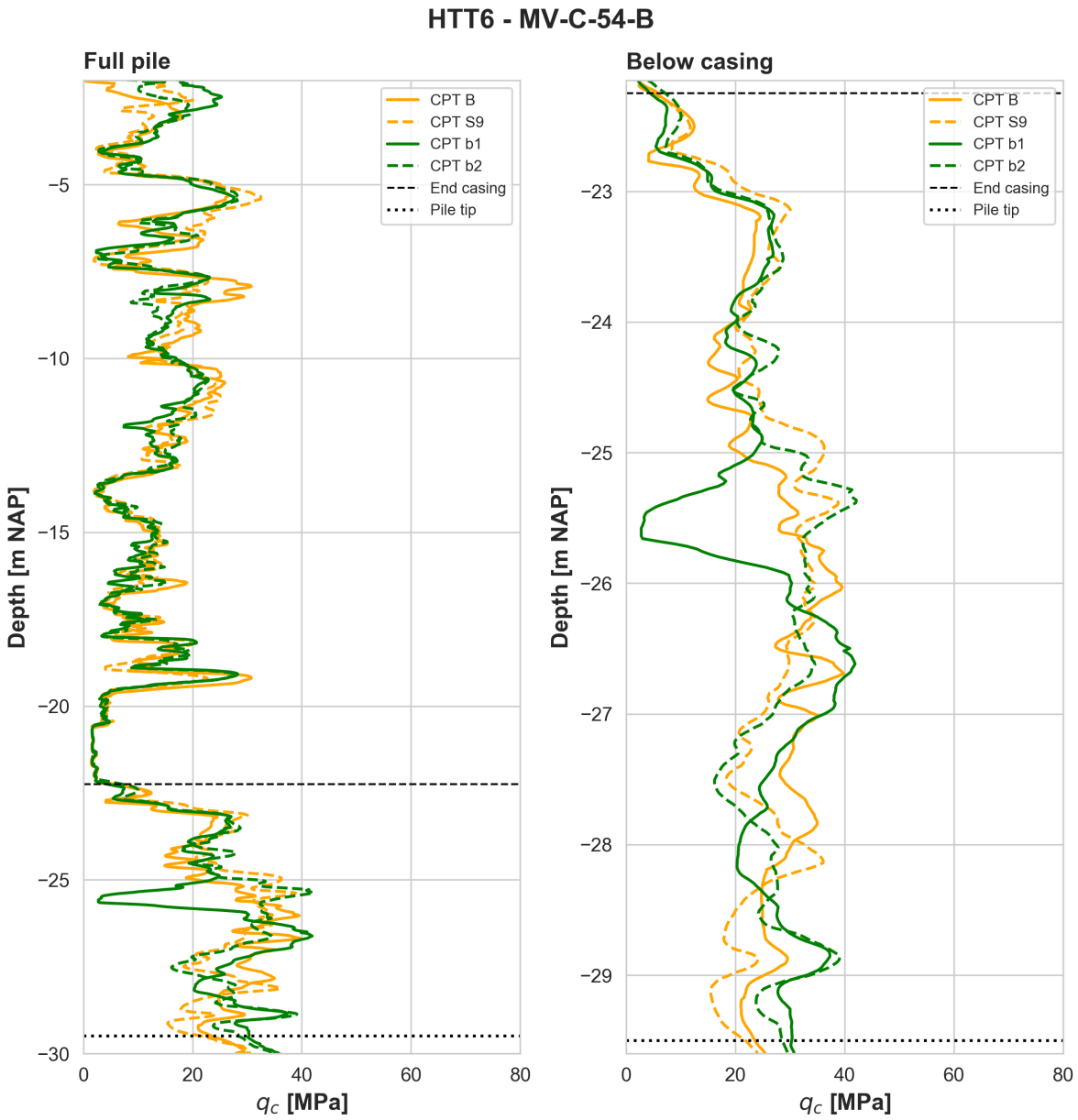

Figure B.6: HTT6 (orange: CPTs before pile installation, green: CPTs after pile installation)

B.1.2. Location of intermediate clay layer

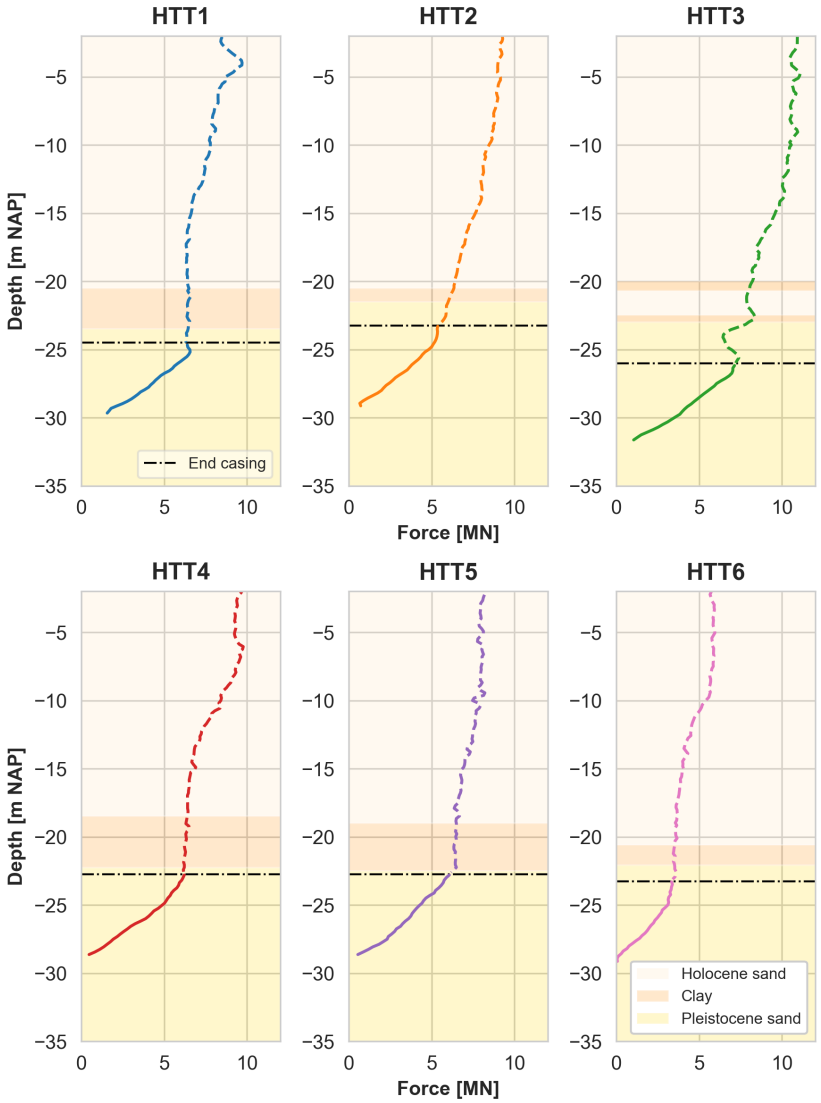

Figure B.7: Location of intermediate clay layer per test pile indicated. The normal force is at which α_t is derived is plotted for each pile (end of casing indicated by dashed line)

.

B.1.3. CPT's before and after installation

Comparison of CPT's before and after pile installation. The deviation of the CPT's before pile installation from the average value (q_{avg}) is denoted above the left plot. This indicates the variability of the soil. The difference between q_{avg} before and after pile installation is denoted above the right plot. This indicates the effect of pile installation on the soil.

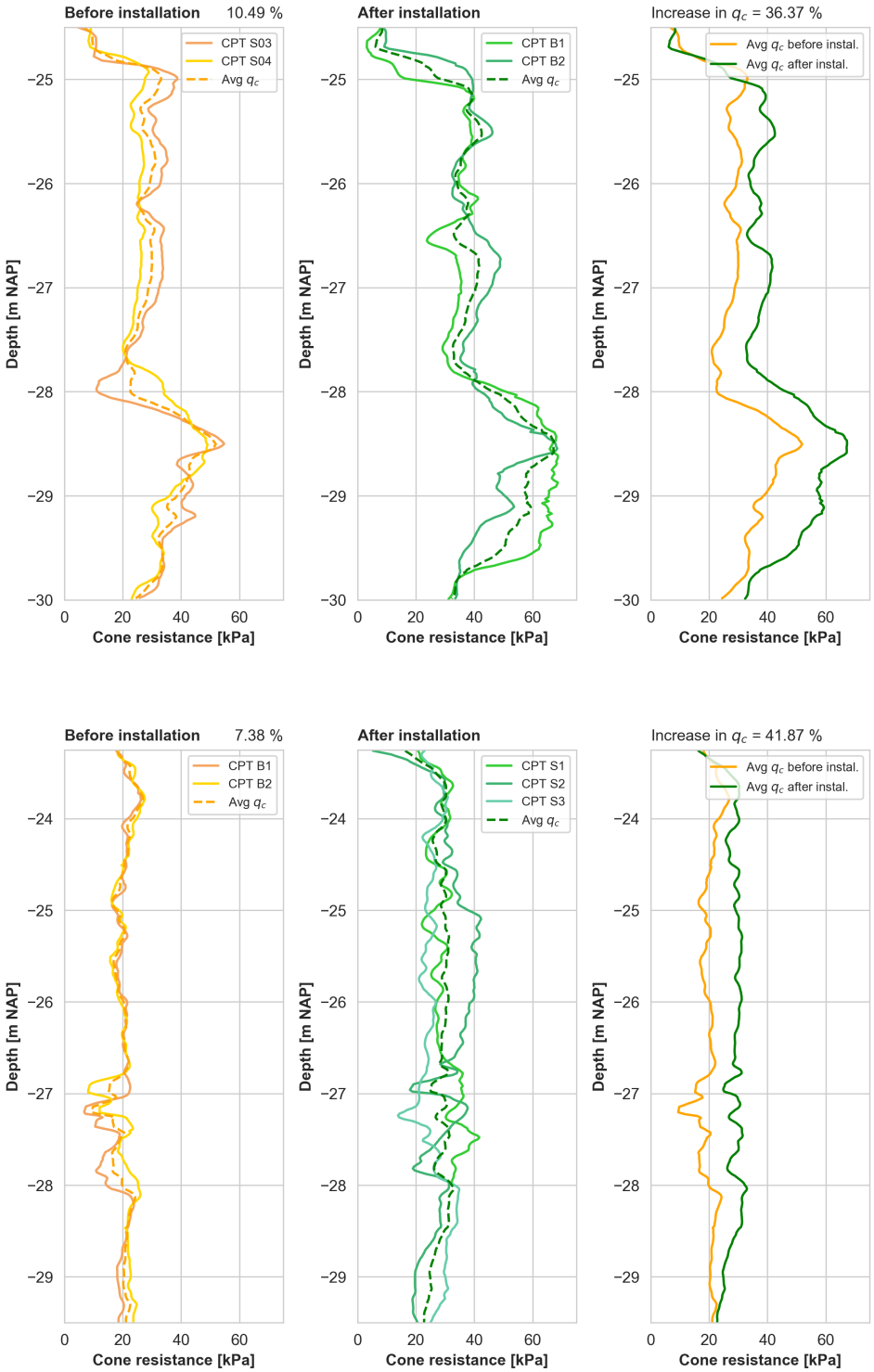

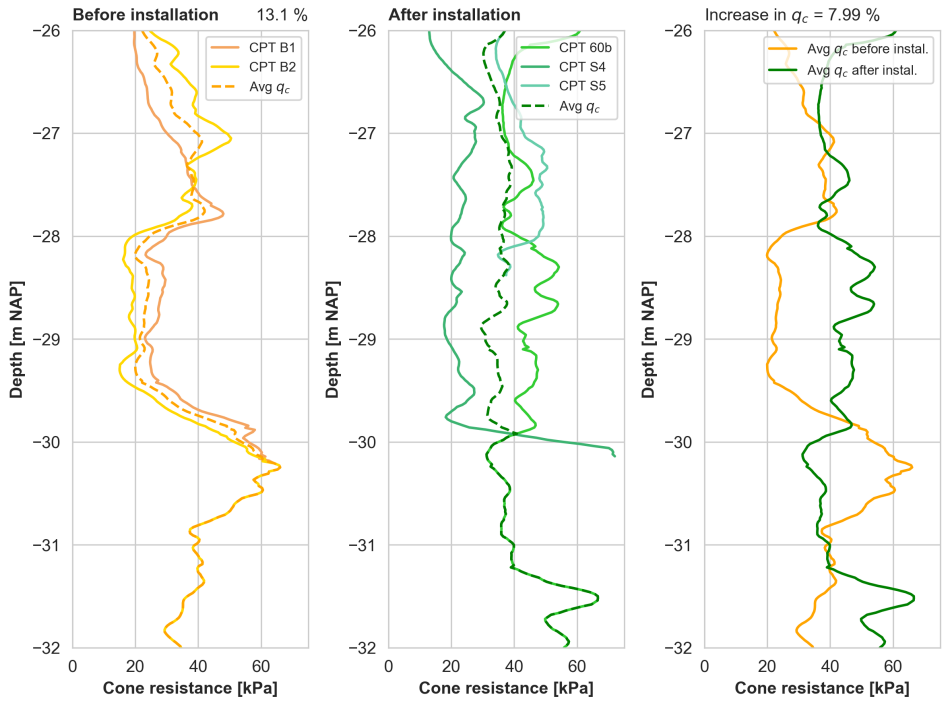
Before installation
13.1 %
CPT B1
CPT B2
Avg q_c
After installation
CPT 60b
CPT S4
CPT S5
Avg q_c
Increase in q_c = 7.99 %
Avg q_c before instal.
Avg q_c after instal.
Depth [m NAP]
Cone resistance [kPa]

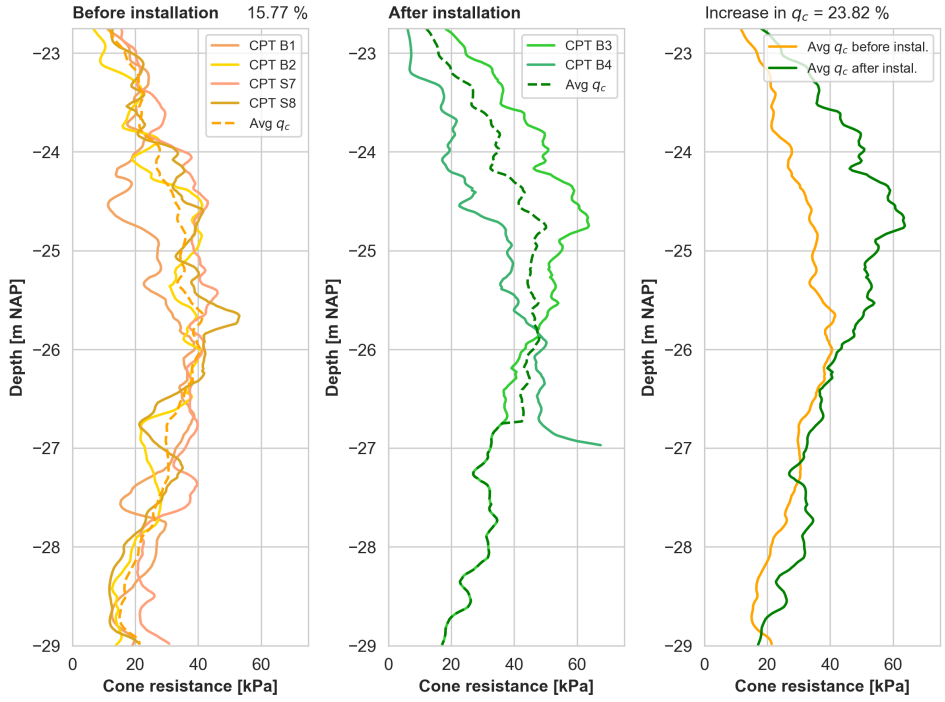
Before installation
15.77 %
CPT B1
CPT B2
CPT S7
CPT S8
Avg q_c
After installation
CPT B3
CPT B4
Avg q_c
Increase in q_c = 23.82 %
Avg q_c before instal.
Avg q_c after instal.
Depth [m NAP]
Cone resistance [kPa]

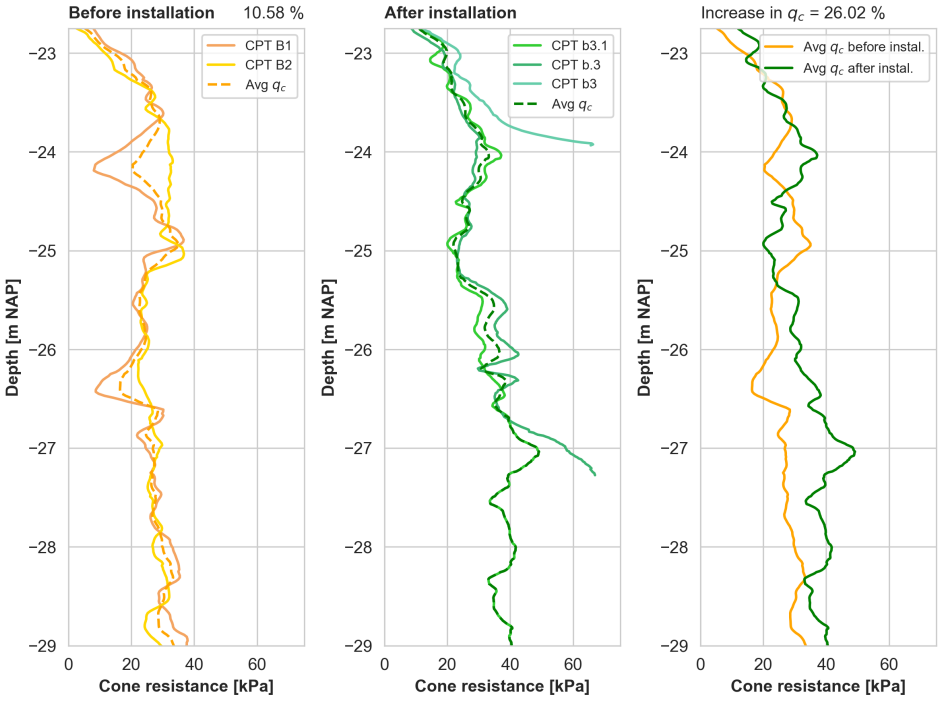
Before installation 10.58 %
CPT B1
CPT B2
Avg q_c
After installation
CPT b3.1
CPT b.3
CPT b3
Avg q_c
Increase in q_c = 26.02 %
Avg q_c before instal.
Avg q_c after instal.
Depth [m NAP]
−23
−24
−25
−26
−27
−28
−29
0
20
40
60
Cone resistance [kPa]

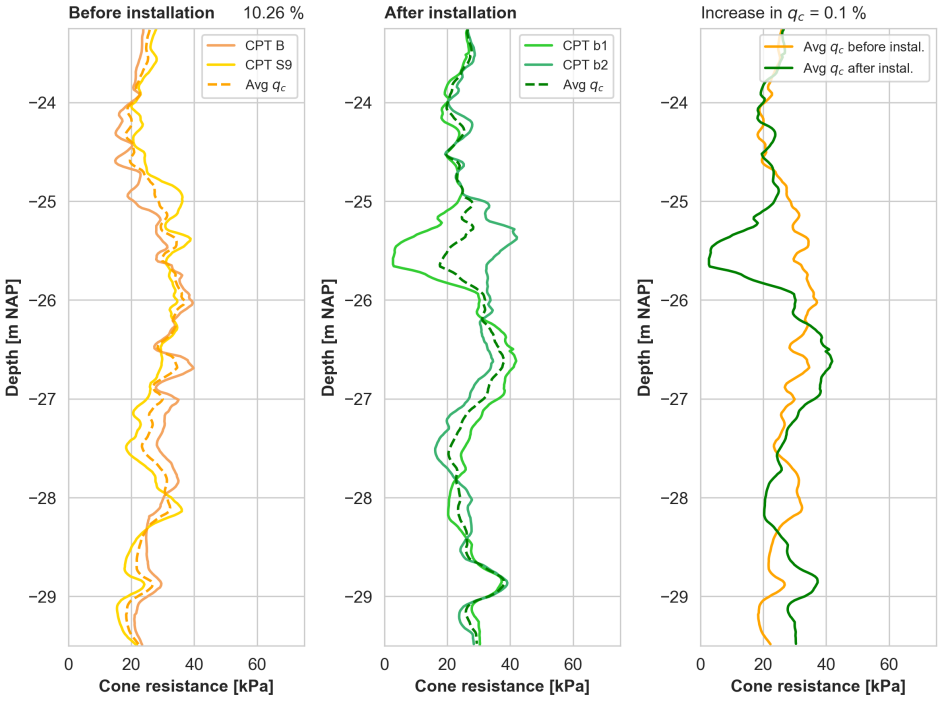
Before installation 10.26 %
CPT B
CPT S9
Avg q_c
After installation
CPT b1
CPT b2
Avg q_c
Increase in q_c = 0.1 %
Avg q_c before instal.
Avg q_c after instal.
Depth [m NAP]
−24
−25
−26
−27
−28
−29
0
20
40
60
Cone resistance [kPa]

B.1.4. Top overview of test piles and CPTs

Figure B.8: Satellite photo of HTT quay wall

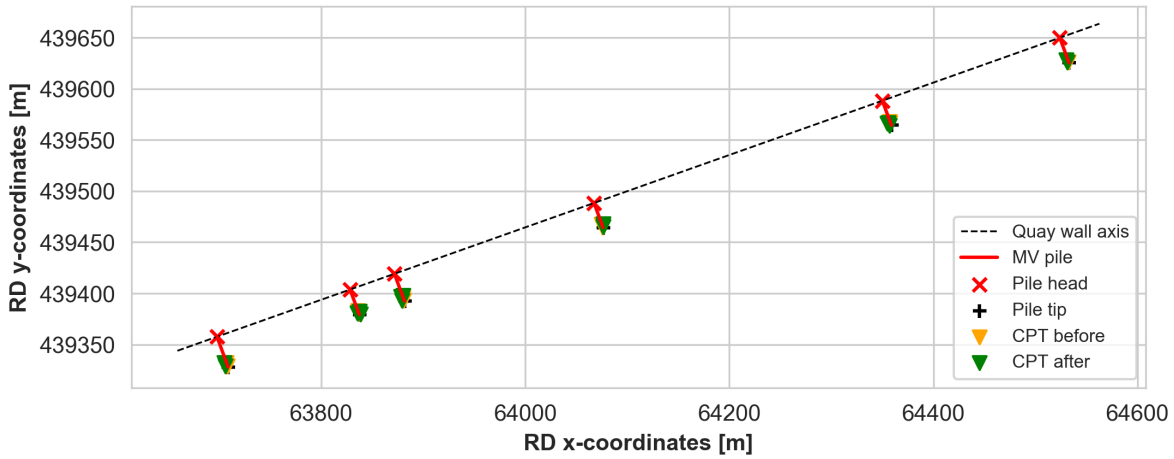

Figure B.9: Global locations overview (RD coordinates)

B.1.5. Top view per test pile

Graphs illustrate the global locations per test pile (RD coordinates). Note that the lines illustrates the designed location of the MV-pile. This is determined based on the location of the pile head, the installation angle and the pile length.

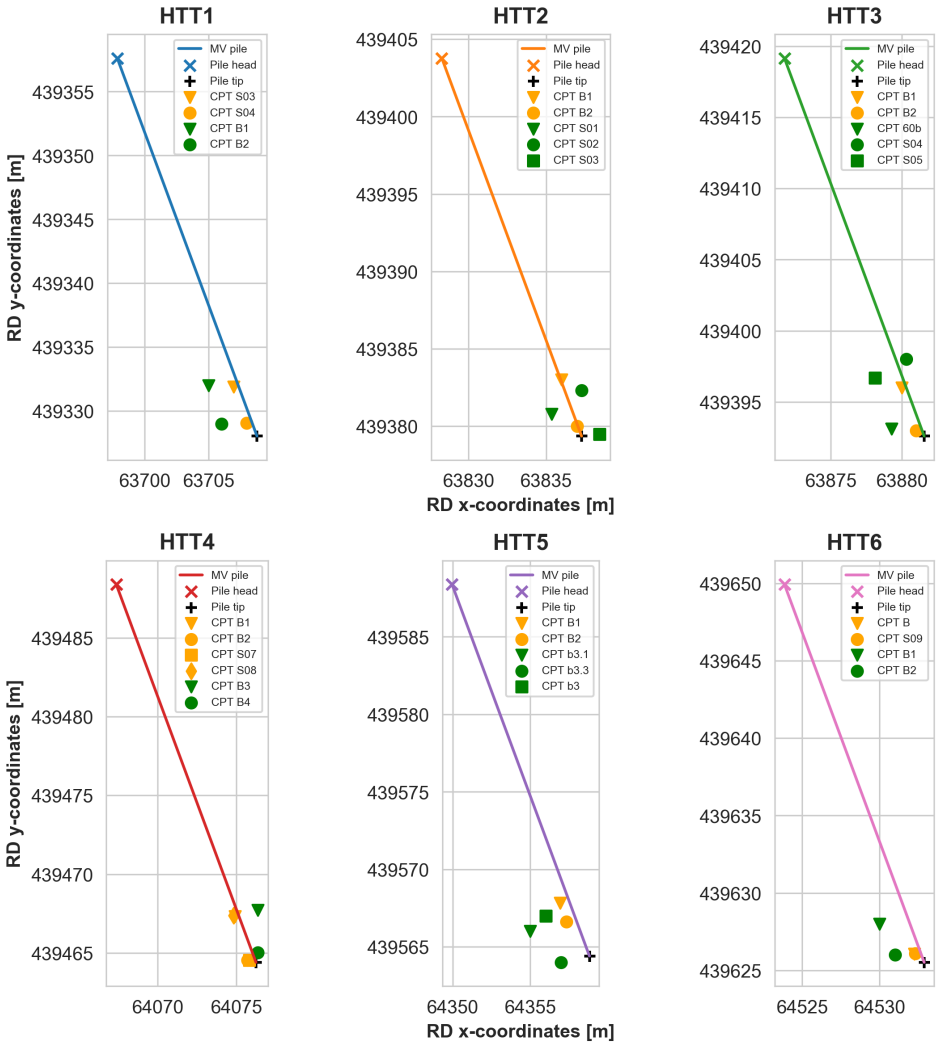

B.2. HTT test data

B.2.1. Creep curves

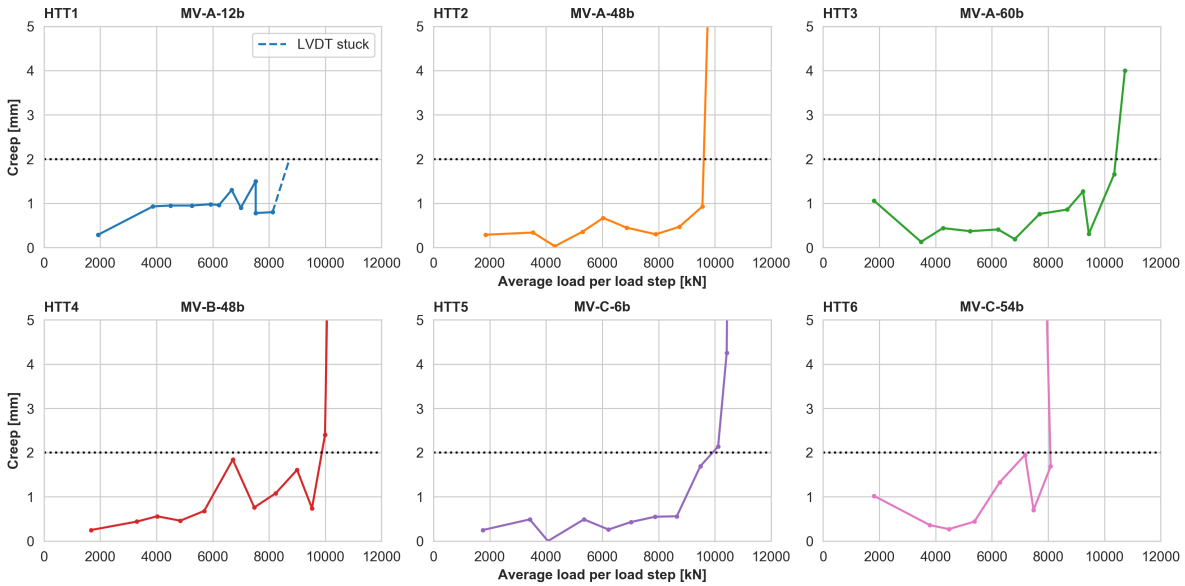

Figure B.10: Graphs illustrating the amount of creep at the end of each load step

B.2.2. Load-displacement data

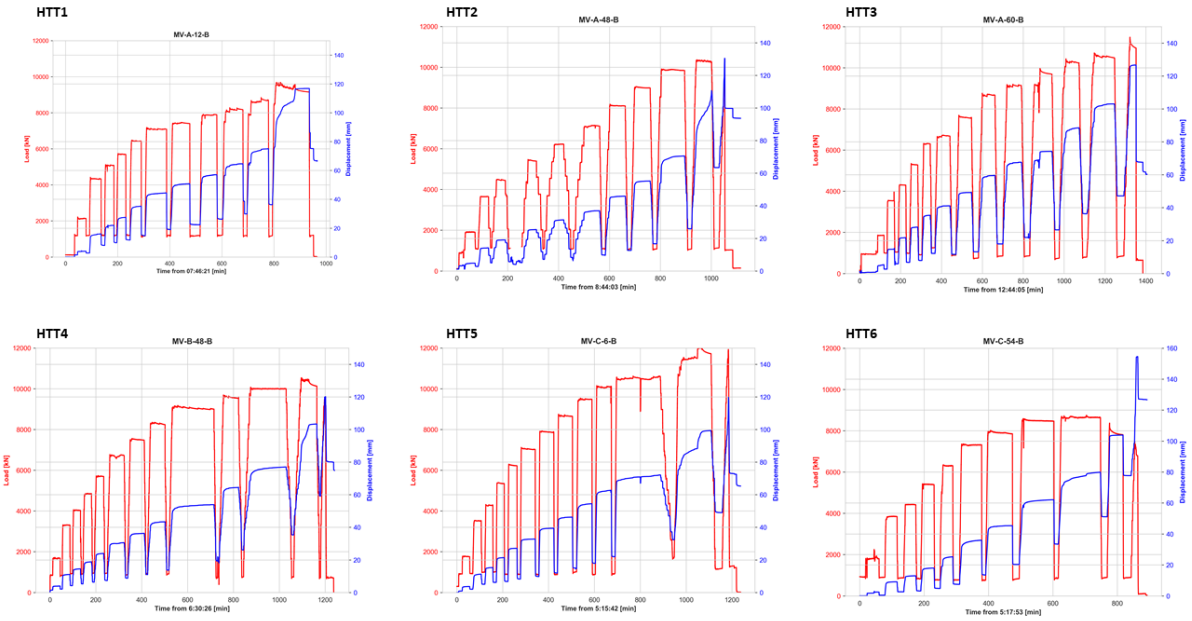

Figure B.11: Applied pile load and pile-head displacement over time

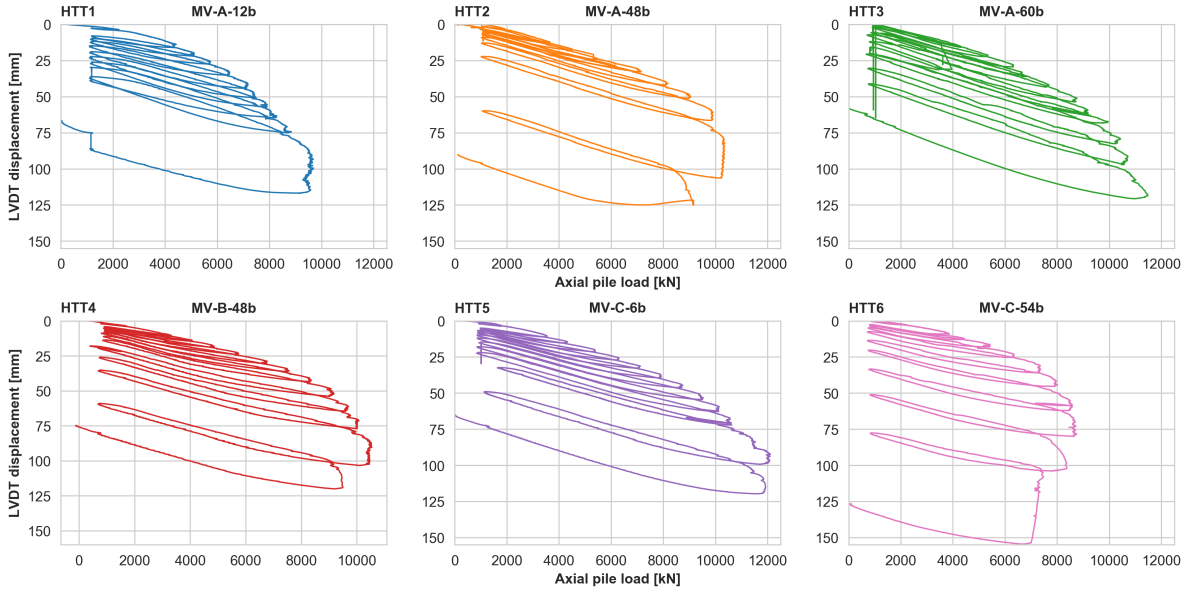

Figure B.12: Load-displacement curves

C

HTT data analysis

C.1. Correlation between cone resistance and installation resistance

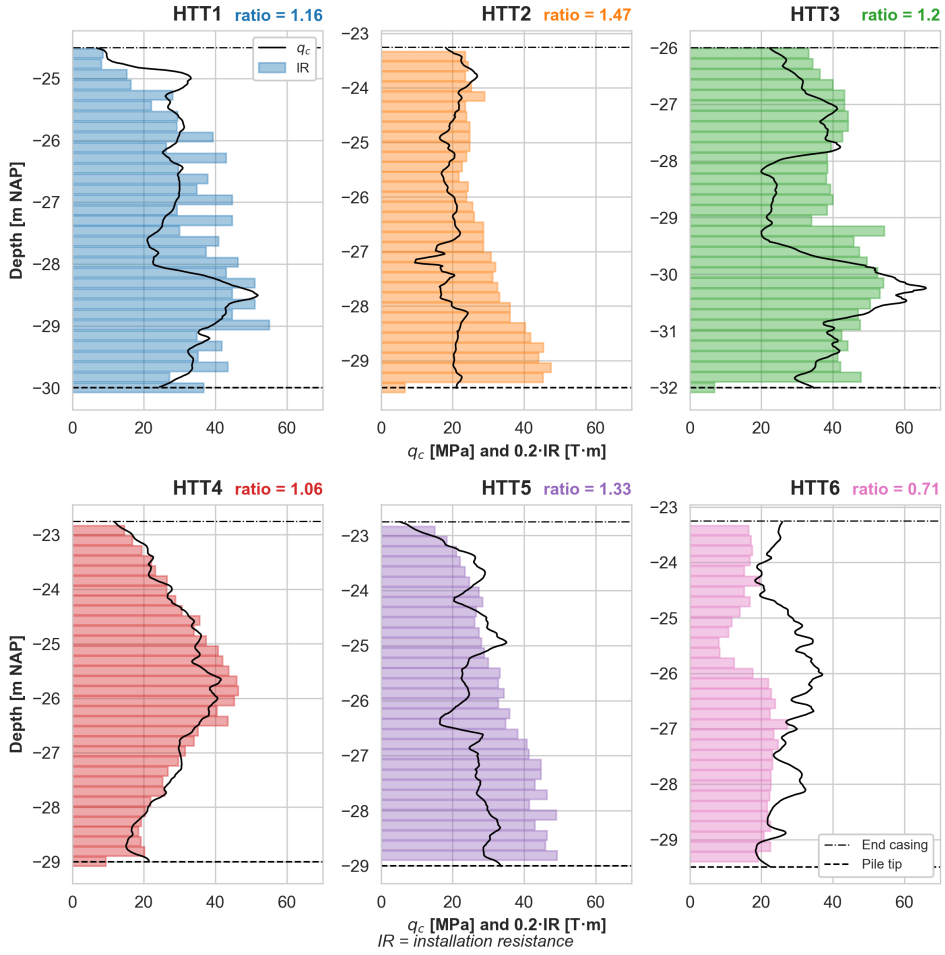

Figure C.1: Correlation between cone resistance (q_c) and installation resistance (IR) per test pile

C.2. Derivation of α_t

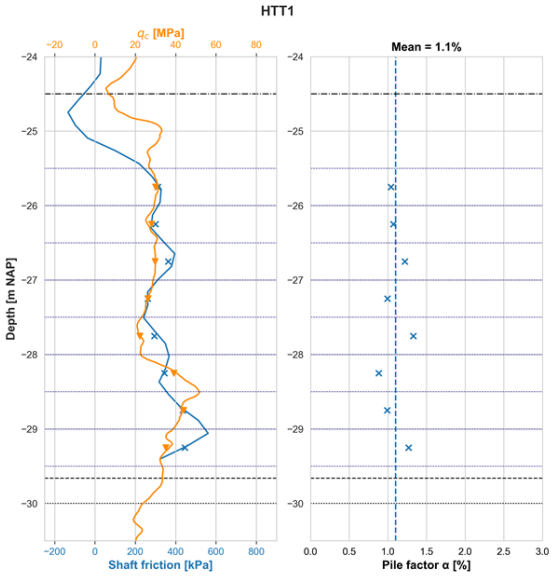

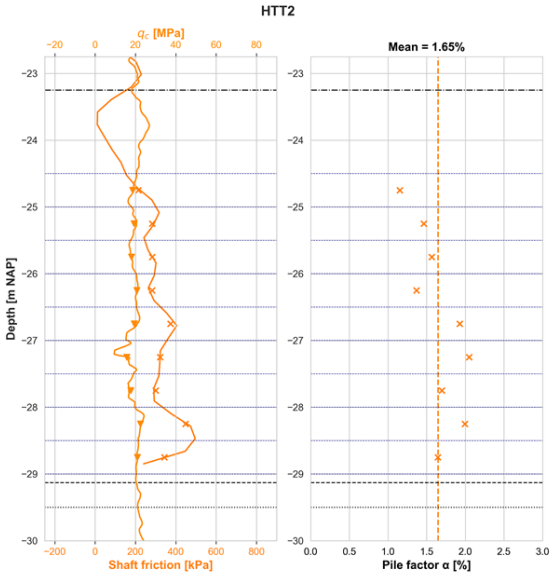

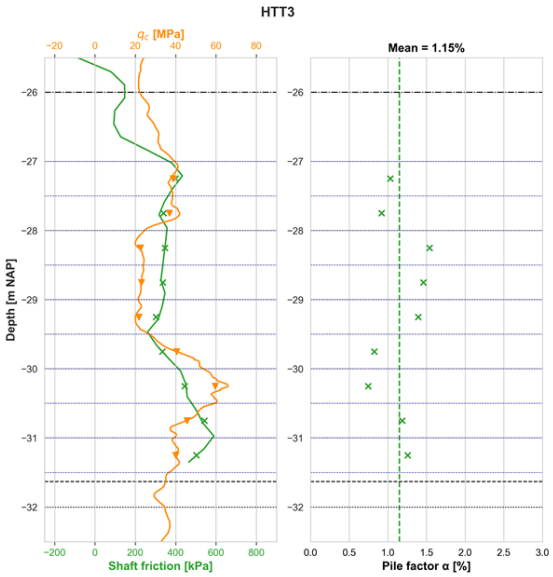

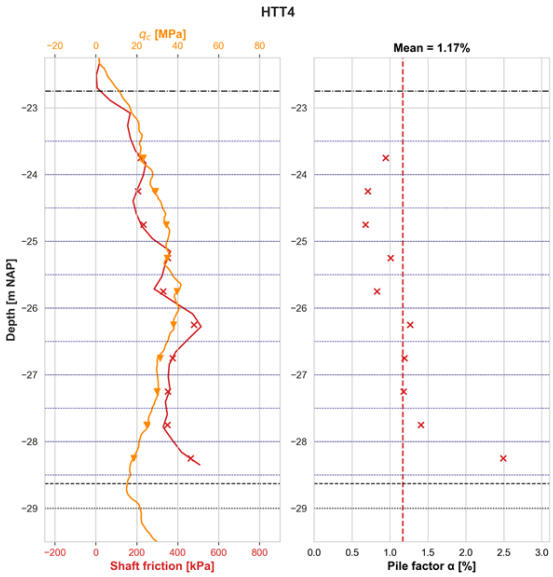

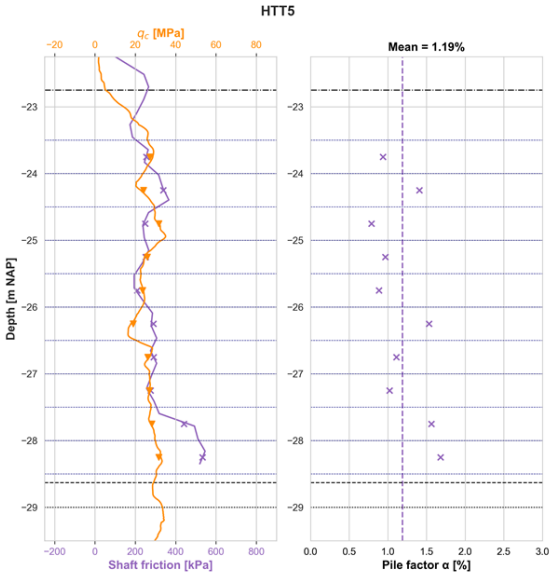
HTT5
q_c [MPa]
Mean = 1.19%
Depth [m NAP]
Shaft friction [kPa]
Pile factor α [%]

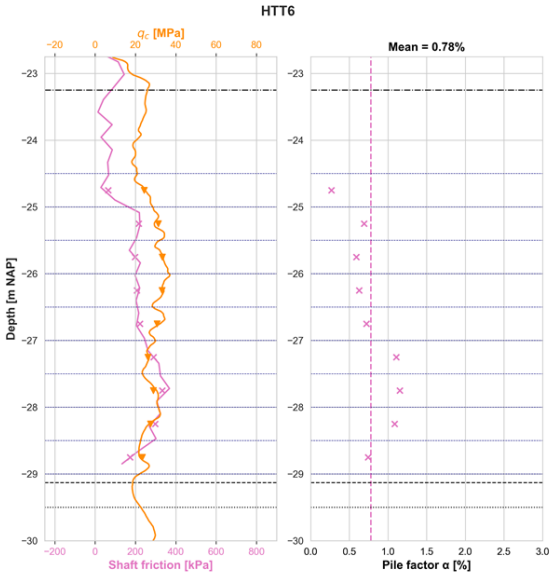
HTT6
q_c [MPa]
Mean = 0.78%
Depth [m NAP]
Shaft friction [kPa]
Pile factor α [%]

C.3. Mobilisation curves

Mobilisation of shaft friction as function of relative pile-soil displacement.

Mobilisation curves

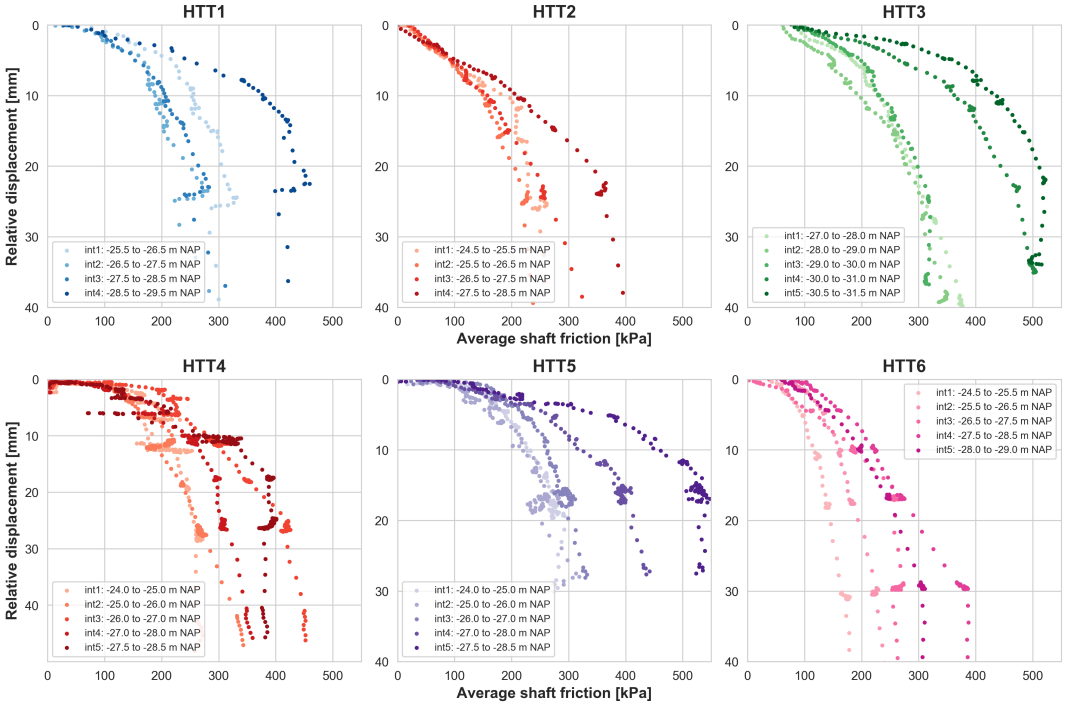

Figure C.2: Mobilisation of shaft friction as function of relative pile-soil displacement per test pile

Normalised mobilisation curves

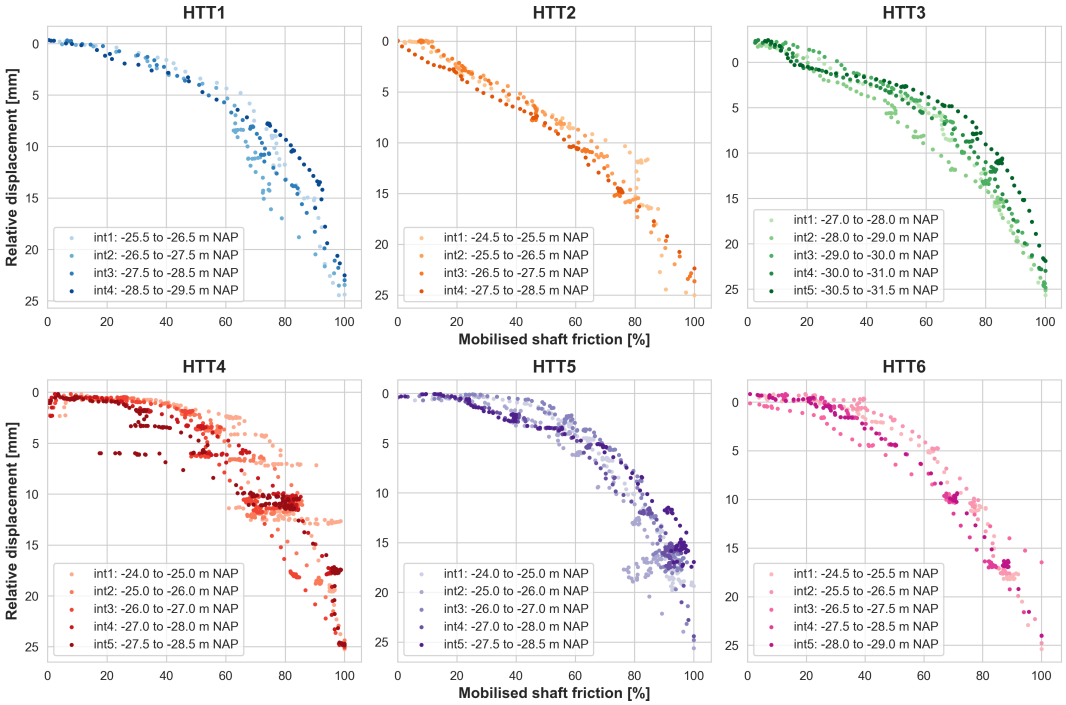

Figure C.3: Mobilisation of normalised shaft friction as function of relative pile-soil displacement per test pile

C.4. Comparison of correlation factors with true measurements

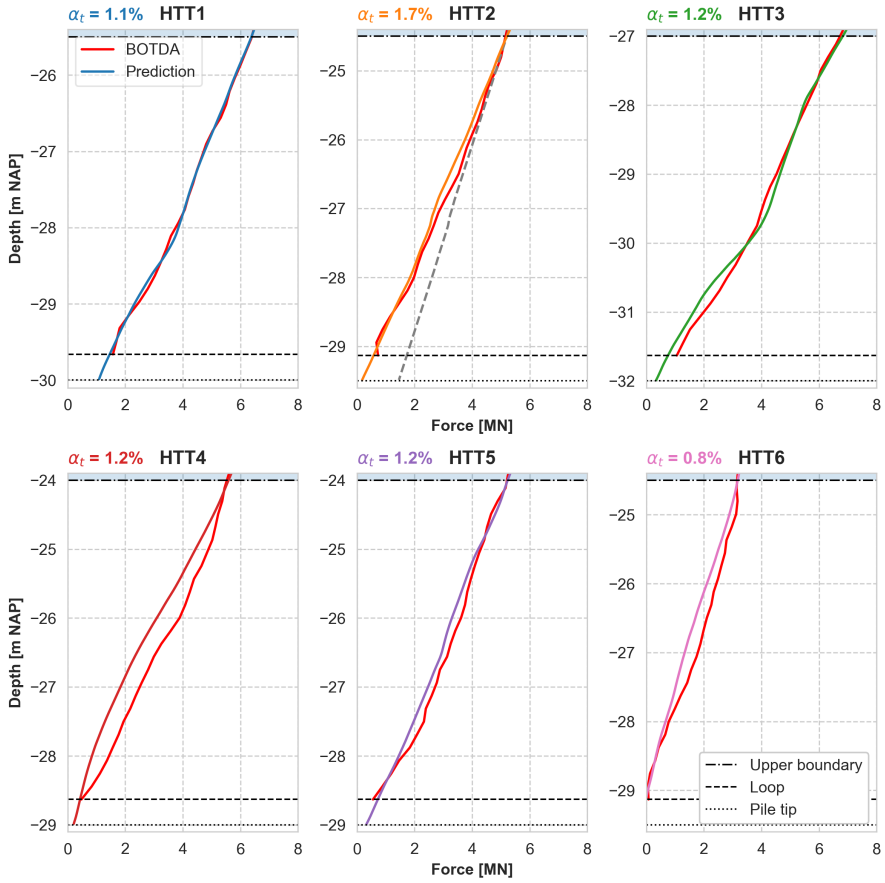

Figure C.4: Predictions for bearing capacity based on derived α_t-values per pile compared to the BOTDA measurements. The blue area indicates the part of the pile at which the distribution of forces is affected by debonding measures in the casing.

C.5. Length reduction of HTT production piles

Zone	Section	Number of piles	Length [m]	New length [m]	Reduction per pile [m]	Reduction per section [m]
A	A1-A3	18	56	51	5	90
	A4-A8	30	53	47.5	5.5	165
	A9-A11	18	54	47.5	6.5	117
B	B1-B20	60	52	44.5	8	480
	B1-B20	60	50.5	44.5	9.5	570
C	C1-C3	18	53	48	5	90
	C4-C11	48	53	45.5	7.5	360
D	D1-D2	14	55	44.5	8.5	119
	D3-D7	35	51	46	5	175
	D8	7	53	46	7	49
Total		308	530.5	465		**2586**

D

Installation data

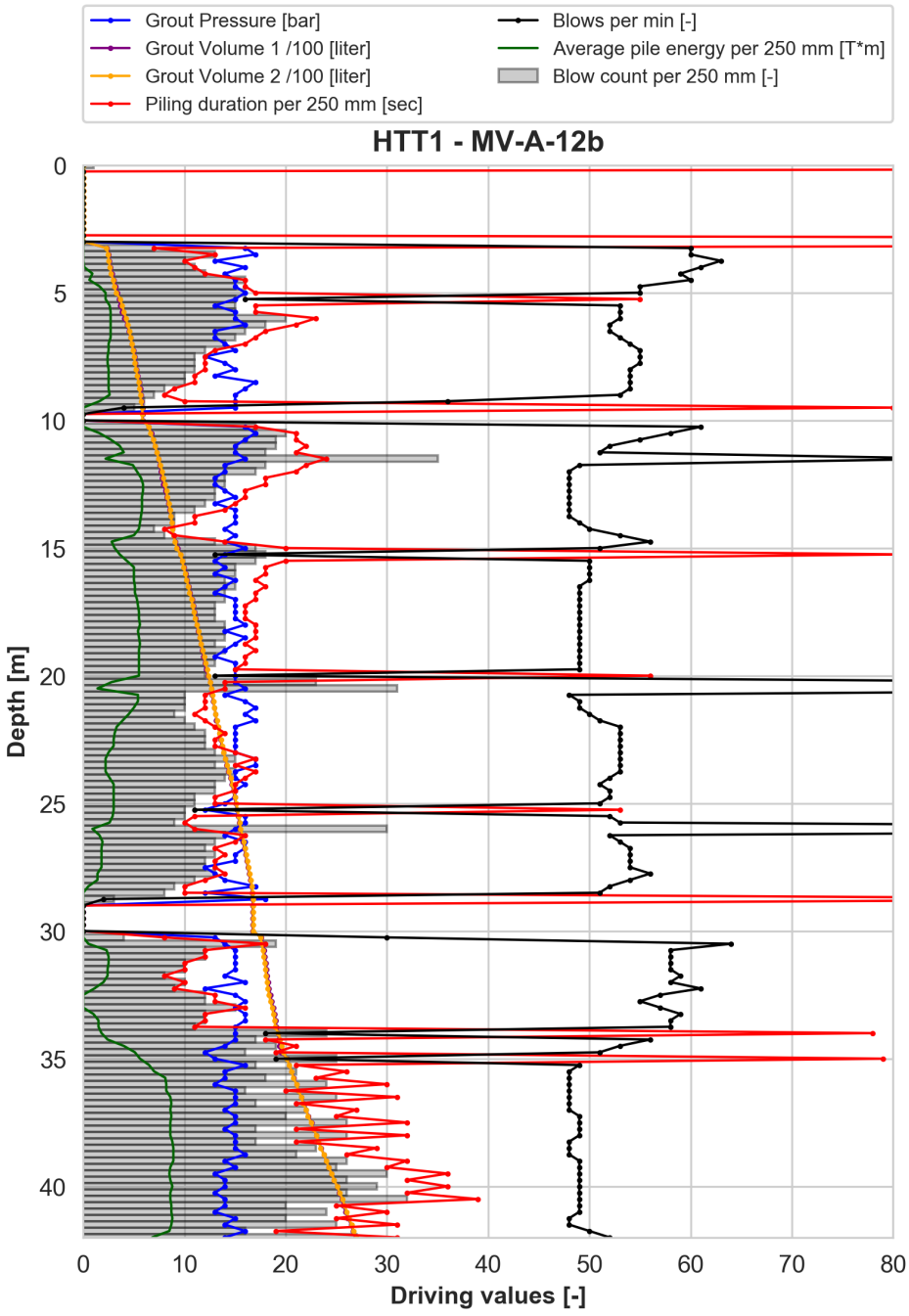

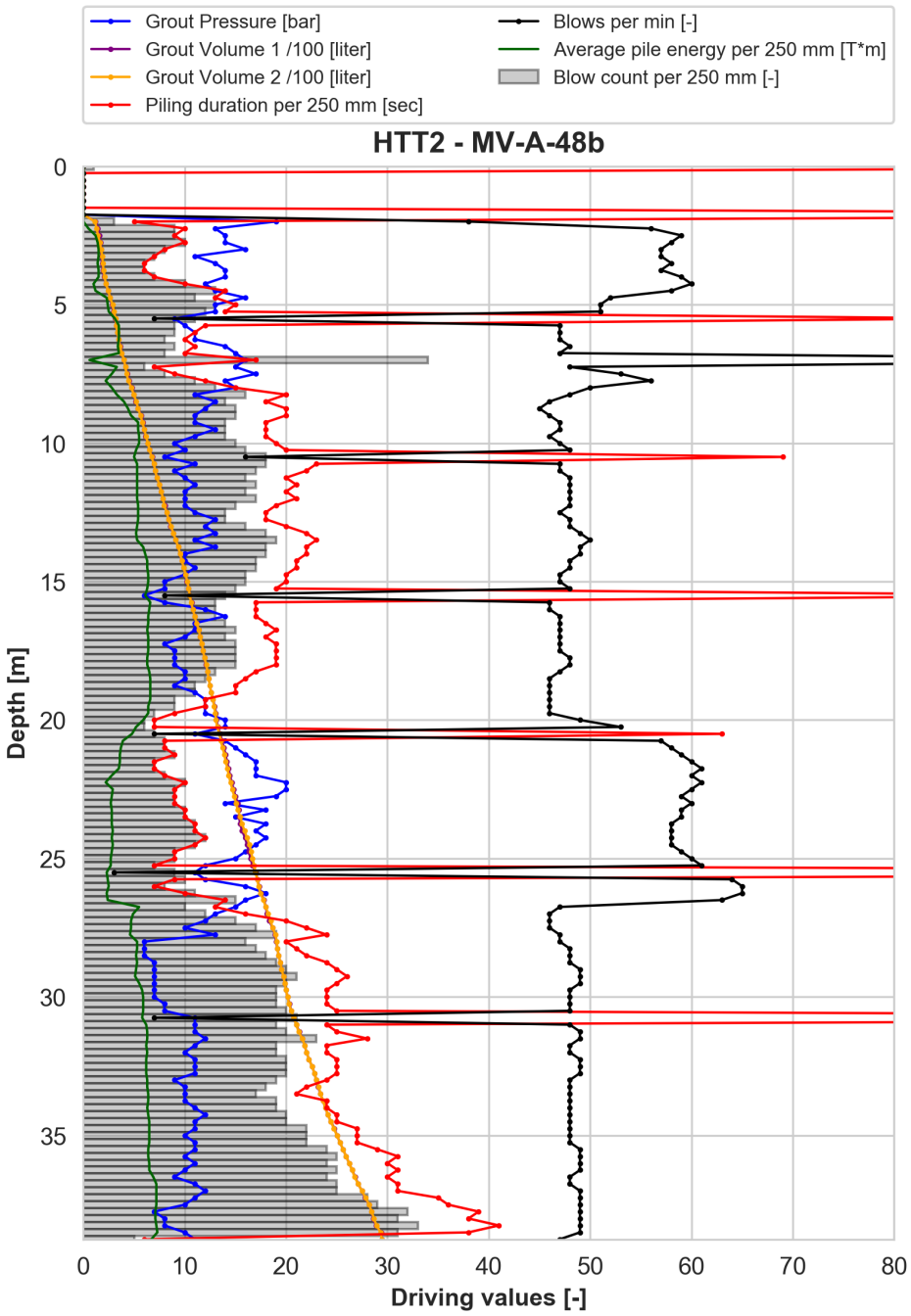
Grout Pressure [bar]
Grout Volume 1 /100 [liter]
Grout Volume 2 /100 [liter]
Piling duration per 250 mm [sec]
Blows per min [-]
Average pile energy per 250 mm [T*m]
Blow count per 250 mm [-]
HTT2 - MV-A-48b
Depth [m]
0
5
10
15
20
25
30
35
0
10
20
30
40
50
60
70
80
Driving values [-]

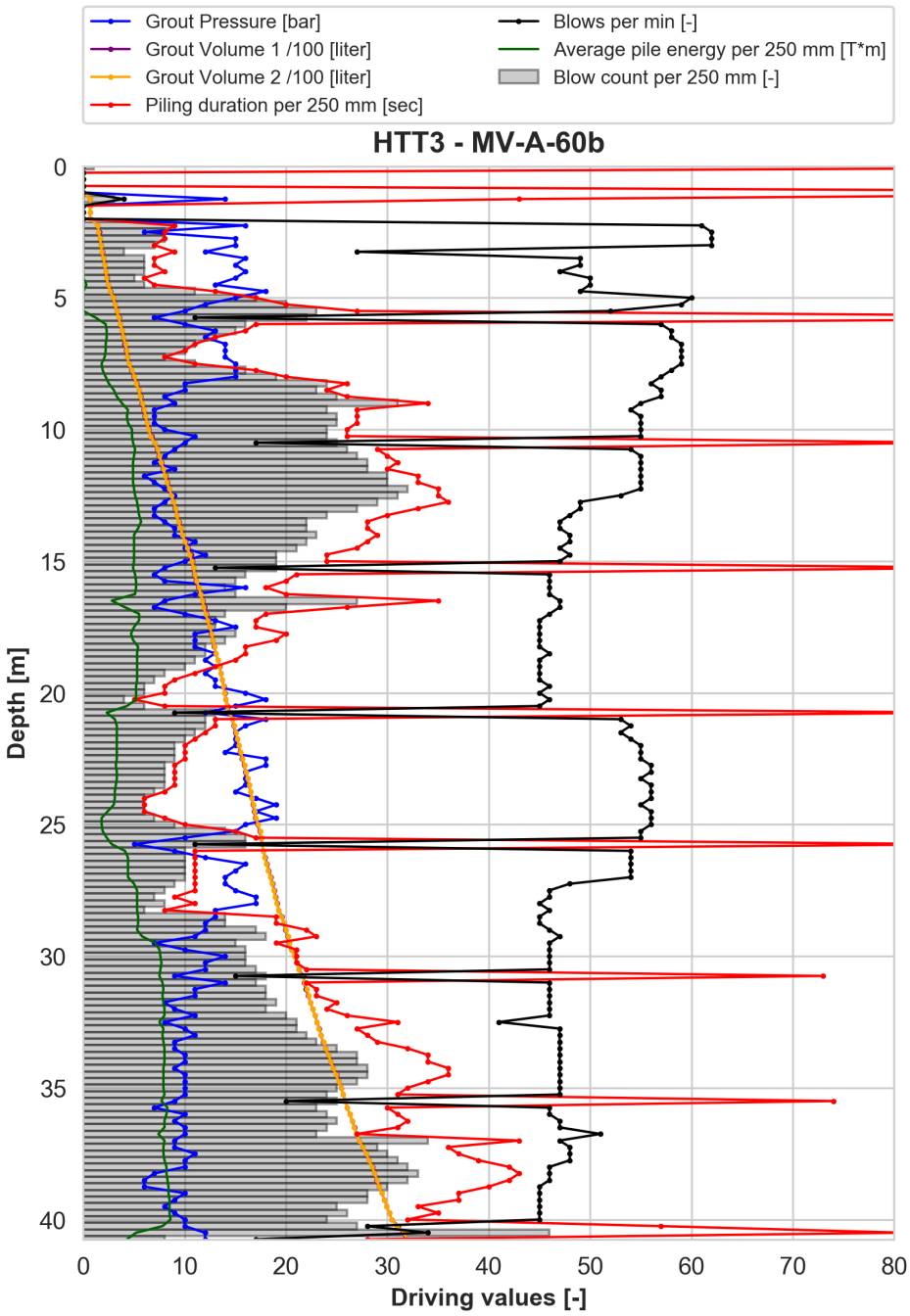
Grout Pressure [bar]
Grout Volume 1 /100 [liter]
Grout Volume 2 /100 [liter]
Piling duration per 250 mm [sec]
Blows per min [-]
Average pile energy per 250 mm [T*m]
Blow count per 250 mm [-]
HTT3 - MV-A-60b
Depth [m]
0
5
10
15
20
25
30
35
40
0
10
20
30
40
50
60
70
80
Driving values [-]

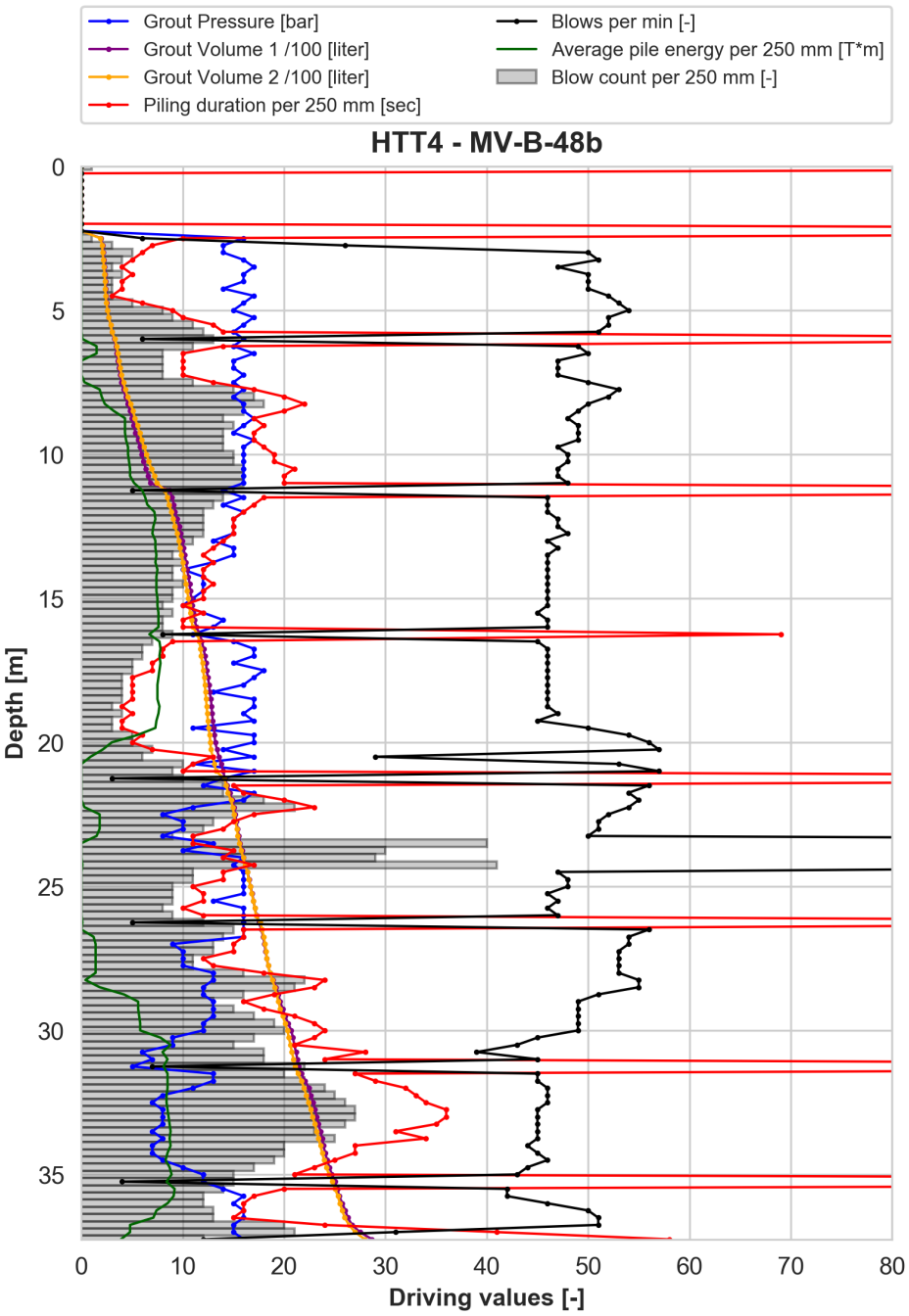
Grout Pressure [bar]
Grout Volume 1 /100 [liter]
Grout Volume 2 /100 [liter]
Piling duration per 250 mm [sec]
Blows per min [-]
Average pile energy per 250 mm [T*m]
Blow count per 250 mm [-]
HTT4 - MV-B-48b
Depth [m]
0
5
10
15
20
25
30
35
0
10
20
30
40
50
60
70
80
Driving values [-]

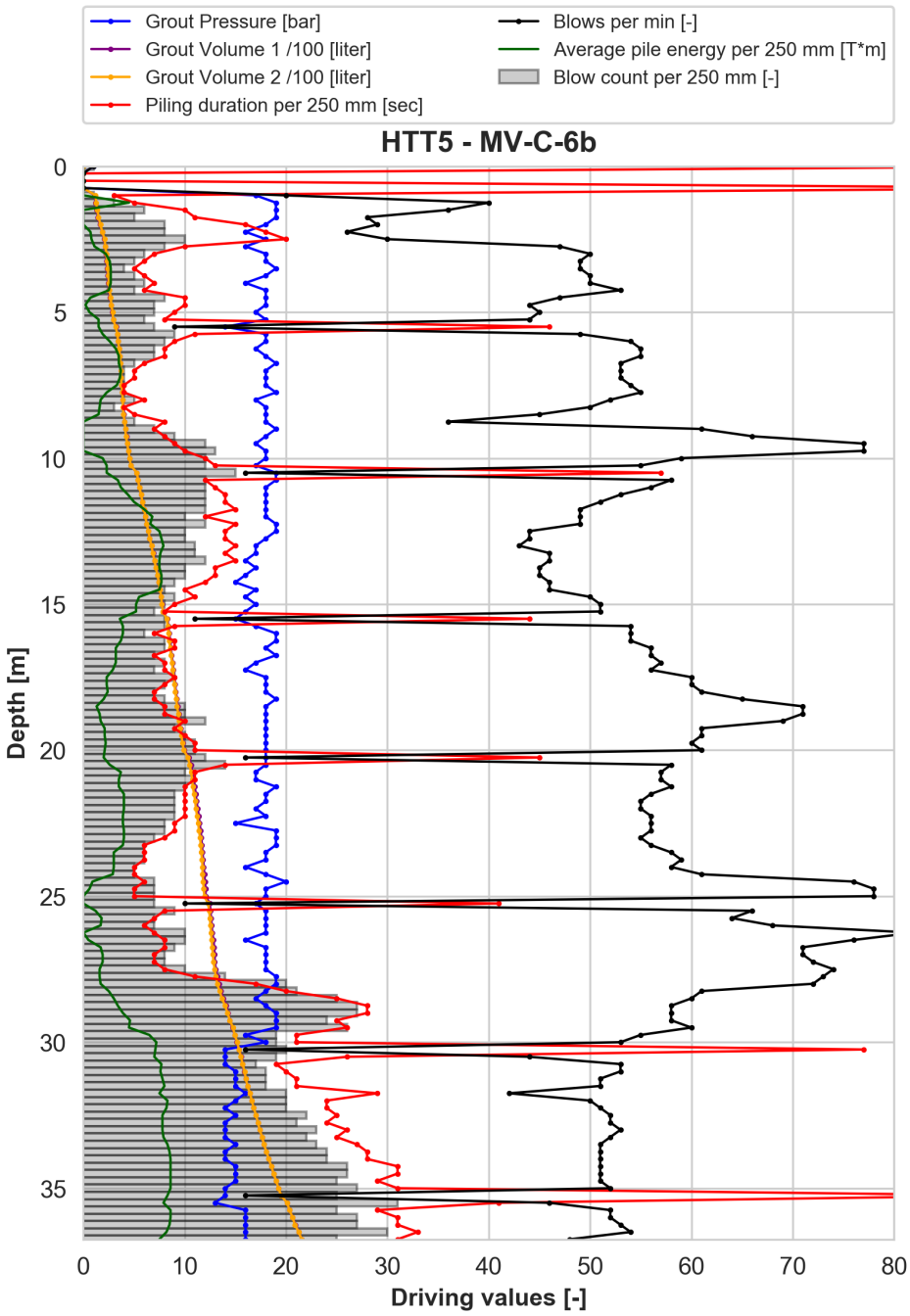
Grout Pressure [bar]
Grout Volume 1 /100 [liter]
Grout Volume 2 /100 [liter]
Piling duration per 250 mm [sec]
Blows per min [-]
Average pile energy per 250 mm [T*m]
Blow count per 250 mm [-]
HTT5 - MV-C-6b
Depth [m]
0
5
10
15
20
25
30
35
0
10
20
30
40
50
60
70
80
Driving values [-]

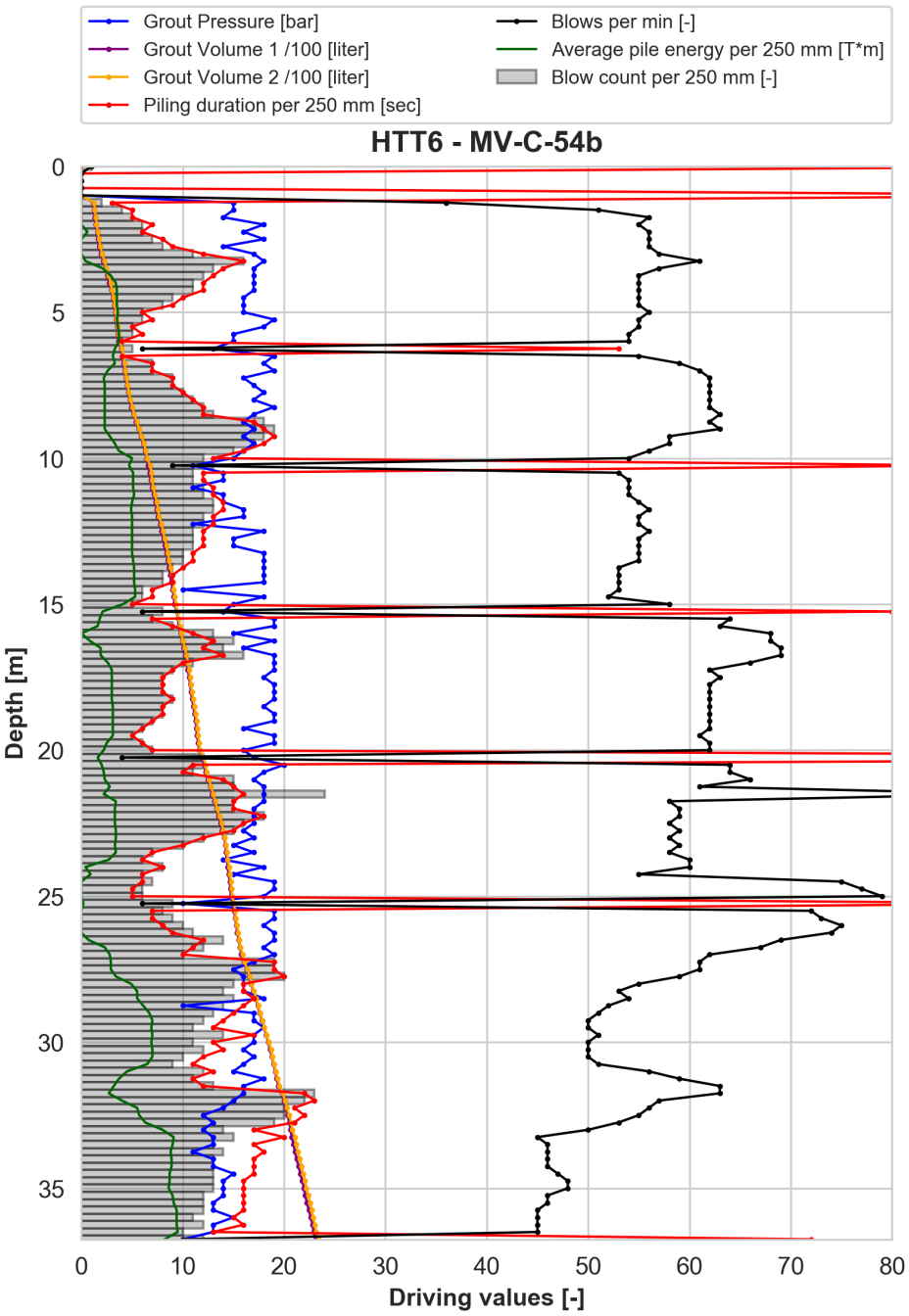
Grout Pressure [bar]
Grout Volume 1 /100 [liter]
Grout Volume 2 /100 [liter]
Piling duration per 250 mm [sec]
Blows per min [-]
Average pile energy per 250 mm [T*m]
Blow count per 250 mm [-]
HTT6 - MV-C-54b
Depth [m]
0
5
10
15
20
25
30
35
0
10
20
30
40
50
60
70
80
Driving values [-]